

**Cobalt and cadmium chalcogenide nanomaterials from
complexes based on thiourea, urea and their alkyl
derivatives: Synthesis and characterization**

BY

Mr E.L MORIFI

STUDENT NUMBER: 20559593

**THIS DISSERTATION IS SUBMITTED FOR THE FULFILMENT OF DEGREE
MAGISTER TECHNOLOGIAE**

FACULTY OF APPLIED AND COMPUTER SCIENCE

DEPARTMENT OF CHEMISTRY

VAAL UNIVERSITY OF TECHNOLOGY

SUPERVISOR : PROF M.J MOLOTO (PhD Chemistry, VUT)

CO-SUPERVISOR : DR. KP MATABOLA (PhD Chemistry, Mintek)

Acknowledgments

I cannot express enough thanks for my supervisor Prof M.J Moloto, who has the attitude and substance of genius, for his exceptional and unlimited support to the last note of the study. During a difficult time when I was in the dark and without knowledge he was very receptive and welcoming. The blessing, help and guidance given by him time to time shall carry me a long way in the journey of life on which I am about to embark.

I also take this opportunity to express a deep sense of gratitude to Mr S. Mpelane for quality results from TEM, Mr S. Nyembe for the XRD analysis and library indexes search (both from Mintek). Mr M Phadi from University of Johannesburg for elemental analysis. Dr N. Moloto for helping in data interpretation. Without helps of the particular that mentioned above, I would face many difficulties while doing this dissertation.

This study has been dedicated to my wonderful family who understood and endlessly encouraged me to never give-up even if the road was too hard. My wife, Mmakgano and son, Junior Laka, who was born when I was in an exchange program in Holland, it was a difficult moment for both of us to appreciate my absent during birth however we had courage and cognisant to realise that in the long-term will benefit us. It will be insensitive to forget my late mother, Monica who sacrificed everything she had, put all needed resources on my disposal and encourage me to study even though she was uneducated.

My gratitude goes to the department of chemistry at Vaal University of Technology (VUT) for allowing me to study in their institution. I am obliged to compliment nanotechnology group for their critics and advices in shaping my study. I speak nanotechnology language because of their constructive criticism.

Last but not list, I would like to acknowledge National Research Foundation (NRF) and HUB & SPOKES at VUT for their constant financial support throughout the study. I should have not made it with an empty stomach.

Finally would like to thank almighty God of ST. Engenas who gave me strength to always shine above meandering points, curves and difficult moments, without being tempted to retaliate with the same kind of force of the opposition.

Table of Content

Title page

Acknowledgments.....	ii
Table of Content	iv
Equation and Schemes	ix
List of Tables	x
List of Figure.....	xi
List of Abbreviations	xiv
Abstract	xv
CHAPTER ONE	1
INTRODUCTION AND BACKGROUND OF NANOPARTICLES	1
1. Introduction and General Background.....	2
1.1 (a) Liposomes.....	4
1.1 (b) Magnetic.....	4
1.1 (c) Dendrimer.....	5
1.1 (d) Nanorods	6
1.1 (e) Fullerenes	6
1.1 (f) Polymeric	7
1.2 Semiconductors.....	7
1.2.1 Quantum dots	8
1.2.2 Core-shells	8

1.2.2 (a) Nucleation mechanism	9
1.2.2 (b) Growth mechanism	10
1.3 Properties of semiconducting nanoparticles	12
1.3.1 (a) Electronic properties from cluster to nanoparticles	12
1.3.1 (b) Optical properties	15
1.3.1 (c) Photoluminescence properties	19
1.3.2 Synthetic methods of nanoparticles	20
1.3.2 (a) Colloidal method	21
1.3.2 (b) Organometallic method	23
1.3.2 (c) Single source precursor method	25
1.4 Aim and Objectives.....	30
1.4.1 Objectives	30
1.5. Problem statement.....	30
CHAPTER TWO	32
SYNTHESIS AND CHARACTERIZATION OF COBALT AND CADMIUM COMPLEXES OF THIOUREA AND UREA	32
2. Introduction.....	33
2.1. Urea and thiourea coordination with the metals.	33
2.2 Experimental Section	41
2.2 (a) Chemical reagents	41
2.3 Instrumentation	41
2.3 (a) FT-IR spectroscopy	41

2.3 (b) Thermogravimetry.....	41
2.3 (c) Microanalysis	41
2.4 Preparation of the complexes.....	42
2.4.1 Methodology	43
2.4.2 Synthesis of cobalt thiourea and urea complexes	44
2.4.2 (a) $\text{CoCl}_2(\text{CS}(\text{NH}_2)_2)_2$	44
2.4.2 (b) $\text{CoCl}_2(\text{CO}(\text{NH}_2)_2)_2$	44
2.4.3 Synthesis of cadmium thiourea and urea complexes	44
2.4.3 (a) $\text{CdCl}_2(\text{CS}(\text{NH}_2)_2)_2$	44
2.4.3 (b) $\text{CdCl}_2(\text{CO}(\text{NH}_2)_2)_2$	45
3. Results and Discussion	46
3.1 (a) FTIR spectral analysis for thiourea and its cobalt and cadmium complexes	46
3.1 (b) FTIR spectra for free urea ligand and its Cd and Co complexes	48
3.2 Thermo gravimetric analysis for complexes.....	52
3.3 Conclusion	54
CHAPTER THREE	55
SYNTHESIS AND CHARACTERAZITION OF NORMAL NANOPARTICLES AND CORESHELL NANOPARTICLES FROM COBALT AND CADMIUM COMPLEXES BASED ON UREA AND THIOUREA.....	55
SECTION A.....	56
Synthesis of nanoparticles and use of single-precursors on urea and thiourea, cobalt and cadmium complexes.....	56

4.1 Introduction.....	56
4.2 Experimental section.....	59
4.2.1 Reagents.....	59
4.2.2 Instrumentation	59
(a) Optical characterization.....	59
(b) X-ray diffraction analysis.....	59
(c) Electron microscopy.....	59
4.2.3 Methodology.....	60
(a) Preparation of nanoparticles from Urea and thiourea, cobalt and cadmium complexes (complex I – IV).....	60
4.3 Results and Discussion	61
4.3.1 Optical properties.....	61
SECTION B	72
Synthesis of core-shell nanoparticles and use of single-precursors on urea and thiourea, cobalt and cadmium complexes.....	72
4.4 Introduction.....	72
4.5.1 Reagents.....	74
4.5.2 Instrumentation	74
(a) Optical characterization.....	74
(b) X-ray diffraction analysis.....	75
(c) Electron microscopy.....	75
4.5.3 Methodology	75

4.5.3.1 Preparation of core-shells nanoparticles from a mixture of two precursors.	75
4.6. Results and Discussions	77
4.6 (a) Synthesis of coreshell nanomaterials based on urea and thiourea cadmium complexes	79
4.6 (b) Synthesis of core-shells nanomaterials based on urea and thiourea cobalt and cadmium complexes.	84
4.6 (c) Synthesis of core-shells nanomaterials based on thiourea and urea cobalt and cadmium complexes	88
4.6 (d) Synthesis of core-shells nanomaterials based on urea and thiorea cobalt complexes..	92
4.6.1 Effect of temperature	96
4.6.1 (a) Synthesis of core-shells nanomaterials based on urea and thiourea cadmium complexes	96
4.7 Conclusion	99
4.9 Summary	100
4.10 Recommendations and future work	102
4.8 References.....	103

Equation and Schemes

Equation 1	9
Equation 2	9
Equation 3	11
Equation 4	12
Equation 5	12
Equation 6	12
Equation 7	17
Equation 8	17
Equation 9	18
Equation 10	18
Equation 11	19
Scheme 1: Schematic of bis(dialkyldithio/seleno-carbamato)cadmium(II)/zinc(II) complex used to prepare nanoparticles of II-VI materials capped with TOP/TOPO.....	27
Scheme 2: Schematic for synthesizing ligand and complex	27
Scheme 3: Structure of urea.	34
Scheme 4: The coordination modes of urea towards metal ions	35
Scheme 5: Structure of thiourea.....	37
Scheme 6: (a) Structure of substituted thiourea showing delocalisation of the p-bond and (b) conformational isomers for both mono and disubstituted alkyl/aryl thiourea.....	39
Scheme 7: Reaction scheme for the synthesis of complexes	43
Scheme 8: Schematic representations for the synthesis of nanoparticles	60
Scheme 9: Schematic representation for the synthesis of core-shell nanomaterials.....	76

List of Tables

Table 1: The wavenumber of the fundamental modes of coordinated thiourea (cm^{-1})	48
Table 2: The wavenumber of the fundamental modes of coordinated urea (cm^{-1}).....	52
Table 3: Reaction conditions for the preparation of nanoparticles from complex I-IV.....	61
Table 4: General variation of concentration and temperature in the preparation of core-shells nanoparticles from complex I, II, III & IV	77
Table 5: Types of core-shells nanoparticles.....	78
Table 6: Variation of concentration in the preparation of CdO:CdS core-shells nanoparticles from complex III & IV	79
Table 7: Band edges and emission maxima.....	80
Table 8: Variation of concentration in the preparation of CoO:CdS core-shells nanoparticles from complex I & III	84
Table 9: Band edges and emission maxima.....	85
Table 10: Variation of concentration in the preparation of CoS:CdO core-shells nanoparticles from complex I & IV	88
Table 11: Band edges and emission maxima.....	89
Table 12: Variation of concentration in the preparation of CoO:CoS core-shells nanoparticles from complex II & I.....	92
Table 13: Band edges and emission maxima.....	93
Table 14: Effect of temperature in the preparation of CdO:CdS core-shells nanoparticles from complex III & IV	96
Table 15: Band edge and emission maxima	97

List of Figures

Figure 1: Types of nanoparticles.....	4
Figure 2: Electronic energy levels of metals and semiconductors as particle size increases from individual atoms to the bulk.	13
Figure 3: Spatial electronic state diagram for bulk semiconductor (a) and (b) nanoparticles	16
Figure 4: Photoluminescence energy diagram	19
Figure 5: FTIR spectra $\text{CdCl}_2(\text{CS}(\text{NH}_2)_2)_2$ and free thiourea ligand, $(\text{CS}(\text{NH}_2)_2)_2$	46
Figure 6: FTIR spectra $\text{CoCl}_2(\text{CS}(\text{NH}_2)_2)_2$ and free thiourea ligand, $(\text{CS}(\text{NH}_2)_2)_2$	47
Figure 7: FTIR spectra $\text{CdCl}_2(\text{CO}(\text{NH}_2)_2)_2$ and free urea ligand, $(\text{CO}(\text{NH}_2)_2)_2$	50
Figure 8: FTIR spectra $\text{CoCl}_2(\text{CO}(\text{NH}_2)_2)_2$ and free urea ligand, $(\text{CO}(\text{NH}_2)_2)_2$	50
Figure 9: TGA curves for Cd-urea and Cd-thiourea complexes.....	53
Figure 10: TGA curves for Co-urea and Co-thiourea complexes.....	54
Figure 11: (a) Absorption spectrum and (b) emission spectrum of CdS nanoparticles synthesized from Cd- thiourea complex.	62
Figure 12: TEM image of CdS nanoparticles prepared at 180°C, 1g precursors: 6g HDA from the Cd-thiourea complex	64
Figure 13: XRD patterns of HDA capped CdS nanoparticles synthesized from Cd-thiourea complexes, at 180 °C.....	65
Figure 14: (a) Absorption spectrum and (b) emission spectrum of CdO nanoparticles synthesized from Cd-Urea complex.	65
Figure 15: TEM image of CdO nanoparticles prepared at 180°C, 1g precursor: 6g HDA from the Cd-urea complex.....	66
Figure 16: XRD patterns of HDA capped CdO nanoparticles synthesized from Cd-urea complexes, at 180 °C.....	67

Figure 17: (a) Absorption spectrum and (b) emission spectrum of CoS nanoparticles synthesized from Co-thiourea.....	68
Figure 18: TEM image of CoS nanoparticles prepared at 180°C, 1g precursor: 6g HDA from the Co-thiourea complex	68
Figure 19: XRD patterns of HDA capped CoS nanoparticles synthesized from Co-thiourea complexes, at 180 °C.....	69
Figure 20: (a) Absorption spectrum and (b) emission spectrum of CoO nanoparticles synthesized from Co-Urea.....	69
Figure 21: TEM image of CoO nanoparticles prepared at 180°C, 1g precursor: 6g HDA from the Co-urea complex.....	70
Figure 22: XRD patterns of HDA capped CoS nanoparticles synthesized from Co-thiourea complexes, at 180 °C.....	71
Figure 23: (a) Absorption spectra (i(1:1), ii(1:2) and iii(1:3)) and (b) emission spectra(i(1:1), ii(1:2) and iii(1:3)) of CdO-CdS nanoparticles synthesized from Cd-Urea and Cd-thiore complexes.	80
Figure 24: TEM images of CdO-CdS nanoparticles prepared at 180°C (a) 1:1, (b) 1:2, (c) 1:3 precursors: 6g HDA from the Co-urea and Cd-thiourea complexes.	82
Figure 25: XRD patterns of HDA capped CdO-CdS core-shell nanoparticles synthesized from Cd-urea and Cd-thiourea complexes in the ratio (a) 1:1, (b) 1:2 and (c) 1:3.	83
Figure 26: (a) Absorption spectra (i(1:1), ii(1:2) and iii(1:3)) and (b) emission spectra(i(1:1), ii(1:2) and iii(1:3)) of CoO-CdS nanoparticles synthesized from Co-Urea and Cd-thiore complexes.	85
Figure 27: TEM images of CoO-CdS nanoparticles prepared at 180°C (a) 1:1, (b) 1:2, (c) 1:3 precursors: 6g HDA from the Co-urea and Cd-thiourea complexes.....	87

Figure 28: XRD patterns of HDA capped CoO-CdS coreshell nanoparticles synthesized from Co-urea and Cd-thiourea complexes in the ratio (a) 1:1, (b) 1:2 and (c) 1:3.	88
Figure 29: (a) Absorption spectra (i(1:1), ii(1:2) and iii(1:3)) and (b) emission spectra(i(1:1), ii(1:2) and iii(1:3)) of CoS-CdO nanoparticles synthesized from Co-thiourea and Cd-Urea complexes.	89
Figure 30: TEM images of CoS-CdO nanoparticles prepared at 180°C (a) 1:1, (b) 1:2, (c) 1:3 precursors: 6g HDA from the Co-thiourea and Cd-urea complexes.....	91
Figure 31: XRD patterns of HDA capped CoS-CdO coreshell nanoparticles synthesized from Co-thiourea and Cd-urea complexes in ratios of 1:1(a), 1:2(b) and 1:3(c).	92
Figure 32: (a) Absorption spectra(i(1:1), ii(1:2) and iii(1:3)) and (b) emission spectra(i(1:1), ii(1:2) and iii(1:3)) of CoO-CoS nanoparticles synthesized from Co-urea and Co-thiourea complexes.	93
Figure 33: TEM images of CoO-CoS nanoparticles prepared at 180°C (a) 1:1, (b) 1:2, (c) 1:3 precursors: 6g HDA from the Co-urea and Co-thiourea complexes.....	94
Figure 34: XRD patterns of HDA capped CoO-CoS coreshell nanoparticles synthesized from Co-urea and C-thiourea complexes in the ratio 1:1(a), 1:2(b) and 1:3(c).	95
Figure 35: (a) Absorption spectrum and (b) emission spectrum of CdO-CdS nanoparticles synthesized from Cd-urea and Cd-thiourea complexes.....	97
Figure 36: TEM images of CdO-CdS particles prepared at 100°C, 1:3 precursors: 6g HDA from the Cd-urea and Cd-thiourea complexes.	98
Figure 37: XRD patterns of HDA capped CdO-CdS coreshell nanoparticles synthesized from Cd-urea and Cd-thiourea complexes, at 100 °C.	99

List of Abbreviations

nm	nanometer
a.u	arbitrary units
cm	centimeter
°C	degree celsius
E_g	band gap
QDs	quantum dots
eV	electron volts
a_B	Bohr radius
a	lattice spacing
d	diameter
e	elementary charge
E	energy
ϵ	dielectric constant
h	Planck`s constant
λ_{exc}	excitation wavelength
ν	frequency
R	radius
T	temperature
t	time
U	urea
tu	thiourea

Abstract

Cadmium and cobalt complexes of urea and thiourea were synthesized using ethanol as a solvent. All complexes were refluxed at 70 - 80 °C, left to cool at room temperature, washed with methanol and acetone to remove impurities and dried at an open environment. The characterization of complexes was done using FTIR spectroscopy, elemental analysis and TGA. The complexes were found to coordinate with the ligands through sulphur and oxygen atoms to the metal, instead of nitrogen. These were as results of wavelength shifting from high to low frequency from spectra of the complexes as compare to their free ligands. These observations make these complexes good candidates for the possible use in synthesis of metal sulphides or oxides nanoparticles. Thermogravimetric analyses of all the complexes were conducted to check the stability of use as precursors for nanoparticles at low and high temperature. A number of thiourea and urea complexes with cadmium and cobalt have been prepared and used in the preparation of metal sulphides/oxides nanoparticles. Complexes start to decompose at low temperature about 100°C and the last decomposition step was at about 800-900°C, which is convenient to thermal decomposition of precursors in the high boiling solvents or capping agent to prepare surface capped metal sulphides/oxides nanoparticles. The complexes were easy to synthesize, low cost and stable in air and were obtained in reasonable yields.

All the complexes reported in this study have been used as single source molecular precursor in the preparation of cadmium oxide, cadmium sulphide, cobalt oxide, cobalt sulphide nanoparticles (normal) and as mixture of any two complexes to form core-shells nanoparticles. Quality nanoparticles synthesis requires three components: precursors, organic surfactants and solvents. The synthesis of the nanoparticles can be thought of as a nucleation event, followed

by a subsequent growth period. Both the nucleation and growth rates were found to be dependent upon factors such as temperature, growth time, and precursor concentration. For a continuous flow system the residence time (at nucleation and growth conditions) was also found to be important. In order to separate the nucleation and growth events, injection techniques were employed to achieve rapid nucleation of nanoparticles with final size dictated by the growth temperature and/or residence time through the growth zone of the reaction system.

Good crystalline normal nanoparticles were obtained from thermolysis of the precursors in hexadecylamine (HDA) as the capping agent at fixed concentrations, temperature and time. All nanoparticles showed a blue-shift in band edges with good photoluminescence behaviour which is red-shifted from their respective band edges and XRD patterns, the crystal structure are in hexagonal phase. The particles showed rods, spheres and hexagonal shapes. Nucleation and growth mechanism brings new avenue in nanostructures called core-shells, which have been reported to have improved luminescence, quantum yields, decreased fluorescence lifetimes, and benefits related to the tailoring of the relative band-gap positions between the two materials. In this study cadmium and cobalt complexes of urea and thiourea were separately dispersed in TOP and injected separately (allowing nucleation/core to occur, followed by the shell) in hot HDA at 180°C for 1hour to yield core-shell nanoparticles. Parameters, such as concentration, temperature and capping molecule as factor affecting nucleation and growth of the core-shells were monitored. The core-shell nanoparticles were characterized by UV/Vis spectroscopy, XRD and TEM. We observed spherical, tripod, bipods, hexagonal and irregular shaped nanoparticle as the concentration of the precursors was increasing, however we were able to form core-shells nanoparticles in one set of experiment 1:3 CdS-CdO, which are assumed to be a reverse type I coreshells nanoparticles. Exciton

absorption peaks at higher energy than the fundamental absorption edge of bulk indicate quantum confinement effect in nanoparticles as a consequence of their small size. XRD patterns, crystals range from hexagonal, cubic and mixture of hexagonal and orthorhombic. A low temperature studies were also conducted a mixture of hexagonal and sphererical shapes with sheets like onion morphology were observed.

CHAPTER ONE

INTRODUCTION AND BACKGROUND OF NANOPARTICLES

1. Introduction and General Background

Nanotechnology as defined for the projects in this chapter arises from the exploitation of the novel and improved physical, chemical, mechanical, and biological properties, phenomena, and processes of systems that are intermediate in size between isolated atoms/molecules and bulk materials, where phenomena length and time scales become comparable to those of the structure. It implies the ability to generate and utilize structures, components, and devices with a size range from about 0.1 nm (atomic and molecular scale) to about 100 nm (or larger in some situations) by control at atomic, molecular, and macromolecular levels. Novel properties occur compared to bulk behaviour because of the small structure size and short time scale of various processes/methods.

Nanotechnology has been identified by many as a key future technology area. Nanotechnology is a field that is closely concerned with the potential economic growth. The emerging of Nanotechnology concerned governments to invest substantial financial resources to further research and development as well as to translate research results into commercial application. Understanding the broad scope and diversity of the nanoscience industry is an important first step in identifying potential opportunities that may be associated with this technology. Current interest in nanotechnology in the world is broad-based and generally spread into small groups. The research themes receiving the most attention include:

- metallic and ceramic nanostructured materials with engineered properties
- molecular manipulation of polymeric macromolecules
- chemistry self-assembling techniques of “soft” nanostructures
- thermal spray processing and chemistry-based techniques for nanostructured coatings
- nanofabrication of electronic products and sensors

- nanostructured materials for energy-related processes such as catalysts and soft magnets
- Nanomachining
- miniaturization of spacecraft systems

In addition, neural communication and chip technologies are being investigated for biochemical applications; metrology has been developed for thermal and mechanical properties, magnetism, micromagnetic modeling, and thermodynamics of nanostructures; modeling at the atomistic level has been established as a computational tool; and nanoprobe have been constructed to study material structures and devices with nanometer length scale accuracy and picosecond time resolution. While generation of nanostructures under controlled conditions by building up from atoms and molecules is the most promising approach, materials restructuring and scaling-down approaches will continue. Exploratory research includes tools of quantum control and atom manipulation, computer design of hierarchically structured materials, artificially structured molecules, combination of organic and inorganic nanostructures, biomimetics, nanoscale robotics, encoding and utilization of information by biological structures, DNA computing, interacting textiles, and chemical and bioagent detectors [1]. Nanoparticles can be classified on the basis of the type of material into metallic, semiconductor and polymeric nanoparticles. Two metallic nanoparticles (that is gold and magnetic nanoparticles) and one semiconductor nanoparticle (that is quantum dots (QDs)) are described here (**Figure 1**).

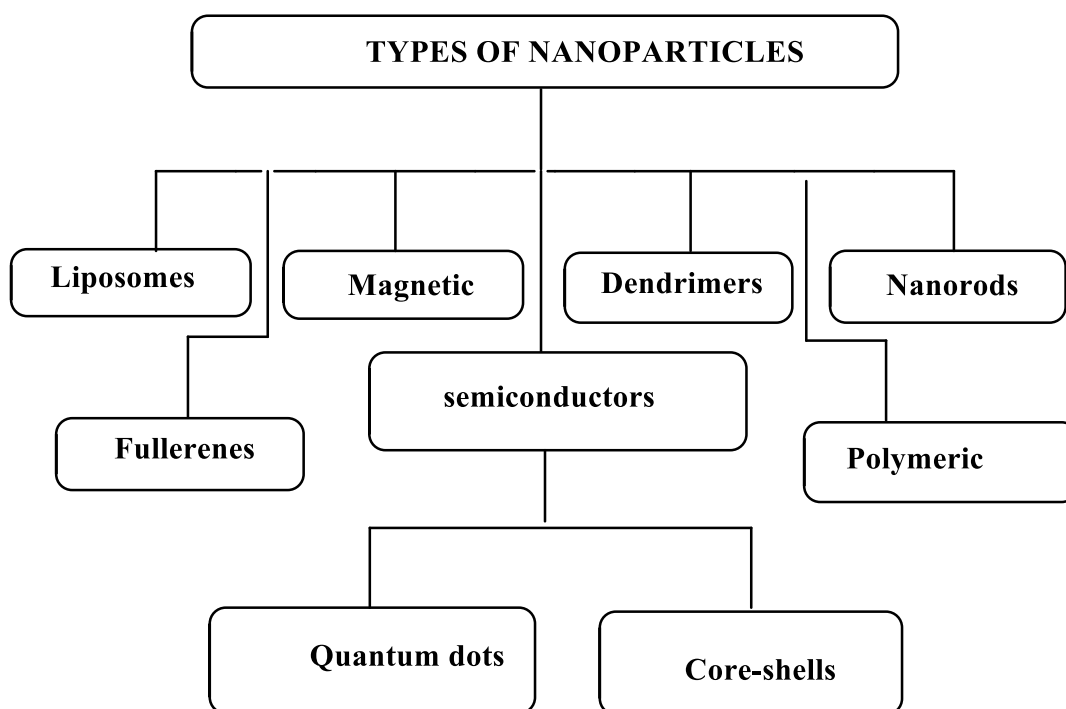


Figure 1: Types of nanoparticles

1.1(a) Liposomes

Liposomes are lipid-based liquid crystals, used extensively in the pharmaceutical and cosmetic industries because of their capacity for breaking down inside cells once their delivery function has been met. Liposomes were the first engineered nanoparticles used for drug delivery but problems such as their propensity to fuse together in aqueous environments and release their payload, have lead to replacement, or stabilization using newer alternative nanoparticles.

1.1(b) Magnetic properties

Super-paramagnetic molecules are those that are attracted to a magnetic field but do not retain residual magnetism after the field is removed. Nanoparticles of iron oxide with diameters in the 5-100 nm range have been used for selective magnetic bio-separations. Typical techniques involve coating the particles with antibodies to cell-specific antigens, for separation from the surrounding matrix. Used in membrane transport studies and are applied for drug delivery and

gene transfection. Targeted delivery of drugs, bioactive molecules or DNA vectors is dependent on the application of an external magnetic force that accelerates and directs their progress towards the target tissue.

1.1 (c) Dendrimers

A dendrimer is a macromolecule which is characterised by its highly branched three-dimensional structure. The structure is always built up around a central multi-functional core molecule and this extremely regular structure contributes to its near-perfect spherical shape. Due to their size, 15 nm, and branching architecture with a relatively hollow core surrounded by a compact surface, dendrimer molecules could be utilised for sensing, catalysis or biochemical activity. They may also find application as light-harvesting antennae and as molecular amplifiers [2]. It has also been suggested that when drug molecules are attached to the periphery, the dendrimer can be used as an efficient drug-delivery platform. Studies have demonstrated potential application of dendrimers as gene carriers [3]. Although linear polymers may be considered to be of nanomeric dimensions, there is one specific group of polymers that is designed to exploit its nanomeric size and characteristics. These are dendrimers and they are large and complex molecules with very well-defined structures. They are almost perfectly monodisperse macromolecules with a regular and highly branched three-dimensional architecture. Dendrimers can act as biologically active carrier molecules in drug delivery, to which can be attached therapeutic agents. They can also be used as scavengers of metal ions, offering the potential for environmental clean-up operations [2].

1.1(d) Nanorods

Typically 1-100 nm in length, nanorods are most often made from semiconducting materials and used in nanomedicine as imaging and contrast agents. Nanorods can be made by generating small cylinders of silicon, gold or inorganic phosphate, among other materials.

1.1(e) Fullerenes

Fullerene can be defined by means of buckyballs and carbon tubes which are carbon based lattice-like and potentially porous molecules. Carbon nanotubes are structures that consist of graphene cylinders closed at either end with caps containing pentagonal rings. They exhibit extraordinary strength and unique electrical properties and are efficient conductors of heat along their length. They exist in single-wall and multi-wall forms. They have been used as composite fibres in polymers and concrete to improve the mechanical, thermal and electrical properties of the bulk product. They have also been used as brushes for electrical motors. Inorganic variants have also been produced [4, 5]. Carbon Buckyballs are the classic three-dimensional carbon nanomaterials. They have a unique structure comprising 60 carbon atoms. These C₆₀ molecules comprise the same combination of hexagonal and pentagonal rings. These spherical molecules were discovered in 1985 and considerable work has gone into their study. However, potential applications have been limited and include catalysts, drug delivery systems, optical devices, chemical sensors and chemical separation devices. The molecule can absorb hydrogen with enhanced absorption when transition metals are bound to the buckyballs, leading to potential use in hydrogen storage [6].

1.1 (f) Polymeric

Polymeric nanoparticles (PNPs) consist of a biodegradable polymer. Biocompatibility is an essential feature for potential application as tissue engineering, drug and gene delivery and new vaccination strategies. Most biodegradable polymers consists of synthetic polyesters like polycyanoacrylate or poly(D, L-lactide) and related polymers like poly(lactid acid) PLA or poly(lactide-co-glycolide) to give a few examples. Latest developments also include natural polymers like chitosan, gelatin, and sodium alginate to overcome some toxicological problems with the synthetic polymers. Polymeric nanoparticles represent a significant improvement over traditional oral and intravenous methods of administration in terms of efficiency and effectiveness [7].

1.2 Semiconductors

Semiconductors are shaping our everyday lives because most of our electronic devices contain a computer chip which can only work because of the special properties of semiconductors. But not just their electric transport properties make them interesting, they also have unique optical properties. Semiconductors in the ground state would behave like an insulator but the low energy gap between the valence band filled with electrons and the empty conduction band makes it relatively easy to optically excite electrons into the conduction band. Semiconductor nanocrystallites whose radii are smaller than the bulk exciton Bohr radius constitute a class of materials intermediate between molecular and bulk forms of matter [8]. Bohr radius which is typically several nanometers for semiconductors [9]. When the size of a nanoparticle exceeds the Bohr radius, the dominant interaction for the electron and hole is their coulombic interaction [10]. For systems with dimensions less than the Bohr radius, increased spatial confinement of the electrons and holes results in both a forced increase in the coulombic interaction energy as well an energy associated simply with carrier confinement.

1.2.1 Quantum dots

A quantum dot is a semiconductor nanocrystal whose size is in the range 1–20 nm. The size of these particles results in new quantum phenomena that yield significant benefits. Material properties change dramatically at this scale because quantum effects arise from the confinement of electrons and holes in the material. These nanostructures confine conduction band electrons, valence band holes, or excitons in all three spacial directions [11]. Size changes other material properties such as the electrical and nonlinear optical properties of a material making them very different from those of the material's bulk form. If a dot is excited, the smaller the dot, the higher the energy and intensity of its emitted light. Hence these very small semiconducting quantum dots provide the potential for use in a number of new applications. The colour of the emitted light depends on the size of the dot, the larger the dot, the redder the light. As the dots become smaller, the emitted light becomes shorter in wavelength yielding emitted blue light. Examples of quantum dots are semiconductor nanocrystals and core-shell nanocrystals, where there is an interface between different semiconductor materials. They have been applied in biotechnology for cell labelling and imaging, particularly in cancer imaging studies [12].

1.2.2 Core-shells

Recent advances in the synthesis of highly monodisperse nanocrystallites [13-15] have paved the way for numerous spectroscopic studies [16] assigning the quantum dot electronic states and mapping out their evolution as a function of size. Core-shell type quantum dots exhibit novel properties making them attractive from both an experimental and a practical point of view [17, 18]. Overcoating nanocrystallite with higher band gap inorganic materials has been shown to improve the photoluminescence quantum yields by passivating surface non-radiative recombination sites. Particles passivated with inorganic shell structures are more robust than

organically passivated dots and have greater tolerance to processing conditions necessary for incorporation into solid state structures. One of the most important aspects of understanding the core-shell is by carefully examining the growth mechanism of nanocrystal which involves two processes, the nucleation followed by the growth.

1.2.2 (a) Nucleation mechanism

Generally, the nucleation is considered as a first stage of embryos formation from nuclei which are only nanometer in size and possible growth to the final particles. In fact, the nucleation is the first formation step of the solid phase from other phases such as solid, liquid and gas. Nucleation occurs and continues with aggregation and clustering of molecules or ions in a supersaturated melt, solution or vapor to form a stable size of solid phase. It seems that supersaturation of solute in the main matrix is the important key to nucleation of particle. Indeed, the driving force for nucleation and growth phenomena is supersaturation. After dissolving the chemical species in a solvent, whether or not of a predetermined nature, to observe the nucleation and growth process the solution must be supersaturated [19, 20]. Supersaturation is the difference between the chemical potential of the solute molecules in the supersaturated (μ) and saturated (μ_s) states respectively. For one molecule, difference is explained by:

$$\Delta\mu = \mu - \mu_s = K_B T \ln \beta \quad (\text{Equation 1})$$

where K_B is the Boltzmann constant and T is the temperature. To simplify, we consider that the activities are equal to the concentrations and can be written as [19]:

$$\beta = C_i/C_s \quad (\text{Equation 2})$$

Here β is the supersaturation ratio, C_i is the concentration of the solute in solution and C_s its saturated or equilibrium concentration. Obviously, this ratio is dimensionless. Moreover, if β

> 1 , the nucleus grows; if $\beta < 1$, the nucleus dissolves; and if $\beta = 1$, nuclei and solution are at equilibrium. However, in a crystallized system, not only there must be a supersaturation condition for the system but also the system must have a number of minute solid bodies, embryos, nuclei or seed which are acting as a core of nucleation to develop crystals [19, 20].

1.2.2 (b) Growth mechanism

Nucleation occurs over some time with constant monomer concentration. Eventually surface growth of clusters begins to occur which depletes the monomer supply. When the monomer concentration falls below the critical level for nucleation (critical supersaturation level), nucleation ends. A general analysis of the growth process is then important to understand nanocrystal synthesis [21]. In general, the surface to volume ratio in smaller particles is quite high. As a result of the large surface area present, it is observed that surface excess energy becomes more important in very small particles, constituting a non-negligible percentage of the total energy. Hence, for a solution that is initially not in thermodynamic equilibrium, a mechanism that allows the formation of larger particles at the cost of smaller particles reduces the surface energy and hence plays a key role in the growth of nanocrystals [22].

A colloidal particle grows by a sequence of monomer diffusion towards the surface followed by reaction of the monomers at the surface of the nanocrystal [23]. Coarsening effects, controlled either by mass transport or diffusion, are often termed the Ostwald ripening process. This diffusion limited Ostwald ripening process is the most predominant growth mechanism and was first quantified by Lifshitz and Slyozov [24], followed by a related work by Wagner [25], known as the LSW theory. The diffusion process is dominated by the surface energy of the nanoparticle. The interfacial energy is the energy associated with an interface due to

differences between the chemical potential of atoms in an interfacial region and atoms in neighboring bulk phases. For a solid species present at a solid/liquid interface, the chemical potential of a particle increases with decreasing particle size, the equilibrium solute concentration for a small particle is much higher than for a large particle, as described by the Gibbs–Thompson equation [26]. The resulting concentration gradients lead to transport of the solute from the small particles to the larger particles. The equilibrium concentration of the nanocrystal in the liquid phase is dependent on the local curvature of the solid phase. Differences in the local equilibrium concentrations, due to variations in curvature, set up concentration gradients and provide the driving force for the growth of larger particles at the expense of smaller particles [27].

The Gibbs-Thompson effect simply introduces a competing effect to the growth [26]. Crystals or particles in general, have a higher vapour pressure the smaller they are, and thus monomers evaporate into solution more easily from smaller particles than from larger ones. Due to the increased surface curvature, the surface atoms are more exposed to the surrounding while experiencing a weaker binding strength to the smaller particle core. Experimentally, the Gibbs-Thompson effect is observed in the lower melting temperature of smaller nanocrystals [28, 29]. The vapour pressure of a crystal of radius can be obtained by calculation by employing the Gibbs-Thompson equation (eq. 3),

$$S_r = S_b \exp(2\sigma V_m / rRT) \quad (\text{Equation 3})$$

Where S_r and S_b are the solubility of the nanocrystal and the corresponding bulk solid, V_m is the molar volume of the material, R is the gas constant and T is the temperature. The

employment of gas equation leads to vapour pressure being expressed as the concentrations of monomers in the vicinity of the surface (eq. 4),

$$C_i = C_\infty \frac{2\sigma}{e^{r dm k B T}} \approx C_\infty (1 + 2\sigma/r dm^k B^T) \quad (\text{Equation 4})$$

Where, C_∞ is the vapour pressure of a flat surface, σ is the surface tension. Formally, the same reasoning is applied to the concentration C_b . The radius of a crystal in equilibrium with the concentration of monomers in the bulk is introduced as the critical size r^* of the growth process

$$C_b = C_\infty \frac{2\sigma}{e^{r^* dm k B T}} \approx C_\infty (1 + 2\sigma/r^* dm^k B^T) \quad (\text{Equation 5})$$

Combining the above two equations, growth rate can be calculated as

$$dr/dt = 2\sigma DC_\infty / d^2_m k B^T \frac{1}{r} (1/r^* - 1/r) \quad (\text{Equation 6})$$

The critical size r^* is characterized by a zero growth rate, as a crystal of the size is in equilibrium with the solution. Nanocrystals smaller than a critical size have negative growth rates (dissolve), while larger ones grow at rates dependent strongly on size. It thus becomes evident that the quantity r^* is actually equal to the critical size r_c that characterizes the position of the energy barrier in the nucleation event.

1.3 Properties of semiconducting nanoparticles

1.3.1 (a) Electronic properties from cluster to nanoparticles

In general, “cluster science” refers to the study of material systems with physical dimensions which are comparable to those of the constituent atoms [30]. At these length scales, which range from 10\AA to over 100 nm, the material systems are discrete particles consisting of as few atoms in molecular clusters to more than 10^7 atoms in larger nanoparticles [31]. In this size regime, material systems are in an electronic configuration which bridges discrete molecular-

like electronic states and the bulk electronic bands which are associated with the material's familiar macroscopic properties [9, 31].

Figure 2: conceptually depicts the bottom-up construction of a bulk material's electronic properties starting with a single atom [30-33]. For both metals and semiconductors, the fundamental building blocks of the material are the constituent atoms in the primitive cells of the crystalline lattice [31]. In general, the primitive cell may contain multiple atoms, but for the sake of clarity, the discussion here focuses on single-atom materials. As two atoms are brought together to form a dimer, the molecular states become an energetically split symmetric and antisymmetric combination of the individual atomic states, and the highest occupied and lowest unoccupied atomic orbitals become the highest occupied and the lowest unoccupied molecular orbitals (HOMO and LUMO, respectively).

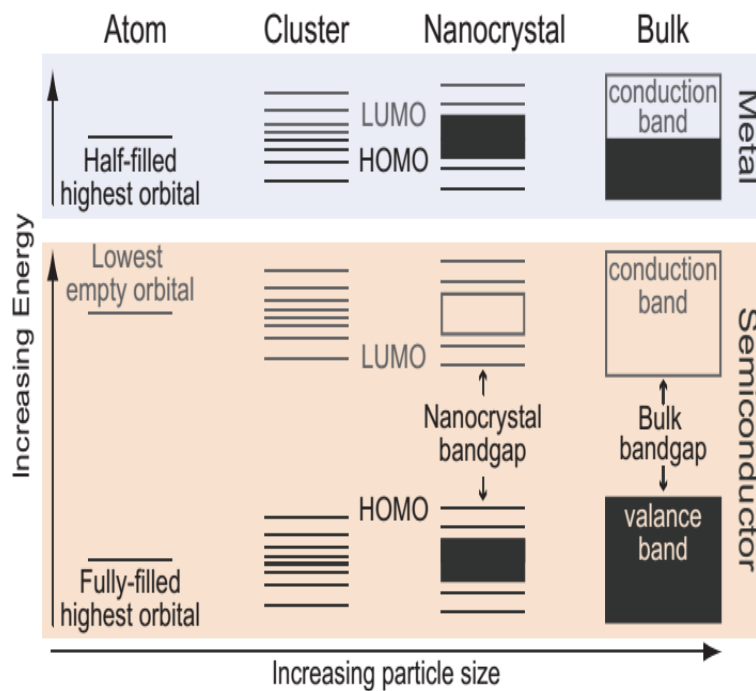


Figure 2: Electronic energy levels of metals and semiconductors as particle size increases from individual atoms to the bulk.

In an identical manner, further splitting occurs in larger clusters with more atoms. Eventually in clusters with a relatively large number of atoms, the splitting becomes negligible (i.e., less than the thermal energy), and the set of closely separated states centred around the original atomic energy level can be considered a quasi-continuous band [30, 31]

The electronic configuration of the constituent isolated atoms is intricately linked to the electronic configuration of the corresponding cluster or bulk material. A band of states forms for each electronic orbital of the single atom that makes up the constituent building blocks [9]. While the energetic centres of the bands are determined by the atomic orbitals, the numbers of states within the bands are determined by the total number of atoms in the system: each atom contributes a single state to the band which can contain two electrons of opposite spin. Therefore, an atomic orbital which contains an even number of valence electrons leads to a filled electronic band in the bulk whereas an odd number of valence electrons leads to a half-filled electronic band. Therein lies the fundamental difference between semiconductors and metals [9].

In metals, where the highest energy individual atomic orbital is filled with an odd number of valence electrons, the highest energy electronic band is only half-filled. This half-filled band called the conduction band which supports electrical conduction due to the nearby, higher energy, vacant states within the top half of the band. In contrast, the highest occupied orbital in semiconductor atoms is filled with an even number of valence electrons leading to complete filling of the top most band called the valence band. Thereby, the closest vacant state for semiconductor electrons lies in the next higher band also referred to as the conduction band and thus inter-band excitation of the electrons is required for significant electrical conductivity.

The difference in occupancy of the highest-filled band between semiconductors and metals has important consequences for their corresponding nanoparticle systems. The amount of splitting between the states in a cluster is not equal [31, 32]; the states in the middle of the quasiband are less separated than those at the edges. Thus, the position of the highest occupied electronic state within this quasiband plays an important role in determining the critical particle size at which a material makes the molecular-to-bulk transition. For metals, where the highest occupied electronic level lies in the middle of the quasiband, nanoparticles assume bulk-like properties at smaller sizes than their semiconductor counterparts in which the highest occupied state lies at the edge of the quasiband. So, while metal clusters quickly become conducting with increasing size, semiconductor nanoparticles preserve molecular-like behaviour of their highest occupied electronic states to notably larger particle dimensions [31]. As a consequence, the task of deliberately tuning the intrinsic electronic states through fabrication is much easier for nanoparticles derived from semiconductor materials as compared to metals [34].

1.3.1 (b) Optical properties

Molecules are, in general, localized entities. In a typical molecular solid, the intermolecular interactions are much weaker than the intermolecular bonding energies so the bulk properties of a molecular solid can usually be analyzed as the sum of individual molecular contributions, with small perturbations from the intermolecular forces. Such weak intermolecular interactions rarely extend beyond the nearest neighbours and the electronic structures of a molecular crystal are usually independent of the size of the crystal. Inorganic semiconductors and metals, on the other hand, consist of a network of ordered atoms with no discernible molecular unit. For a semiconductor crystal, electronic excitation consists of a loosely bounded electron - hole pair, usually delocalized over a length much longer than the lattice constant [35]. As the diameter of the semiconductor crystalline approaches this exciton Bohr diameter, its electronic

properties start to change. This is the so- called quantum confinement effect, which can be observed as a blue shift in the band gap or exciton energy [36, 37].

A spatial electronic state diagram showing the quantum confinement effect is shown in **Figure 3**. As the cluster properties are intermediate between molecules and bulk semiconductors, the quantum size effect can best be explained with hybrid molecular and semiconductor languages.

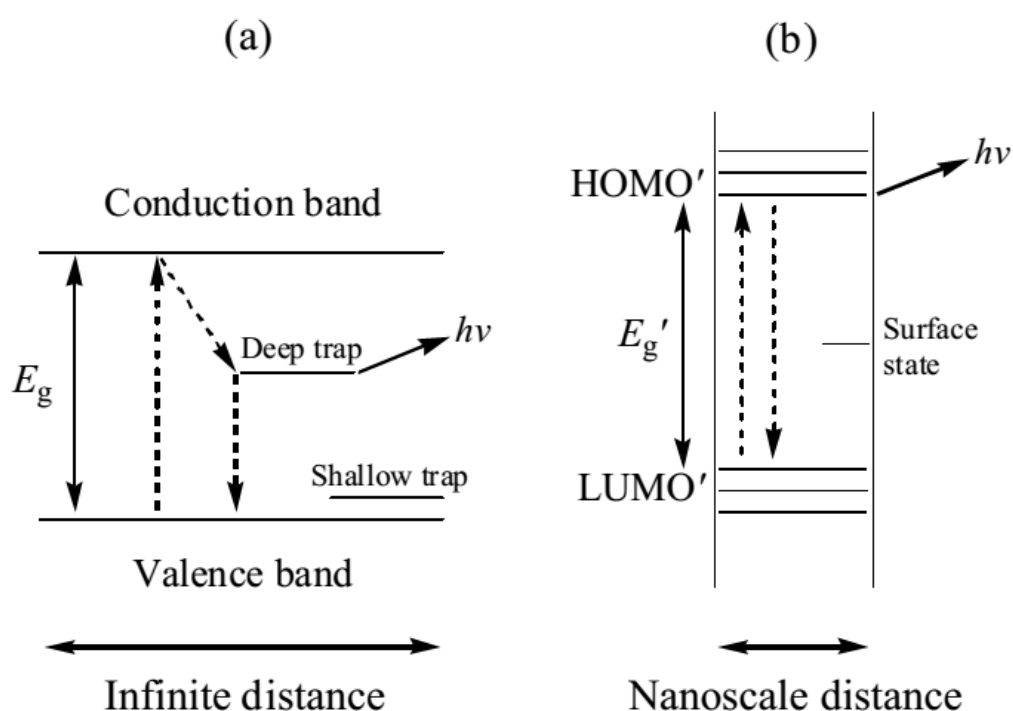


Figure 3: Spatial electronic state diagram for bulk semiconductor (a) and (b) nanoparticles

An important parameter of a semiconductor material is the width of the energy gap that separates the conduction from the valence energy bands (**Figure 3:(a)**). In semiconductors of macroscopic sizes, the width of this gap is a fixed parameter, which is determined by the material's identity. However, the situation changes in the case of nanoscale semiconductor particles with sizes smaller than ~10 nm (**Figure 3: (b)**). This size range corresponds to the regime of quantum confinement for which electronic excitations “feel” the presence of the

particle boundaries and responds to changes in the particle size by adjusting their energy spectra. Quantum size effects have been observed experimentally for many nanocrystalline semiconductors [38, 39]. In addition to quantum size effects, coating nanoparticles with different materials is a preferred way of controlling the dimensions of the bandgap of nanoparticle quantum dots [40]. The optical absorption spectrum of a nanocrystallite semiconductor provides an accessible and straightforward method for the evaluation of quantum size effects. The absorption of a photon, leading to excitation of an electron from a valence band to the conduction band, is associated with the band gap energy (E_g). The absorption of photons with energy similar to that of the band gap, $h\nu = E_g$, leads to an optical transition producing an electron in the conduction band of the semiconductor along with a hole in the valence band. Absorption of photons with energy much greater than E_g leads to excitations above the conduction-less processes. The absorption (A) of light by a semiconductor material with thickness (l) can be expressed by an expression analogous to the Beer law (eq. 7), where α represents the absorption coefficient of the solid and is a function of the radiation frequency.

$$A = \alpha l \quad (\text{Equation 7})$$

All electronic transitions are subject to selection rules: for semiconductors the requirements (beside $h\nu = E_g$) are that the wave vector, K , should be conserved. K_{photon} is small when compared with the wave vectors of the electron before (K_e) and after excitation (K'_e) (eq. 8).

$$\begin{aligned} K_e + K_{\text{photon}} &= K'_e \\ K_e &= K'_e \end{aligned} \quad (\text{Equation 8})$$

The absorption coefficients of a photon for a given energy (eq. 9) is proportional to the probability (P_{if}), the density of states in the initial state (n_i), and the density of available

final state (n_f). This process must be summed for all possible transitions between states separated by an energy difference equal to the energy of the incident photon.

$$\alpha(h\nu) = \sum P_{if} n_i n_f \quad (\text{Equation 9})$$

Semiconductors in which there is conservation of the wave vector for optical transitions are referred to as direct band gap semiconductors and have large absorption coefficients. A useful expression relating the absorption coefficient and the photon energy of a direct transition near the threshold is given by eq. 10 [41]. Semiconductors where lowest electronic transition, between the valence band and the conducting band, is formally forbidden are said to have an indirect band gap and normally have small absorption coefficient.

$$\alpha(h\nu) = (E_g - h\nu)^{1/2} \quad (\text{Equation 10})$$

The energy gap of a quantum dot depends on the size of the dot. The larger the size is, the lower is its absorption and fluorescence energy (red shift). The smaller the dot is, the higher is its absorption and fluorescence energy (blue shift). There are two ways that can be used to determine the band gap energy (eV) of the prepared nanocrystalline semiconductor. One easy way is to experimentally estimate it from the spectrum, with the second one being achieved by calculation. Both methods agree that a shift to lower wavelength of the prepared semiconductor nanoparticles, as compared to the bulk materials gives a measure of the finite size of the particle [11]. There are special phenomena that are used to define nanoparticles of certain sizes. Some of those properties are higher stability and larger gap. These properties are very important since they play a crucial role in differentiating semiconductor nanoparticles from bulk semiconductors. The correlation between band gap size and particle stability was explained by simple bonding descriptions in which the highest occupied molecular orbital and lowest unoccupied molecular orbital gap give a measure of the orbital overlap. However, the above mentioned statement was found to be true only for nanoparticles prepared from group

II-IV [42]. In their work, Brus *et al.* [43] differentiated small particles from bulk semiconductor particles by stating that the band gap of small particles is greater than that of the bulk semiconductors. Band gap of the nanoparticles can simply be calculated from eq. 11,

$$E = hc/\lambda \quad (\text{Equation 11})$$

where E is the band gap energy, h is the Planck's constant, c is the velocity of light and λ is the absorption edge in reflectance spectra [44].

1.3.1 (c) Photoluminescence properties

Photoluminescence (PL) is the light of a material that is emitted from optical excitation. It is one of the kinds of the more general phenomenon of luminescence, namely the emission of optical radiation resulting from various types of excitation which are Bio-chemical or chemical changes, electrical energy, subatomic motions, reactions in crystals, or stimulation of an atomic system. Nowadays the theory can be explained by means of bio-, chemi-, electro-, thermo-, radio-luminescence, etc.

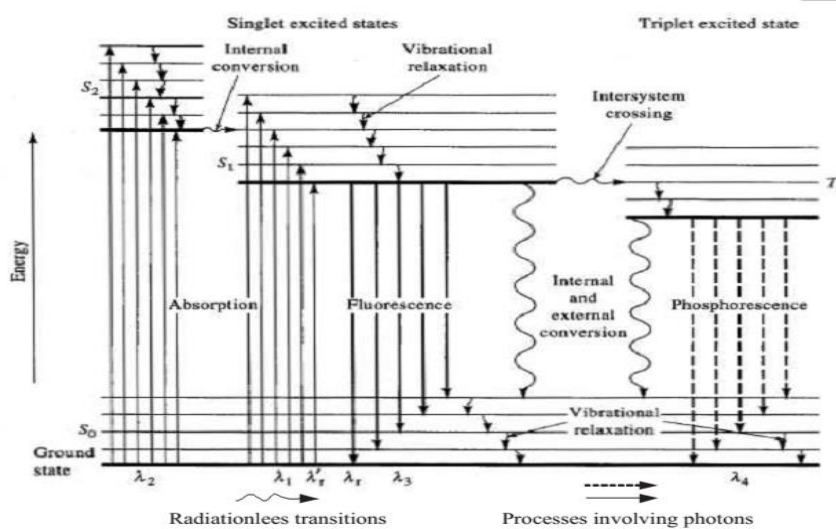


Figure 4: Photoluminescence energy diagram[45]

When a beam of light with sufficient energy is incident on a material, X-rays/photons are absorbed, become excited and move to the high energy level. Eventually the electrons lose energy and return to the ground state (fluorescence process). If this vibration relaxation is radiative, the emitted light can be translated to photoluminescence signal. The measured intensity of this signal gives the relative rates of radiative and non-radiative (termed internal conversion- generally internal conversion is an inefficient process and is probably only a small fraction of the total excitation energy in most molecules) recombinations. Recently this phenomenon is also refer to fluorescence or phosphorescence, in which is a type of luminescence that occurs naturally in many minerals and metallic compounds, in some organic compounds, and in some living organisms such as marine fauna and insects (the most familiar one being the firefly, whose light flashes are produced by bioluminescence). Phosphorescence is distinguished from fluorescence for two main reasons: a) in phosphorescence there is a longer time period between the excitation and the emission of light; b) phosphorescence may continue for some time (even hours) after the exciting source has been removed, while fluorescence ceases when excitation is off.

1.3.2 Synthetic methods of nanoparticles

When atoms or molecules organize into condensed systems, new collective Phenomena develop. The cooperative interactions produce the physical properties we recognize as characteristic of bulk materials. Like atoms or molecules, nanocrystals may also be used as building blocks of condensed matter. Synthetic routes enabling controlled manipulation of nanocrystals into the glassy and ordered states of matter lead to the preparation of close-packed nanocrystalline solids. The assembly of nanoparticles opens up the possibility of fabricating new solid-state materials and devices with novel physical properties, as the interactions

between proximal nanocrystals give rise to new collective phenomena. The synthesis of nanoparticles is very critical in order to produce materials of quality. The properties of the resulting particles determine its quality and thus a number of methods have been developed.

1.3.2 (a) Colloidal method

The colloidal route was the first reported method used to synthesize nanoparticles and involves controlled precipitation reaction in a homogenous solution. Colloidal semiconductor nanocrystals are synthesized from precursor compounds dissolved in solutions, much like the traditional chemical processes. The synthesis of colloidal semiconductor nanoparticles is based on a three-component system which is (i) precursors, (ii) organic surfactants, and (iii) solvents. When a reaction medium is heated to a sufficiently high temperature, the precursors chemically transform into monomers. Once the monomers reach a high enough supersaturation level, the crystal growth starts with nucleation process (indicated in section 2.2.1). The temperature during growth process is one of the important factors in determining optimal conditions for the nanoparticles growth. It must be high enough to allow the rearrangement and annealing of atoms during synthesis process while being low enough to promote particles growth. Another critical factor that has to be stringently controlled during nanoparticles growth is the monomer concentration.

The growth process of nanocrystals can occur in two different regimes, (i) focusing and (ii) defocusing. At high monomer concentrations, the critical size (the size where nanocrystals neither grow nor shrink) is relatively small, resulting in growth of nearly all particles. In this regime, smaller particles grow faster than large ones (since larger crystals need more atoms to

grow than small crystals) resulting in focusing of the size distribution to yield nearly monodisperse particles. The size focusing is optimal when the monomer concentration is kept such that average nanocrystal size present is always slightly larger than the critical size. When the monomer concentration is depleted during growth, the critical size becomes larger than the average size present, and the distribution defocuses. Weller group [46] synthesized nanocrystallites of Zn_3P_2 and Cd_3P_2 by the injection of phosphine (PH_3) into solutions containing metal salts; control of particle size was achieved by varying the phosphine concentration and the temperature of the reaction. Samples of both Zn_3P_2 and Cd_3P_2 showed remarkable quantum size effects, as observed by changes in the colour of the products. Hexametaphosphate was used as a stabilizer to prevent particle aggregation. The solubility of inorganic salts can be used to prepare more complex structures by such methods and examples include: CdS/ZnS [47], CdSe/AgS [48], HgS/CdS [49], PbS/CdS [50], CdS/HgS [51], ZnS/CdSe [52] and ZnSe/CdSe [53] core-shells nanoparticles. Reiss et al [54] and many other authors [55] have also reported that the luminescence properties are much more stable and less sensitive to surface ligand exchange as compared to “bare” core nanocrystals. This effect is a fundamental prerequisite for the use of nanocrystals in applications such as biological labelling and light-emitting devices, which rely on their emission properties [56-60]. The main constraints on the production of such structures involve the relative solubility of the solids and lattice mismatches between the phases. The preparation of “quantum dot quantum well systems” such as CdS/HgS/CdS [61] has also been reported in which an HgS quantum well of 1–3 monolayers is capped by 1–5 monolayers of CdS .

Yang et al [62] in his work indicated that doping semiconductor nanoparticles with conventional impurities allows the control of the number of carriers (electrons and holes) in semiconductors, which has built the foundation for *p-n*-junction based semiconductor devices,

such as computer chips [63]. However, *n*- and *p*-type doping of semiconductor nanoparticles by conventional impurities has been unsuccessful through a colloidal synthesis, in part, because of the difficulties in introducing the impurities into colloidal nanoparticles [64-67]. Alternatively, most efforts have focused on doping semiconductor nanoparticles with magnetic impurities [64]. To date, a variety of semiconductor nanoparticles have been doped with Mn, as well as other magnetic impurities such as Co, Ni, Eu, and Tb [68-70].

1.3.2 (b) Organometallic method

Preparation of semiconductor nanocrystals by means of organometallic approaches requires high-temperature (200-360 °C) thermolysis of organometallic precursors in the presence of coordinating solvents (so-called stabilizing agents). A narrow particle size distribution can be achieved via temporal separation of the fast nucleation event from the following slow growth of the pre-formed nuclei. Organometallic precursors are rapidly injected into a very hot (300-320°C) stabilizing solvent resulting in the fast formation of nucleation, on injection of precursor into a hot reaction vessel a slight drop of temperature usually is the process where nucleation is terminated. The time of subsequent growth at desired parameters such as concentration, temperature and the proper choice of stabilizing agents provide control over the particle size. Murray, Norris and Bawendi [71] in their work that high quality quantum dots became readily available in appreciable yields. In their paper they showed that CdE (E=S, Se, Te) semiconductor nanoparticles, with a close control of their size, can possibly be obtained by the injection of dimethyl-cadmium and the respective chalcogenide source into a hot solvent such as tri-n-octylphosphine oxide (TOPO). The injection of these precursors into the hot solvent (typically between 200-300°C) results in a short burst of nuclei which are generated in homogeneous solution. This rapid nucleation depletes to a large extent the reactants and limits

the occurrence of further nucleation and subsequent growth occurs almost exclusively through Ostwald ripening.

The molecules of the high boiling point solvents normally used also have the capability to coordinate to the nanocrystals surfaces, hence acting as barriers against the nanoparticles into bulk powders. The quantum dots produced by this method and similar strategies are of high quality, i.e. they consist of nanocrystals with narrow size distributions and organically capped surfaces. The size of the nanocrystals can be controlled by adjusting experimental parameters such as the type of solvent, reaction temperature and time, with the size of the particles increasing with increasing reaction temperature. Also control on the injection rate and temperature on further additions of molecular precursors to the reacting mixture, allows control of the shape and type of the polymorph observed in the final quantum dots [72]. The original TOPO method has been successfully implemented to coat the quantum dots core with a higher bandgap semiconductor (typically, ZnS). This can be achieved by injection of solutions of dimethyl or diethylzinc and hexamethyldisilathiane ((TMS)₂S) into the hot solvent containing the core CdE nanoparticles [73]. The major drawback of the above method is the high toxicity and difficult manipulation associated to some of the starting chemicals. For instance Cd(CH₃)₂ is extremely toxic and pyrophoric, and these limitations become more relevant for high temperature synthesis. Although maintaining some of the conceptual characteristics of the original synthetic method [74], alternatives to this approach have emerged in the following years.

One of these approaches was introduced by Trindade and O'Brien [75, 76] in which they involves the thermal decomposition of single-molecular precursors, i.e. a source compound

that contains in the same molecule the elements required for the formation of the semiconductor, such as alkyldiseleno- or alkylthiocarbamate metal complexes. This method is particularly attractive when readily available air-stable precursors can be employed in a one-step process to obtain nanocrystalline materials; this has been clearly the case of the synthesis of several metal sulphides from dithiocarbamate or xanthate complexes [76, 77]. This approach has also been investigated to coat CdSe quantum dots with ZnS and CdS, either by the thermal decomposition of the respective metal dithiocarbamate complexes [78] or via sonochemical decomposition of metal xanthates [79].

1.3.2 (c) Single source precursor method

Single source precursor method has been identified to be one of the precise methods for reproducibility of results in the synthesis of nanoparticles. There are number of advantages related to the single source precursor method:

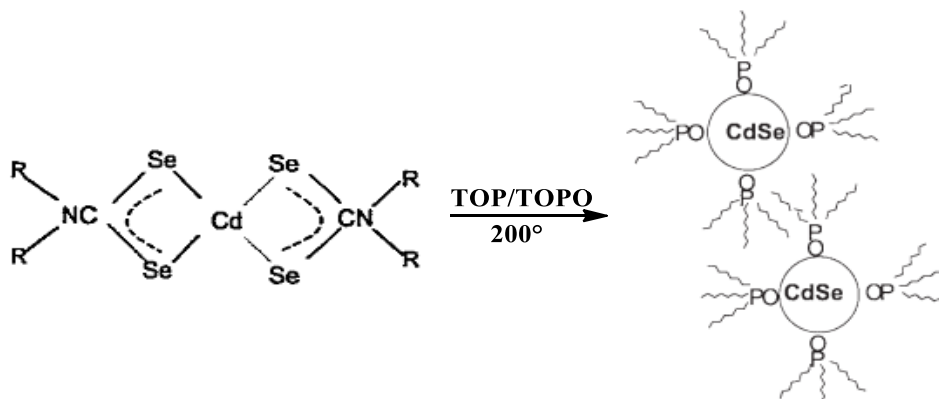
- Single source routes avoid the need for volatile, sometimes toxic and/or pyrophoric precursors.
- Some II-VI and III-V nanoparticles are air sensitive. All precursor synthesis is carried out under anaerobic conditions, with the resulting precursors being air and moisture stable.
- One non-volatile precursor is involved, purification of which is easier than that of two or more volatile precursors, and hence there is less chance of the incorporation of impurities into the nanoparticles.
- Low temperature deposition routes are possible.
- Although there are theoretical models predicting the optical properties of semiconductor nanoparticles, the properties of nanoparticles obtained by new synthetic routes are

sometimes hard to anticipate and may lead to particles with unique and unanticipated, but useful, properties.

Many potential single-molecular precursors have been described in the literature and were originally intended for use in the growth of semiconductor thin films from CVD techniques, but proved problematic because of their low volatility and lack of stoichiometric control. Some compounds used by others include the preparation of II-V nanoparticles of Cd_3P_2 from $[\text{MeCdP}(\text{tBu})_2]_3$ [80, 81]. Brus et al [82] produced nanoparticles of CdSe from the pyrolysis of the single-molecular precursor $\text{Cd}(\text{SePh})_2$ and from the single-molecular precursor $[\text{Cd}(\text{SePh})_2]\text{-}[\text{Et}_2\text{PCH}_2\text{CH}_2\text{PEt}_2]$, and Wells et al [83] reported the synthesis of GaP nanoparticles from the thermolysis of $[\text{X}_2\text{GaP}(\text{SiMe}_3)_2]_2$ ($\text{X} = \text{Br}, \text{I}$) and from the thermolysis of $(\text{Cl}_3\text{Ga}_2\text{P})_n$. Barron et al [84] took the gallium- and indium-selenium clusters, $[(\text{tBu})\text{GaSe}]_4$ and $[(\text{EtMe}_2\text{C})\text{InSe}]_4$, and decomposed them to produce nanoparticle materials of GaSe and InSe , respectively. However, large particles possessing wide size distributions were obtained in most cases, most likely because of the solid state thermolysis method employed and the absence of a capping agent, both of which fail to separate the nucleation and growth processes involved.

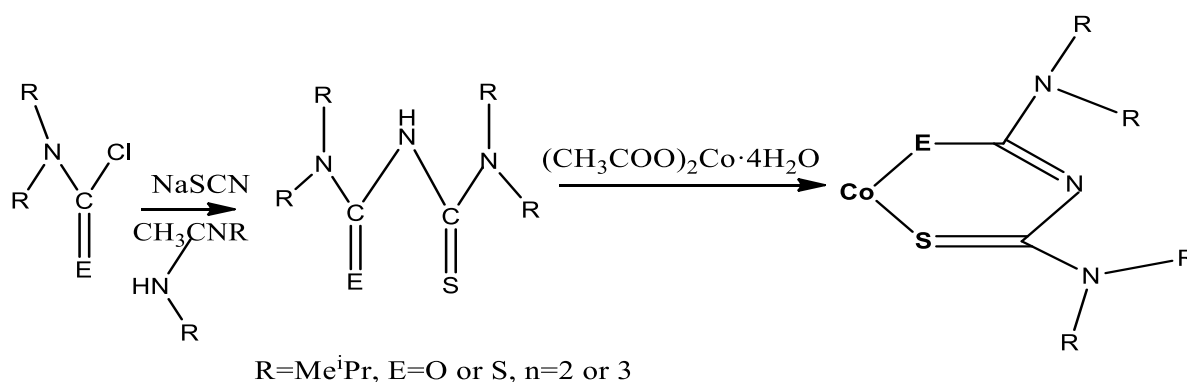
Trindade and O'Brien [85] first reported the use of cadmium dithio- and diselenocarbamate complexes as precursors for the preparation of TOPO capped II-VI materials. Bis(dialkylthio/seleno-carbamato)cadmium(II)/zinc(II) compounds were thermolysed in TOPO or in 4-ethylpyridine to prepare MS and MSe nanoparticles ($\text{M} = \text{Cd}, \text{Zn}$) (Scheme 1). However, these preparations have been limited by the costs associated with high-temperature oxygen-free equipment and the risks of using toxic organic phosphines. Therefore, the

application of a novel, facile synthetic strategy, which uses a faster reaction process, and relatively nontoxic chemicals, to the preparation of MS and MSe based QDs is highly desirable.



Scheme 1: Schematic of bis(dialkyldithio/seleno-carbamato)cadmium(II)/zinc(II) complex used to prepare nanoparticles of II-VI materials capped with TOP/TOPO.

Ramasamy [86] reported the synthesis of cobalt complexes of 1,1,5,5-tetramethyl-2,4-dithiobiuret, $(\text{Co}(\text{N}(\text{SCNMe}_2)_2)_3)$ (1), and 1,1,5,5-tetraisopropyl-2-thiobiuret, $(\text{Co}(\text{N}(\text{SOCN}^i\text{Pr}_2)_2)_2)$ (2), and their use for the selective synthesis of Co_{1-x}S and Co_4S_3 phase cobalt sulphide nanoparticles (Scheme 2).



Scheme 2: Schematic for synthesizing ligand and complex

Ramasamy et al[85] further synthesized Cobalt sulphide nanoparticles by the thermal decomposition of complex1 in hot surfactant solution (230°C , octadecylamine (ODA) and hexadecylamine (HDA), 1hour, oleylamine (OA)). The nanoparticles prepared from complex

1 were hexagonal Co_{1-x}S and cubic and hexagonal Co_{1-x}S for complex 2, with size and shape dependent upon the reaction time and capping agent. TEM confirmed mixture of cubic and hexagonal complex 2 and irregular shapes complex 1 and the particles were monodispersed. At 250 °C, more spherical nanoparticles were observed and at 270 °C variously shaped nanoparticles including triangular prisms, trapezoids, rods, hexagons and spheres were obtained.

The mixture of shapes in the nanoparticles can be explained by kinetic and thermodynamic: The factors controlling the shapes of inorganic nanocrystals involve competition between thermodynamic and kinetic factors [87, 88]. According to this model, after the formation of a preferred crystalline phase seed, the final morphology of the nanocrystals is mainly determined by the growth process through a balance between kinetic growth and thermodynamic preference. At high temperature, the reaction is under thermodynamic control and the most stable form of nanocrystal is generally preferred. At lower temperature, the reaction may be under kinetic control and selective anisotropic growth may occur. Ramasamy et al in his study concluded that, the deposition at 230 °C produced a mixture of spherical and irregular shapes of nanoparticles. When the temperature is increased to 250 °C, the product is controlled by thermodynamics and the nanoparticles are predominantly spherical. The sphere can be considered as a preferred shape of minimized surface area under limiting thermodynamic control [87] However, at the highest temperature of 270 °C, the transformation of small nanoparticles into other particle geometries probably occurs via the Ostwald ripening process [89].

Jun et al [90] reported core-multi-shell structure quantum dots prepared by inserting an interlayer, such as CdS and ZnSe between the CdSe core and ZnS shell in order to reduce the lattice parameter difference. The core-multi-shell structure was prepared by one step process to grow CdS and ZnS shells on a CdSe core. The authors used CdO, octadecylphosphonic acid (ODPA), TOPSe and trioctylamine (TOA) as a solvent to prepare CdSe core. The shell was carried out by using cadmium acetate dihydrate, zinc acetate, and TOPS as starting materials, oleic acid (OA) as a capping agent, and TOA as a solvent. Because this method has significant advantages: (i) being less toxic, (ii) insensitive to air and moisture, (iii) easier to purify, and (iv) providing highly monodisperse QDs with a high PL efficiency. Protiere and Reiss [91] used the air-stable monomolecular precursor zinc ethylxanthate ($\text{Zn}(\text{ex})_2$) in combination with zinc stearate to synthesize the monodispersed CdS/ZnS core/shells QDs exhibiting efficient blue emission in the range of 440-480 nm with quantum yield (QY) of 35-45%. Chen et al [92] applied a monomolecular precursor of zinc diethyldithiocarbamate ($\text{Zn}(\text{DDTC})_2$) for the synthesis of stable purple/blue emitting CdS/ZnS core-shells QDs with their emission peak tunable between 375 and 475 nm and the maximum QY of 50%. It should be pointed out that the single-source molecular precursor method [93-95] (an individual molecule acting as the source of both metal and chalcogen in nanoparticle synthesis) route offers the distinct advantages of mildness, safety, and simplified fabrication procedure and equipment, when compared with the most popularly employed successive-ion layer adsorption and reaction (SILAR) method for shell growth [92, 96]

1.4 Aim and Objectives

Aim of the study is to synthesize and characterize cobalt and cadmium chalcogenide nanoparticles based on thiourea, urea and their alkyl derivatives.

1.4.1 Objectives

- To synthesize cobalt and cadmium complexes from their based ligands (thiourea and urea)
- Characterization of complexes by employing elemental analysis (EL), Fourier Transform Infrared (FTIR) spectroscopy and thermo gravimetric analysis (TGA).
- Synthesis of nanoparticles by varying conditions such as concentration and temperature to yield the following features:
 - A mixture of both two metal chalcogenides nanoparticles
 - A combination of conditions to give the subsequent growth of core shell nanomaterials.
- Characterization of the metal chalcogenide nanoparticles and core-shell nanomaterials by using Ultraviolet-Visible (UV-VIS), Photoluminescence (PL) spectroscopy, Fourier Transform Infrared (FTIR) spectroscopy, Transmission Electron Microscopy (TEM) and Powder X-ray Diffraction (PXRD).

1.5. Problem statement

Several studies on different nanostructures like nanoparticles, nanowires, nanorods, nanospheres, nanoflowers, nanofibers, nanotubes, and core-shell structures have been developed for enhancing the light harvesting within the electrodes, without sacrificing the surface of material. The review of literature reveals an increasing interest in the new designs

of nano-porous electrode based on the core-shell configuration. The use of core-shell nanostructures to lower the charge recombination which is based on the hypothesis that a coating layer built up an energy barrier at the semiconductor/electrolyte interface and, thus, retard the reaction between the photo-generated electrons and the redox species in electrolyte. Many reported methods use colloidal route which involves two separate solutions of the core and shell materials which does not often give enough conclusive evidence of the formation of core-shell nanomaterials especially based on TEM, absorption spectroscopy and XRD analysis. In an effort to unravel and understand more on the formation of core-shells, single source precursors will be explored in a scenario of combining two complexes with different chalcogenide and metal sources. This is the first time attempts like this have been made and can possibly bring more insight into the making of core and the shell as they will both be made in the same pot and under the same conditions. The disadvantage with the approach is the inability to control the core and that can only be controlled by the choice of the complexes and their thermal stabilities. The variation in the amounts of the precursors has potential in determining the formation of the core in that mixture of the two complexes.

CHAPTER TWO

SYNTHESIS AND CHARACTERIZATION OF COBALT AND CADMIUM COMPLEXES OF THIOUREA AND UREA

2. Introduction

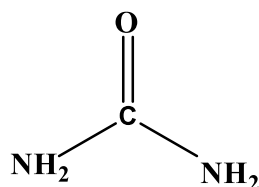
2.1. Urea and thiourea coordination with the metals

The rich coordination chemistry of transition metals has led the design and development of novel ligands with unique structures and functional characteristics [97-100]. Currently significant efforts are being directed towards the design of specific ligand architecture in synthetic and applied chemistry [101]. One such area is the study of the coordination chemistry of the transition metals, such as zinc, cadmium, mercury, cobalt and lead in attempt to design specific ligands that can selectively bind these metals[102-104]. Recently, the coordination chemistry of cobalt and cadmium (II) has received increased attention mainly due to their significance and impact on the environment and human body [105, 106]. In fact, the toxic effect of cadmium (II) is associated with its competition with cobalt for a variety of important binding sites in cells such as gene regulation [107].

Urea may be prepared in the laboratory by the interaction of ammonia with carbonyl chloride, alkyl carbonates, chloroformates or urethans. Industrially [108-111], urea is prepared by allowing liquid carbon dioxide and liquid ammonia to interact, and heating the formed ammonium carbamate at 130-150°C under about 35 atmospheric pressure. The carbamate is decomposed to form urea and water according to the following reaction;

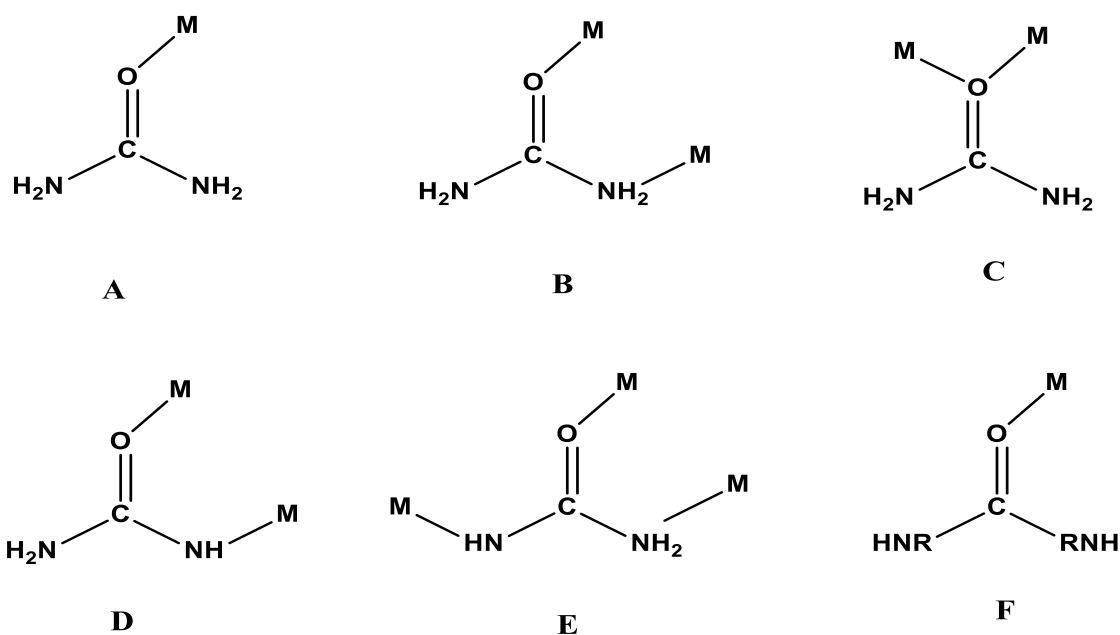


Urea is also extensively used in the paper industry to soften cellulose and has been used to promote healing in infected wounds and many other applications in the field of medicine [112, 113].



Scheme 3: Structure of urea.

Crystal structure studies have shown that in solid urea, both nitrogen atoms are identical. Bond length measurements [114] in urea give the C-N distance as 1.37 Å, while, in aliphatic amines the C-N bond length is 1.47 Å. This indicates that the C-N bond in urea has some double bond character (about 28%). Complexes of urea with some metal ions are used as fertilizers [115-117]. Complexes of urea with zinc sulphate and nitrate, $[\text{Zn}(\text{CON}_2\text{H}_4)_6]\text{SO}_4 \cdot \text{H}_2\text{O}$ and $[\text{Zn}(\text{CON}_2\text{H}_4)_4](\text{NO}_3)_2 \cdot 2\text{H}_2\text{O}$ have very important application in this field [118]. These complexes were found to increase the yield of rice more than a dry mixture of urea-zinc salt does. Calcium nitrate-urea complex, $[\text{Ca}(\text{urea})_4](\text{NO}_3)_2$, [119, 120] was used also as an adduct fertilizer. For example, metal-urea complexes have a pharmaceutical application that the platinum-urea complex was recorded a significant effect as an antitumor agent [121]. Urea (U) usually coordinates as a monodentate ligand through the oxygen atom, forming a $\text{C}=\text{O} \cdots \text{M}$ angle considerably smaller than 180° , in accordance with the sp^2 hybridization of the O atom (A in Scheme 3). The rare N,O-bidentate coordination mode (B in Scheme 3) has been found in a very limited number of cases [122, 123], while in $[\text{Hg}_2\text{Cl}_4\text{U}_2]$ each U molecule bridges the two Hg^{II} atoms through the oxygen atom [124] (C in Scheme 3). Of particular chemical or biological interest is the ability of U to undergo metal-promoted deprotonation [125]; the monoanionic ligand H_2NCONH^- adopts the μ^2 (D in Scheme 3) and μ^3 (E in Scheme 3) coordination modes. The urea and its derivatives such as the N, N'-dimethylurea and N, N'-diethylurea (Scheme 3) have only been found to coordinate as monodentate ligands through the oxygen atom (F in Scheme 3).



M - Metal,
R- alkyl group

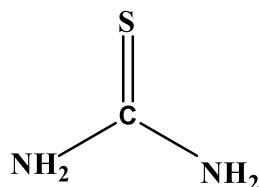
Scheme 4: The coordination modes of urea towards metal ions

Infrared spectra of urea have been observed by several investigators [126-131]. The normal vibrations of the urea molecule were calculated by Kellner [132] on the assumption of the non-planar model. However, on the basis of the dichronic measurement of the infrared band arising from the N-H stretching vibration by Waldron and Badger [133] and the proton magnetic resonance absorption measurement made by Andrew and Hyndman [134], it is concluded that urea molecule has a planar structure. Yamaguchi [135], assigned all of the observed frequencies in the spectra of urea. To the two vibrations of the frequencies 1686 and 1603 cm^{-1} , there are considerable contributions of both CO stretching and NH_2 bending motions, whereas Stewart [136] assigned the 1686 cm^{-1} band to CO stretching vibration and the 1603 cm^{-1} band to NH_2 bending motion. The calculations studied by Yamaguchi showed that for the band at 1686 cm^{-1} , the contribution of the NH_2 bending motion is greater than that of CO stretching motion. The band at 1629 cm^{-1} corresponds to almost pure NH_2 bending vibration. The NH_2 bending motion of A_1 type is equal to that of B_2 type. The A_1 type band

should have a frequency of about 1630 cm^{-1} , if there is no coupling between NH_2 bending and CO stretching motions.

Urea possesses two types of potential donor atoms, the carbonyl oxygen and amide nitrogen. Penland et al [137] studied the infrared spectra of urea complexes to determine whether coordination occurs through oxygen or nitrogen atoms. The electronic structure of urea may be represented by a resonance hybrid of structures A-F as shown in scheme 3 with each contributing roughly an equal amount. If coordination occurs through nitrogen, contributions of structure B will decrease. This results in an increase of the CO stretching frequency with a decrease of CN stretching frequency. The N-H stretching frequency in this case may fall in the same range as those of the amido complexes. If coordination occurs through oxygen, the contribution of structure A will decrease. This may result in a decrease of the CO stretching frequency but no appreciable change in NH stretching frequency. Since the vibrational spectrum of urea itself has been analyzed completely [135], band shifts caused by coordination can be checked immediately. For example, the effect of the coordination on the spectra of the complexes of urea with Pt(II) and Cr(III) in which the coordination occurs through nitrogen and oxygen atoms, respectively [137]. The mode of coordination of urea with metal ions seems to be dependent upon the type and nature of metal. Pd(II) coordinates to the nitrogen, Fe(III), Zn(II), and Cu(II) coordinate to the oxygen, whereas Co(II) and Cd(II) coordinate with either nitrogen or Oxygen of urea [137]. In urea-metal complexes, if a nitrogen-to-metal bond is present, the vibrational spectrum of this complex differs significantly from that of the free urea molecule. The N-H stretching frequencies would be shifted to lower values, and the C=O bond stretching vibration ($\nu(\text{C=O})$) would be shifted to higher frequency at about 1700 cm^{-1} [138].

Thiourea (TU) is one of the few simple organic compounds having high crystallographic symmetry. It crystallizes in the rhombic bipyramidal division of the rhombic system and behaves as a good ligand [139].

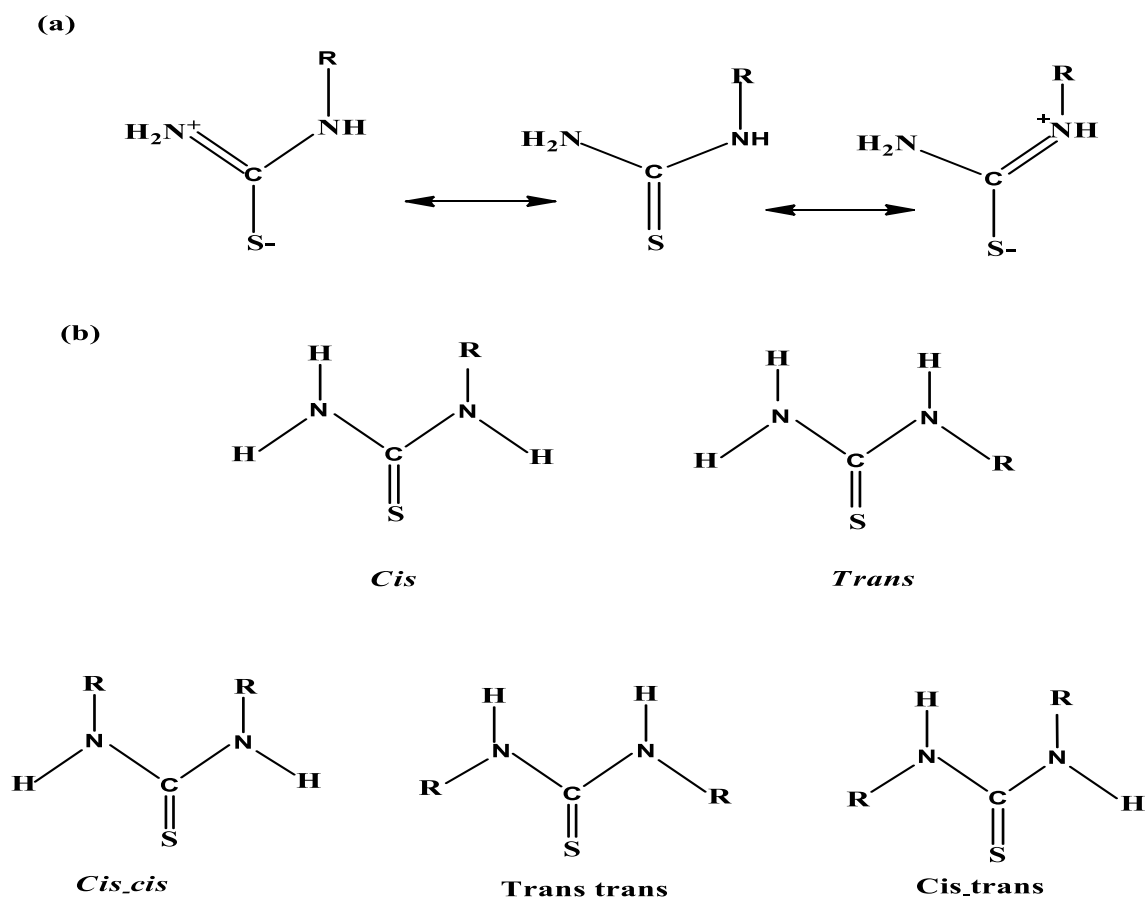


Scheme 5: Structure of thiourea.

The crystal structure of thiourea has established the coplanarity of the C, N and S atoms in the molecule [140]. Thiourea molecules also possess a large dipole moment and have the ability to form an extensive network of hydrogen bonds. Due to these two properties thiourea molecules can be used as inorganic matrix modifier [141, 142]. The thiourea molecule can also coordinate with metal ions to form stable coordinate complexes. Thiourea as such is a centrosymmetric one, but when it is coordinated with metal ions it becomes a non centrosymmetric material, which is an essential property for a crystal to exhibit non-linear optical activity [143]. Metal complexes of thiourea are commonly called semiorganics, and benefit from both the advantageous properties of the organic and the inorganic part of complex [144]. In particular the coordination compounds formed by the organic ligand thiourea and metal ions with d^{10} electronic configuration (Zn^{2+} , Co^{2+} , Cd^{2+} , Hg^{2+}) have recently received renewed attention. This interest arises due to its high non-linear optical properties and the convenient preparation of semiconducting materials based on CdS through the thermal decomposition of these complexes [145, 146]. The study of infrared absorption spectra of stable Werner type coordination complexes formed from metal salts with 2, 4 or 6 mol of thiourea (TU) molecule has been reported by many authors [147-151]. Yamaguchi and Penland [140] studied the infrared absorption spectra of complexes of thiourea with manganese cobalt, nickel, zinc,

copper, mercury, cadmium and lead. They concluded that, the complexation exists between metal and sulphur only rather than between metal and nitrogen. Other researchers mentioned out that thiourea are potentially capable of forming coordinate bonds through both sulphur and nitrogen even though the extremely low basicity of the ligand [152] militates against the formation of nitrogen metal bonds.

The chemistry of substituted thiourea derivatives has attracted attention because of their potential use as reagents for the separation of metal ions [153] and in biological applications such as their use: as antibacterial [154, 155], antiviral [156] or antifungal agents [157, 158]. In addition to their applications, the ligands are of interest as they possess various potential donor sites: the sulphur atom of the C-S group and the nitrogen atom of the NH, NHR' or NRR' groups (where R= R'= alkyl or aryl groups). Several studies have been made on the coordinating ability of these ligands mainly with aim of determining the coordination mode. The *N*-alkyl substituted thiourea, with the coplanar N₂CS skeletal atoms can take two possible conformational forms, *trans* and *cis* whereas three different conformations are possible for *N,N*-dialkyl substituted thioureas the *cis-cis*, *trans-trans* and *cis-trans* isomers. NMR studies have been in efforts to determine the extent of the rotation about the S=CN bond in thioureas [159-162]. A number of studies on the structural conformation of *N*-methylthiourea have been carried out, both in the solid state and solution [163-165].



Scheme 6: (a) Structures of substituted thiourea showing delocalisation of the p-bond and (b) conformational isomers for both mono and disubstituted alkyl/aryl thiourea.

It was confirmed by Mido et al. [166] through Raman and IR and X-ray structural analyses of *N*-methylthiourea that the compound assumes the *cis* configuration in the solid state. Lane et al.[163]studied the infrared spectra of several thiourea derivatives in the solid state. They found that *N,N*-dimethylthiourea and *N,N*-diethylthiourea were *trans-trans* isomers. Subsequent studies on the coordination of these molecules were made using infrared spectra to determine their binding sites [167-174]. In most complexes they bind through the sulphur atom although there are examples of complexes with *N*-bonded to alkylthiourea derivatives [175]. The cadmium(II) and copper(I) complexes show marked similarity in their structures in that they form clusters [176], dinuclear [177] or polynuclear complexes [178, 179] whereas other complexes are monomeric [173, 174]. There is a substantial downshift in the vibrational frequencies of C- S bond when coordinated to a metal, suggesting considerable interactions

between the thiourea molecules and the metals [167]. The structures of thiourea complexes have been reported [180, 181]. The molecular structure of $[\text{CdCl}_2(\text{CS}(\text{NH}_2)_2)_2]$ consisted of tetrahedral but $[\text{PbCl}_2(\text{CS}(\text{NH}_2)_2)_2]$ is polymeric polyhedral linked together by bridging sulfur and chloride atoms and coordination number of seven around lead atoms was observed by Wharf *et al* [182]. Malik *et al* [183] reported the crystal thiourea compound and complex in which they mentioned that the cadmium thiourea complex contain the central atom in distorted square planar geometry, whose edges are shared by two sulphur atoms of the thiourea and two chlorine atoms from the metal source. Further mentioned that the two thiourea units are *trans* to each other. The Cd1-C11, Cd1-C12, Cd1-S1 and Cd1-S2 bond distances are 2.4438(4), 2.4233(4), 2.5511(4) and 2.5588(4) respectively. Cadmium and cobalt has strong ability to bond with chalcogenides to form semiconducting material which has been applied to many areas due to their suitable band gaps (approximately 2.3 - 2.6 eV) and strong photo-response in the visible region. The cadmium and cobalt chalcogenides in nano-scale has special luminescence properties and semiconductor quantized performance. These outstanding properties makes cadmium and cobalt chalcogenides nanoparticles attractive candidates for functional materials and widely used in many fields such as solar cells, photo-detectors, photo-electrochemistry, photo-chromism and electro-chromic materials [13].

2.2 Experimental Section

2.2 (a) Chemical reagents

Cobalt(II) chloride hexahydrate, cadmium(II) chloride, urea and, thiourea obtained from Sigma Aldrich, were used as purchased. Acetone, methanol and n-butyl alcohol (analytical grade) obtained from Sigmaaldrich were used without further purification and distilled water was also used as solvents.

2.3 Instrumentation

2.3 (a) FT-IR spectroscopy

Infrared spectra were recorded on FT-IR Perkin Elmer 400 spectrometer. Spectra were collected over the range from 400 to 4000 cm^{-1} . The powder complexes were placed on the instrument sample holder and subjected to analysis

2.3 (b) Thermogravimetry

The sample preparation for thermogravimetric analysis was done by weighing 10 mg of the complexes. These complexes were decomposed at temperature range of 50 to 930 $^{\circ}\text{C}$. This analysis was performed on a Perkin Elmer Pyris 6 TGA under an inert atmosphere of dry nitrogen, and heating rate of 10 $^{\circ}\text{C}.\text{Min}^{-1}$.

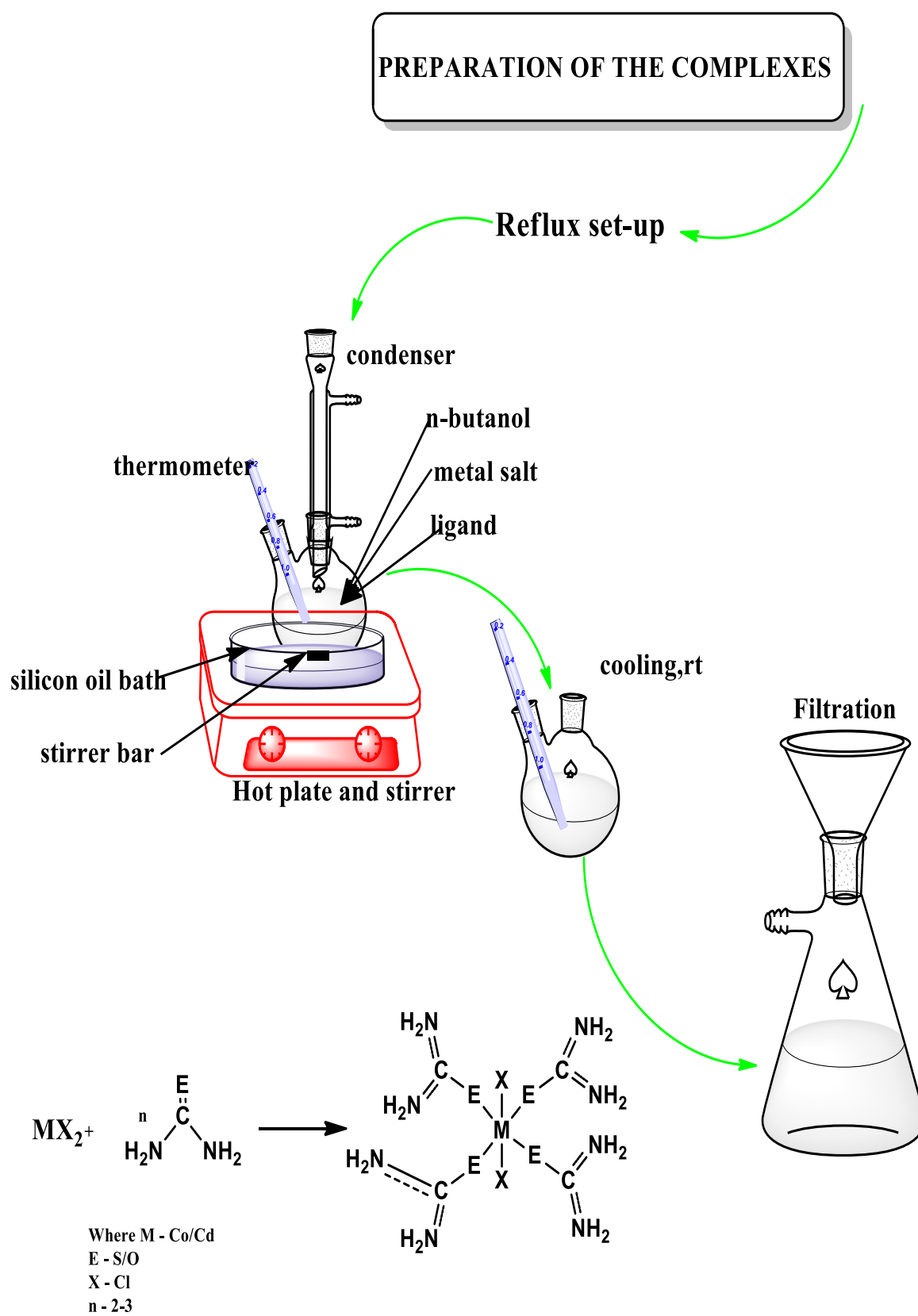
2.3 (c) Microanalysis

Microanalysis was performed on a CARLO ERBA elemental analysis for determination of C, H, N and S.

2.4 Preparation of the complexes

All the complexes were prepared by the general reaction scheme 3, whereby all the atoms required in a deposited material are present in a single molecule. All cadmium complexes of thiourea and urea were refluxed in ethanol/methanol as solvents while cobalt complexes are refluxed in n-butyl in stoichiometric amounts. The respective complexes were obtained in reasonable yield and prepared for analysis.

2.4.1 Methodology



Scheme 7: Reaction scheme for the synthesis of complexes

2.4.2 Synthesis of cobalt thiourea and urea complexes

2.4.2 (a) $\text{CoCl}_2(\text{CS}(\text{NH}_2)_2)_2$

$\text{CoCl}_2 \cdot 6\text{H}_2\text{O}$ (2.38 g, 0.01 mol) was dissolved in 30 ml n-butanol and thiourea (3.04 g, 0.02 mol) was added. The mixture was refluxed for 3 hours on heating until complete dissolution of the entire solid is attained. After this solution had cooled to room temperature, benzene was added until a slight permanent turbidity is produced. Further cooled in an ice chest resulted in a blue solid precipitating. The precipitate was filtered washed twice with ethanol and acetone under vacuum. Yield: 75%; Elemental analysis: Calcd. C:17.1, H:3.7, N:19.9. Found: C:17.2, H:3.77, N:21.8. Significant IR bands cm^{-1} : N-C-N- 1391(vs), C-S- 721 (m) and N-H 3390 (m).

2.4.2 (b) $\text{CoCl}_2(\text{CO}(\text{NH}_2)_2)_2$

$\text{CoCl}_2 \cdot 6\text{H}_2\text{O}$ (2.38 g, 0.01 mol) was dissolved in 30 ml n-butanol and urea (3.04 g, 0.025 mol) was added. The mixture was refluxed for 3 hours on heating until complete dissolution of the entire solid is attained. The solution was cooled to room temperature resulting in a purple colour. The precipitate was filtered washed three times with acetone under vacuum. Yield: 62%; Elemental analysis: Calcd. C:6.3, H:4.2, N:18.5. Found: C:6.5, H:3.9, N:16.5. Significant IR bands cm^{-1} : C-O- 1632 (m) and N-H 3494 (m)

2.4.3 Synthesis of cadmium thiourea and urea complexes

2.4.3 (a) $\text{CdCl}_2(\text{CS}(\text{NH}_2)_2)_2$

$\text{CdCl}_2 \cdot 6\text{H}_2\text{O}$ (2.5 g, 0.01 mol) was dissolved in 30 ml ethanol and thiourea (3.5 g, 0.05mol) was added. The mixture was refluxed for 3 hours on heating until yielding a white solution. The white solution was left for cooling in a room temperature, filtered and

washed three times with methanol and acetone and left to dry under vacuum. Yield: 82%, Elemental analysis: Calcd. C:5.2, H:2.4, N:16.7, S:19.1. Found: C:4.36, H:2.8, N:16.22. Significant IR bands cm^{-1} : N-C-N- 1411(vs), C-S- 726 (m) and N-H 3390 (m)

2.4.3 (b) $\text{CdCl}_2(\text{CO}(\text{NH}_2)_2)_2$

$\text{CdCl}_2 \cdot 6\text{H}_2\text{O}$ (2.5 g, 0.01 mol) was dissolved in 30 ml methanol and urea (3.5 g, 0.029 mol) was added. The mixture was refluxed for 3 hours on heating until yielding a white solution. The white solution was left for cooling in a room temperature, filtered and washed three times with acetone and left to dry under vacuum. Yield: 80%: Elemental analysis: Calcd. C:4.2, H:3.8, N:18.5. Found: C:3.73, H:3.6, N:17.9. Significant IR bands cm^{-1} : C-O- 1604 (m) and N-H 3483 (m)

3. Results and Discussion

All Co and Cd complexes of thiourea and urea were refluxed in different solvents in stoichiometric amounts. The respective complexes were obtained in reasonable yield and their melting points were taken indicating the presence of monomers. In this regard, the infrared studies were conducted to elucidate bonding of the metal to the respective sulphur atom.

3.1 (a) FTIR spectral analysis for thiourea and its cobalt and cadmium complexes

Thiourea has a large dipole moment and an ability to form extensive network of hydrogen bonds. A thermochemistry study with an emphasis on the fundamental measure of the total coordinate bond strength conducted by Moloto et al [184] showed that thiourea has a low basicity and, in aqueous solution, forms complexes with metal ions which are of similar stability to that of the protonated ligand itself.

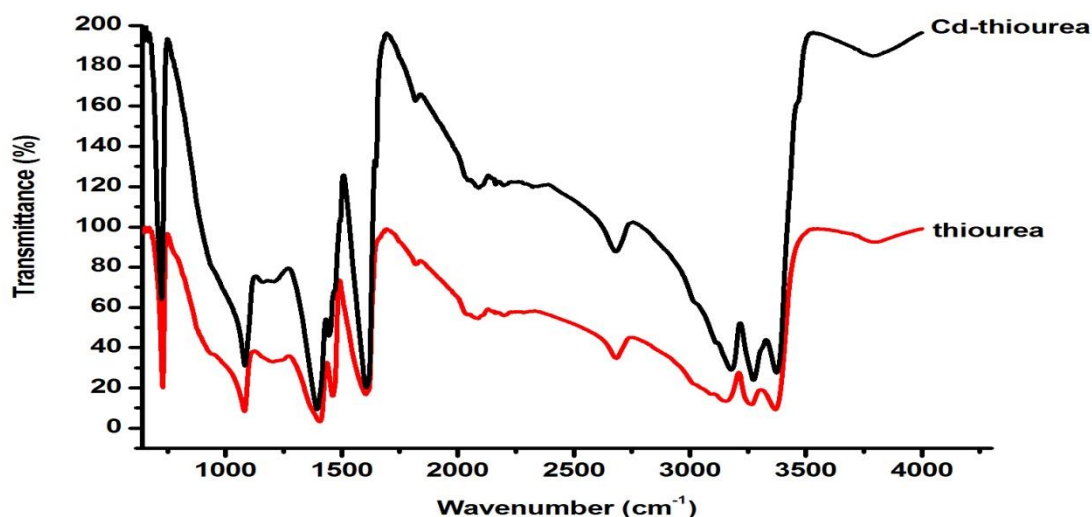


Figure 5: FTIR spectra $\text{CdCl}_2(\text{CS}(\text{NH}_2)_2)_2$ and free thiourea ligand $(\text{CS}(\text{NH}_2)_2)_2$

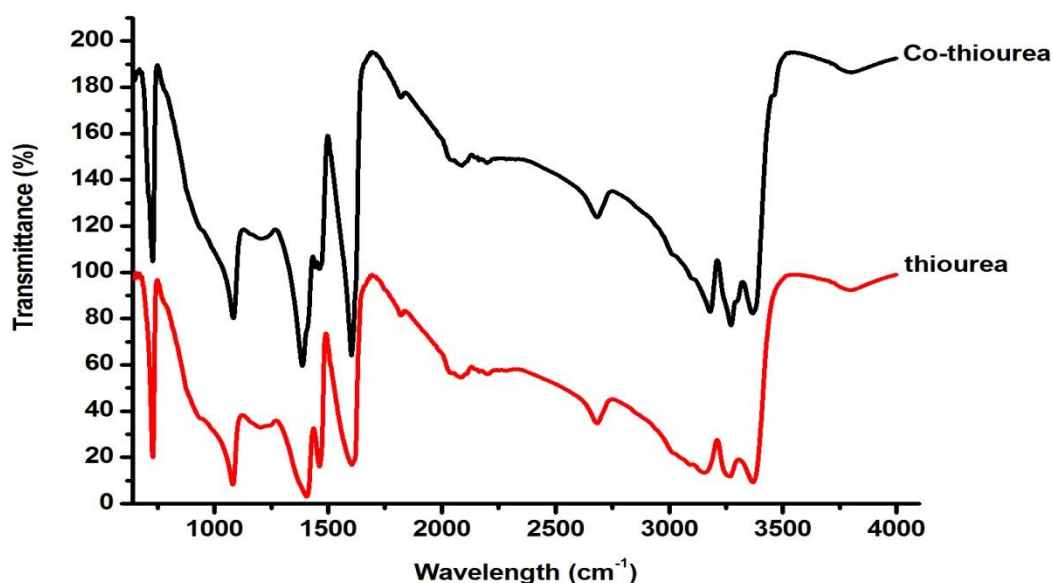


Figure 6: FTIR spectra $\text{CoCl}_2(\text{CS}(\text{NH}_2)_2)_2$ and free thiourea ligand $(\text{CS}(\text{NH}_2)_2)_2$

The S-C-N bending modes for the Co and Cd complexes observed at 1496 and 1473 cm^{-1} as expected (**Figure 5 & 6**) showed a decrease in the frequency shifts to 1484 and 1467 cm^{-1} , respectively on coordination of the sulphur atom to the metals. It is evident that coordination of the thiourea makes the unpaired electrons on the sulphur atom less available for bonding with the other thiourea molecule and readily available to bond with the metal. The N-H absorption bands are not shifted to the lower frequency which indicates that nitrogen to the metal bonds is not present and the bonding must be between the sulphur and the metal. Similarly from the N-C-N stretching mode at 1472 cm^{-1} there are no observable features of the M-N bond but much enhanced sensitivity to coordination through sulphur. Absorption at 1092 cm^{-1} is attributable to NH_2 rocking mode, which is also not affected by the formation of a metal-sulphide bond. The free ligand show a band observed at 732 cm^{-1} , which is due to contribution of C-S stretching and has shifted to a lower frequency 721 and 726 for Co-thiourea and Cd-thiourea complexes respectively. This signify a decrease in the double bond character of the $\text{C}=\text{S}$ which confirms the sulphur coordination of thiourea to cobalt and cadmium metals. Yamaguchi

et al [183, 185] reported that the NCN and CS frequencies are respectively increased and lowered on sulphur coordination while the opposite occurs on nitrogen coordination.

Table 1: The wavenumber of the fundamental modes of coordinated thiourea (cm^{-1})

Band assignment	thiourea	Cd- thiourea	Co- thiourea	Relative intensity
N-H Stretching symmetric	3172	3180	3189	medium
N-H stretching asymmetric	3392	3390	3390	medium
N-H bend symmetric	3278	3281	3282	medium
N-H deformation	1617	1618	1607	strong
N-H rocking	1092	1086	1099	medium
N-H stretch	3791	3823	-	weak
N-H wagging vibration	718	730	711	strong
NCN stretching	1399	1411	1391	very strong
C-S stretching	732	726	721	medium

3.1 (b) FTIR spectra for free urea ligand and its Cd and Co complexes

Complexes of urea with some metal ions such as $[\text{Zn}(\text{urea})_6]\text{SO}_4 \cdot \text{H}_2\text{O}$ and $[\text{Zn}((\text{urea})_4)(\text{NO}_3)_2 \cdot 2\text{H}_2\text{O}]$ are used as fertilizers [117, 186-188]. Crystal structure studies of urea showed that in solid urea, both of the nitrogen atoms are identical.⁶ Urea usually

coordinates as a monodentate ligand through the oxygen atom, forming a $\text{C}=\text{O} \cdots \text{M}$ bond. The rare N,O-bidentate coordination mode has been observed in a very limited number of cases [189-192]. Raman and infrared spectra of urea have been studied by several scientists [193-203]. Urea possesses two types of potential donor atoms, the carbonyl oxygen and amide nitrogen atoms. Penland et al [204] studied the infrared spectra of urea complexes to determine whether coordination occurs through oxygen or nitrogen atoms. If coordination occurs through nitrogen CO stretching frequency is expected to increase with a decrease of CN stretching frequency, the NH stretching frequency in this case may fall to the same range as those of the amido complexes.

On the other hand if coordination occurs through oxygen CO stretching frequency decreases but with no appreciable change in NH stretching frequency. Since the vibrational spectrum of urea itself has been analyzed [202], band shifts caused by coordination can easily be checked, for example, the effect of the coordination on the spectra of the complexes of urea with Pt(II) and Cr(III) in which the coordination occurs through nitrogen and oxygen atoms, respectively [204]. The mode of coordination of urea with metal ions seems to be dependent upon the type and nature of metal ions. Pd(II) coordinates to the nitrogen, whereas Fe(III), Zn(II), and Cu(II) coordinate to the oxygen of urea [204]. In urea-metal complexes, if a nitrogen-to-metal bond is present, the vibrational spectrum of this complex differs significantly from that of the free urea molecule. The N-H stretching frequencies would be shifted to lower values, and the C=O bond stretching vibration, ($\nu(\text{C}=\text{O})$) would be shifted to higher frequency at about 1700cm^{-1} [205].

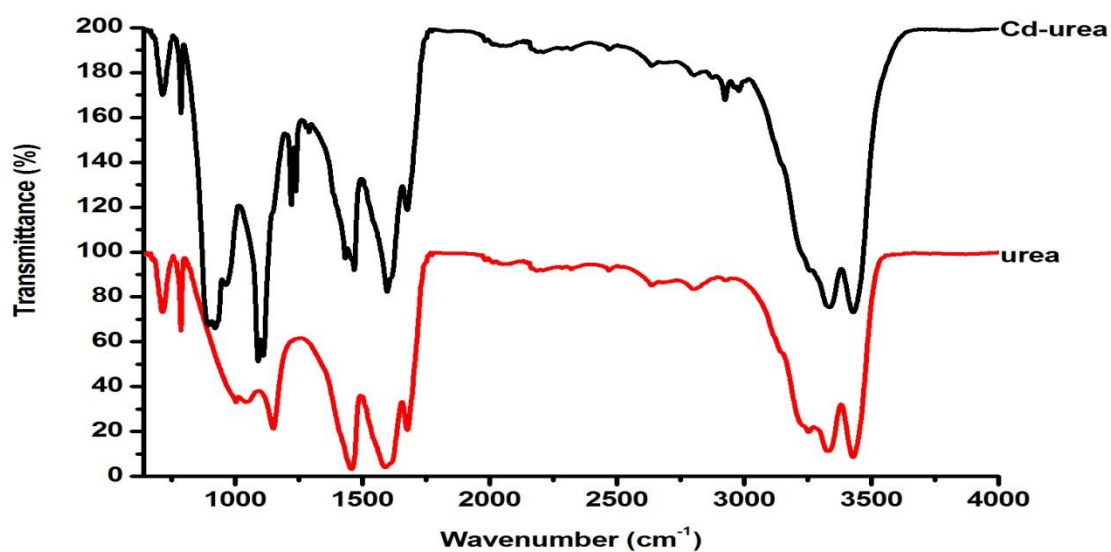


Figure 7: FTIR spectra $\text{CdCl}_2(\text{CO}(\text{NH}_2)_2)_2$ and free urea ligand $(\text{CO}(\text{NH}_2)_2)_2$

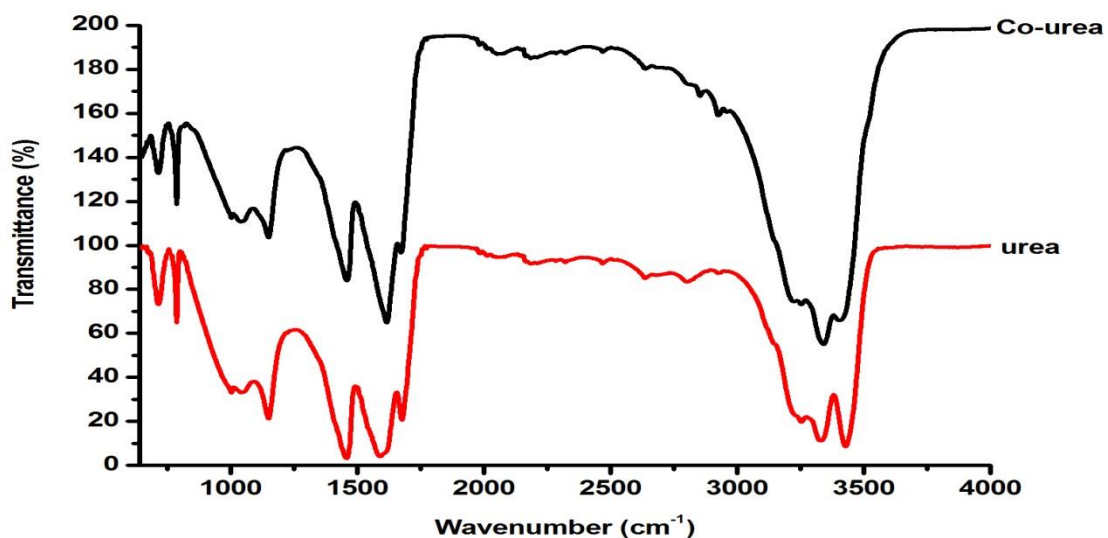


Figure 8: FTIR spectra $\text{CoCl}_2(\text{CO}(\text{NH}_2)_2)_2$ and free urea ligand $(\text{CO}(\text{NH}_2)_2)_2$

The carbonyl group region where expected three strong bands are observed little difficult in differentiating the $\text{C}=\text{O}$ stretching bands from NH_2 deformation bands. The medium bands at 1604 and 1632 cm^{-1} in the complex with Cd and Co respectively, are assigned to $\text{C}=\text{O}$ stretching vibration (**Figure 7 & 8**). This assignment is based on the fact that the frequency value of CO bands with

different metals in our complexes is in the order $\text{Cd} < \text{Co}$. This order agrees well with heat of formation of the MCl_4^{2-} ions [206], the order which can be considered as a criterion of electron acceptor power of the transition metals. A similar trends has been found in other works, such as the second ionization potential of transition metals [207] and metal depended frequency shifts in number of coordination compounds[208-210].

All in plane vibration of NH_2 groups show small frequency shifts. These may be due to the change in environment or consequence of the breaking of the coupling between NH_2 bending and OCN skeleton vibration. A number of normal coordinates analyses of urea indicate that substantial vibration mixing of $\text{C}=\text{O}$ stretching is present in urea [211-217]. However on formation of metal to oxygen bond, the coupling between the $\text{C}=\text{O}$ stretching and NH_2 bending vibration in complexes are assigned to bands appearing in the region of $1632 - 1684 \text{ cm}^{-1}$. Because of the lack of appropriate spectral data concerning with the out of plane vibration of uncoordinated urea which refer to, assignment of two peaks below 900 cm^{-1} by arranging them in such a way that their order of frequency values consistent with the order of those obtained from normal coordination analyses [213, 215].

Table 2: The wavenumber of the fundamental modes of coordinated urea (cm⁻¹)

<i>Band assignment</i>	<i>urea</i>	<i>Cd- urea</i>	<i>Co- urea</i>	<i>Relative intensity</i>
N-H Stretching symmetric	3347	3404	3393	medium
N-H stretching asymmetric	3439	3483	3494	medium
N-H bend symmetric	3285	-	3190	medium
N-H deformation	1615	-	-	strong
N-H rocking	1167	1134	1113	medium
N-H torsion	722	-	-	weak
C-N stretching	1467	1472	1475	strong
C=O stretching	1640	1604	1632	medium

3.2 Thermo gravimetric analysis for complexes

Thermal decomposition studies on metal complexes have brought information on the mechanism and steps of decomposition by heating, and therefore permit determination of kinetic parameters of the reaction [218, 219]. Thermal decomposition has been done due to interest in the isolation and identification of the solid decomposition products of complexes, interesting decomposition intermediate has been produced. Metal compound of thiourea and urea represent an extensive series of sulphur and oxygen bonded complexes with well-

established structures. Thermal decomposition of nickel (II) thiourea [220] and Zinc (II) urea compounds [117, 186-188], and acetylthiourea complexes of molybdenum [221] and cadmium (II) [222] have been done. Thermal decomposition of thiourea and urea complexes of cadmium, copper and cobalt in static air led to the formation of metal sulphide/oxide in a main degradation step between 200-300°C. In the study thermogravimetric analysis were considered to study the physical behavior of cobalt and cadmium complexes based on thiourea and urea to explore stability and identify the decomposition products formed, including the volatile organic material.

Figure 9: shows the TGA curves for thiourea and urea cadmium complexes. Cd-urea complex show two steps decomposition with a sudden loss of weight on heating until 178°C which can be associated with loss of water and some volatile impurities remained during purification. The second decomposition started at 560°C, a period of slow loss of weight led to the formation of the metal oxide, which was completed at about 663°C. The TGA curve of Cd-thiourea complex displayed the beginning of weight loss at 208°C to 400 °C, in which most of organic molecules from the ligand are lost, followed by chlorides at a slow period of weight loss from 650 to 750°C, which led to formation of metal sulphide, shown in **Figure 9**.

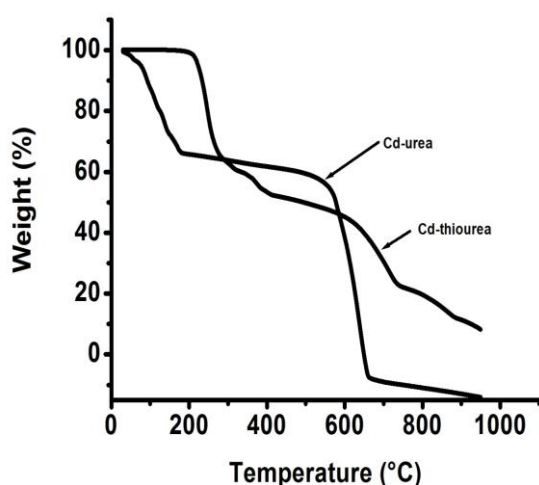


Figure 9: TGA curves for Cd-urea and Cd-thiourea complexes

The TGA curves in **Figure 10** indicate the two-step decomposition of Co-urea and Co-thiourea complexes. Co-thiourea complexes display first decomposition at 200°C to 320 °C, whereas Co-urea complexes decompose immediately on heating to 175°C. These periods of weight loss can be associated with the water, impurities and some organic molecules from the ligand. There is a slow weight loss of the two complexes which led to the formation of metal sulphide and oxide at a final temperature of 800°C.

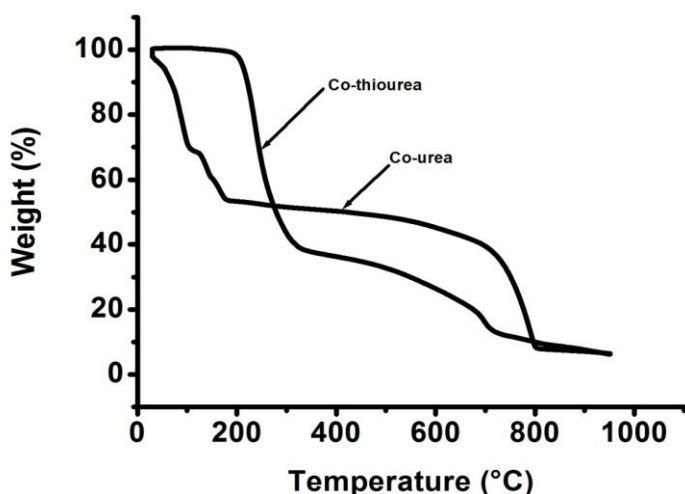


Figure 10: TGA curves for Co-urea and Co-thiourea complexes

3.3 Conclusion

The cobalt and cadmium complexes based on their thiourea and urea ligand were successfully synthesized. Following various measurements performed on these complexes which were consistent confirmed the purity of these complexes. The synthetic methods of these complexes produced reasonable yield which to be used in the second part of the study for the preparation of nano-materials. FTIR spectroscopy confirmed the bond of the metal to sulphur and/or Oxygen. TGA shows a residue of less than 10% which is in good agreement theoretical formation of metal sulphide and oxide form the prepared complexes.

CHAPTER THREE

SYNTHESIS AND CHARACTERIZATION OF NANOPARTICLES AND CORESHELL NANOMATERIALS FROM COBALT AND CADMIUM COMPLEXES BASED ON UREA AND THIOUREA

SECTION A

Synthesis of nanoparticles and use of single-precursors on urea and thiourea, cobalt and cadmium complexes

4.1 Introduction

The most widely used quantum dots to date are II-IV semiconductor nanocrystals. Nanocrystalline materials have attracted much attention in recent years due to the change, at nanoscale, which occurs when their crystallite radius becomes comparable to the exciton Bohr radius. Cobalt and cadmium of respective sulfide and oxides are among the widely studied II–VI group semiconductors because they show significant quantum confinement effects which influence their electrical and optical properties[223, 224]. They have found applications particularly in photovoltaic, photonic, and optoelectronic devices and sensors [225]. Preparation methods for the synthesis of high quality and nearly monodispersed semiconductor nanoparticles of quantum dots have typically utilized tri-n-octylphosphine oxide (TOPO), hexadecylamine (HDA) and trioctylphosphine (TOP) as these compounds provide the most controlled growth conditions[226]. Bawendi and co-workers [13] showed that injection of the metal-organic precursors into a hot reaction pot with TOPO and TOP as solvents resulted in a short burst of homogenous nucleation and narrow size distribution. Size control is primarily achieved by varying reaction conditions [13]. Moloto *et al* showed that incorporating alkylamines such as HDA into the synthesis led to much improved quantum yield [227].

Like manganese, iron, and copper, cobalt exhibits several possible oxidation states Co^{2+} , Co^{3+} and Co^{4+} and several types of coordination such as tetrahedral, pyramidal, and octahedral[228-230]. Consequently, cobalt oxides offer a wide-field for the creation of many frameworks, not only stoichiometric oxides but also non-stoichiometric oxides, involving a mixed valence of

cobalt and/or the presence of oxygen vacancies. A property which distinguishes the cobalt oxides from other 3d metal oxides deals with the ability of cobalt to be present in various spin states, that is, low spin (LS), high spin(HS),and intermediate spin(IS) [231].

In cobalt oxides, the selection decided by the Hund's coupling makes that Co^{2+} is always in high spin state $t_{2g}^5 e_g^2$ ($S=3/2$), whereas Co^{4+} usually adopts the low-spin state $t_{2g}^5 e_g^0$ ($S=1/2$) due to the crystal field splitting. In contrast, for Co^{3+} the three different spin states are possible, that is, low-spin $t_{2g}^6 e_g^0$ ($S=0$), high-spin $t_{2g}^4 e_g^2$ ($S=2$), and intermediate spin $t_{2g}^5 e_g^1$ ($S=1$) due to the fact that crystal field splitting very sensitive to changes in the Co-O bond length and Co-O-Co bond angle, modifying easily the spin state of Co^{3+} . Spin state transitions can, therefore, be easily provoked by varying the temperature and the pressure, applying a magnetic field and photon and/or by tuning the structural parameters (oxygen content and type of counteraction) of the material [232-234]. Cobalt sulphide (CoS) form a II-IV compounds with considerable potential for application in electronic devices[235]. It can be used in solar energy as absorbers[236], ultra high density magnetic recording[237], anodes for Li-ion batteries[238] and catalysts for hydrodesulphurization and dehydro-dearomatization[239]. And also, the cobalt sulphide also finds novel applications in selective coatings and solar cells, optical filters, temperature sensors, optical wave guides and IR detectors[240-249]. It is of particular interest that the properties of cobalt sulphide are strongly dependent on the particle size, shape, distribution and surface. Therefore, the crystal structure and optoelectronic properties of CoS may be varied depending on the micro environment of layered inorganic matrices. It is also notable that the properties, morphologies and stoichiometric compositions were affected by various synthetic routes[250]. They are one of the most complex metal sulfides systems, with a number of phases and chemical

composition. Their chemical composition have many phases such as Co_4S_3 , Co_9S_8 , CoS , Co_{1-x}S , Co_3S_4 , Co_2S_3 and CoS_2 [251].

Amongst quantum dots including cadmium with chalcogenide materials such as sulphur, oxygen and selenium are the easiest one to be synthesized. High temperatures and high pressures are not required for the synthesis cadmium chalcogenides. Cadmium chalcogenides as a kind of semiconductor material has been applied to many areas due to its suitable band gap (approximately 2.3 - 2.6 eV) and strong photo-response in the visible region [252]. The cadmium chalcogenides in nano-scale has special luminescence properties and semiconductor quantized performance. These outstanding properties make cadmium chalcogenides nanoparticles attractive candidates for functional materials and widely used in many fields such as solar cells, photo-detectors, photo-electrochemistry, photo-chromism and electro-chromic materials [253-257]. Thiourea behaves similar to urea as far as the structure is concerned (chapter 2). The use of these ligands (thiourea and urea) as complexes with transition metals such as cadmium and cobalt, to form precursors for II-VI semiconductor nanoparticles has attracted some interest, due to the presence of sulphur and oxygen atoms from thiourea and urea respectively. The thiourea unit consists of one sulfide and hence the binding to the metal centre upon formation of complexes would be through the sulphide, whereas urea consist of one oxygen and the binding will occur through oxygen. The stability of the complexes is enhanced by the chelating ability of the ligand to the metal ions. This resulted in an interest of thiourea and urea complexes of cadmium and cobalt as potential single source precursors for the synthesis of nanoparticles.

4.2 Experimental section

4.2.1 Reagents

Cobalt (II) chloride hexahydrate, cadmium (II) chloride, urea, thiourea obtained from Sigma Aldrich, were used as purchased. Acetone, methanol and n-butyl alcohol (analytical grade) were used without further purification and distilled water was also used as solvents.

4.2.2 Instrumentation

(a) Optical characterization

Absorption spectra of the particles were measure using a Perkin Elmer Lambda 20 UV-VIS Spectrophotometer. The samples were place in quartz cuvettes (1-cm path length) with toluene as the solvent. Emission spectra of the particles were recorded on a Perkin Elmer LS 45 photoluminescence (PL) spectrometer with a xenon lamp at room temperature. The samples were placed in glass cuvettes (1 cm) with toluene as solvent.

(b) X-ray diffraction analysis

X-ray diffraction (XRD) patterns on powdered samples were carried out in the 2θ on a D8 diffractometer. Samples were placed in silicon zero background sample holder. Measurements were taken using a glancing angle of incidence detector at an angle of 2° , for 2θ values over $20^\circ - 60^\circ$ in steps of 0.05° with a scan speed of $0.01^\circ 2\theta.s^{-1}$.

(c) Electron microscopy

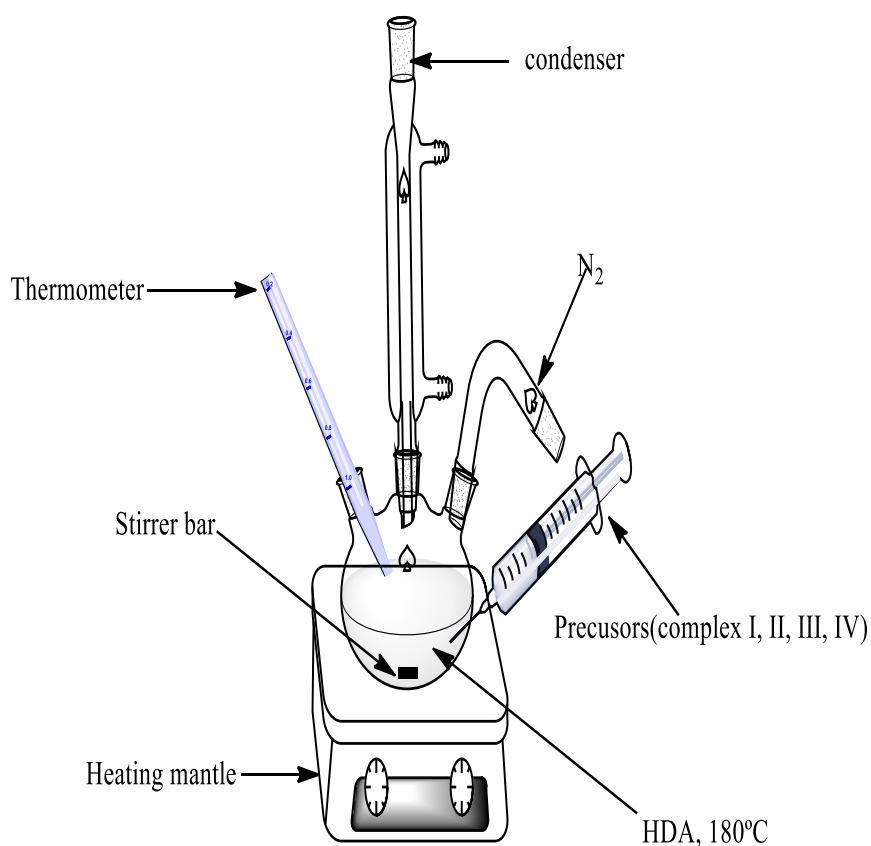
The images were obtained using high resolution transmission electron microscope (HRTEM Joel JEM-2100 microscope) operating at 200 kV. The samples were prepared by placing a drop

of dilute solution of sample in toluene on to a copper grid. The sample was allowed to dry completely at room temperature.

4.2.3 Methodology

(a) Preparation of nanoparticles from Urea and thiourea, cobalt and cadmium complexes (complex I – IV)

Hexadecylamine (HDA) 6g was heated to 180°C under nitrogen environment. For each precursor 1g was dispersed in 5ml trioctylphosphine (TOP) and injected into the hot solution of HDA. The reaction was maintained at 180°C for 1hour. The solution was cooled to approximately 70°C at room temperature. After cooling the reaction mixture, an excess of acetone was added. The precipitate formed were isolated by a centrifuge, washed with acetone three times to remove some of the capping agent and dried in an open air environment.



Scheme 8: Schematic representations for the synthesis of nanoparticles

Table 3: Reaction conditions for the preparation of nanoparticles from complex I-IV

Material (g)	HDA (g)	Temperature (°C)	Time (minutes)
CdS	6	180	60
CdO	6	180	60
CoS	6	180	60
CoO	6	180	60

4.3 Results and Discussion

4.3.1 Optical properties

(a) CdS nanoparticles prepared from thiourea complexes

UV-visible and photoluminescence spectroscopy are a very useful techniques for characterization of metal chalcogenide nanoparticles. Small metal chalcogenide nanoparticles exhibit a high optical absorbance due to the existence of discrete energy levels of electron and particular of specific states. The UV-vis absorption spectrum of CdS nanoparticles is shown in **Figure 11(a)**. The spectra were recorded in absorption mode and all samples were prepared by dissolving the nanocrystallites in toluene.

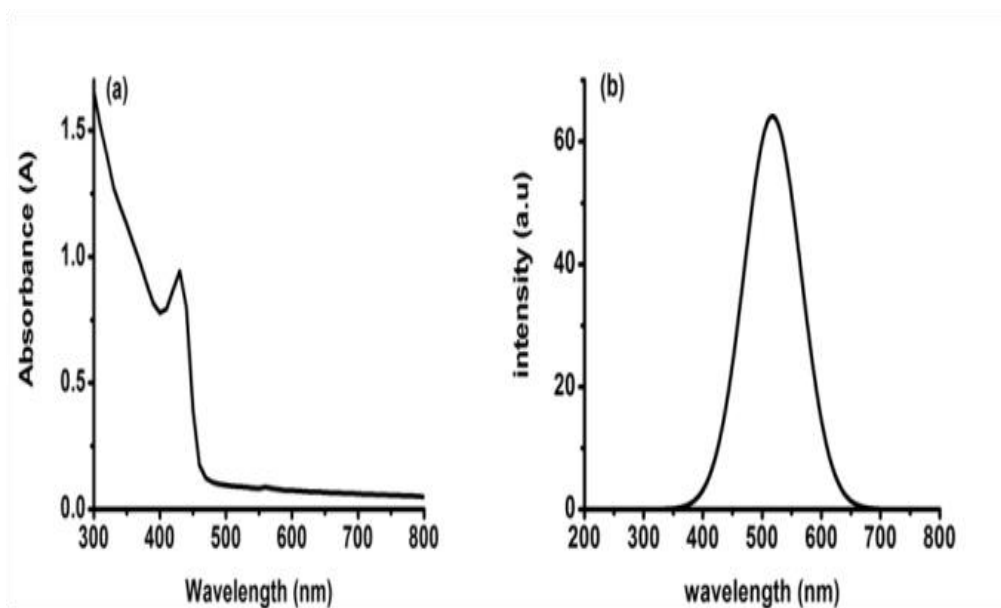


Figure 11: (a) Absorption spectrum and (b) emission spectrum of CdS nanoparticles synthesized from Cd- thiourea complex.

The bulk crystallites of CdS usually observed the interband adsorption spectrum with a band edge around 515 nm. There is a blue shift of the adsorption band edge with related to the bulk as results of formation of nanoparticles. In the study **Figure 11(a)** the band edge is observed at 466 nm nm and the absorption peak at 429 nm. The blue-shift in band-edge was further explained using the work reported by Cheon and co-workers [258]. Cheon and co-workers discovered that not only the size of the nanoparticle has an influence on the band-gap but shape also plays an important role [37]. In the case of rods, length and the width both have a contribution in the resultant band-edge. Therefore the blue-shifts in band-edge can be explained by the notion that the morphology of the particles has a great influence on the optical properties of the nanoparticles. With spherical particles, the diameter of the particle can be related to the optical properties of the particles, whereas with rod- or wire-like particles, the diameter does not account for the properties of the particles. Other reason accounting for the blue shift can be associated with agglomeration of the particles due to ageing and external factors such as temperature which exhibits less stability to the capping material allowing factors such as oxygen to penetrate into the pores of the particles.

A similar feature for the UV-vis spectrum of the nanoparticles of CdS has been reported by Moloto *et al* [259] and Hoyer *et al* [260]. Moloto *et al* reported that the growth process of nanoparticles involves a delicate balance between kinetic and thermodynamic control. Hoyer *et al* [260] reported that capping agents are an important component in the synthesis of the nanoparticles. In general its main purpose is to solubilise and disperse the nanocrystals and the reactants involved in the growth thereby controlling the speed of the reaction. The solvent molecules need to bind and unbind dynamically on the surface of the growing crystals. Once a molecule detaches from the surface of the nanocrystal, new atomic species (monomers) can be incorporated into the nanocrystal, and thus it can grow. When referring to these characteristics of the solvent molecules, they are termed surface ligands, or surfactants. In a synthesis the solvent can be a mixture of different species, including pure solvent and pure surfactants.

The emission maxima of CdS **Figure 11(b)** show a red-shift from its respective absorption band-edges. The emission peak of CdS at 533 nm was assigned to the surface trap induced fluorescence, as a result of recombination of an electron trapped in a sulfur vacancy with a hole in the valence band of CdS [261]. One explanation for the luminescent emission of CdS is that either free electrons and holes or excitons recombine in the pure lattice so that this emission is “lattice” emission. Also, CdS luminescence can be related with specific lattice defects [262]. TEM is also a very useful technique in characterization of the size and shape of the nanoparticles. CdS nanoparticles using cadmium thiourea as precursor have been synthesized in HDA.

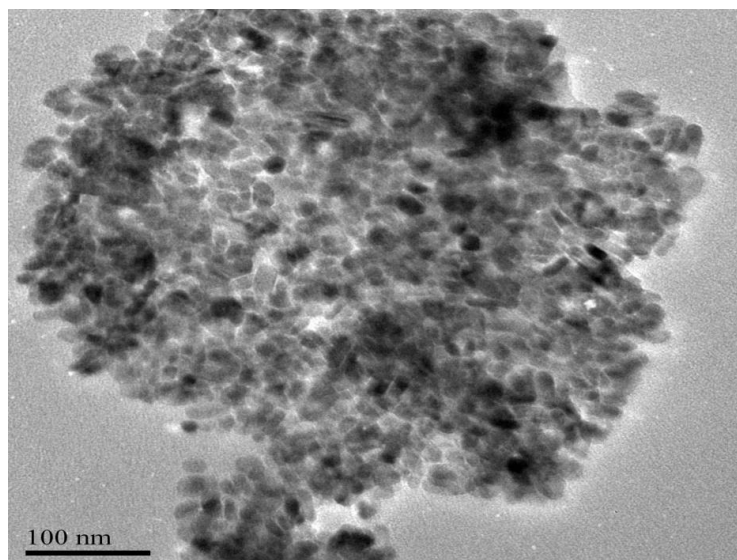


Figure 12: TEM image of CdS nanoparticles prepared at 180°C, 1g precursors: 6g HDA from the Cd-thiourea complex

The particles show some level of agglomeration whilst rods and spherical shapes with size average of 2 to 3 nm in width and 4 to 25 nm in length and a diameter of 3 nm are observed (**Figure 12**). The difference in particle size and agglomeration could be due to a combination of factors, such as the temperature, reaction time, capping agent nature and concentration of precursors used. Structural characterization of CdS nanoparticles as previously reported by Bawendi *et al* [263] that CdS exists either as the cubic or hexagonal phase and the existence of a mixture of cubic and hexagonal phase with the predominance of one over the other. In the present study CdS nanoparticles are in predominance of hexagonal phase (**Figure 13**). The diffractive patterns can be indexed to 100, 002 and 101 planes and other peaks confirm the structure to be hexagonal phase in nature for CdS. The sharpening of the peaks on the diffractogram is a clear indication of large particles

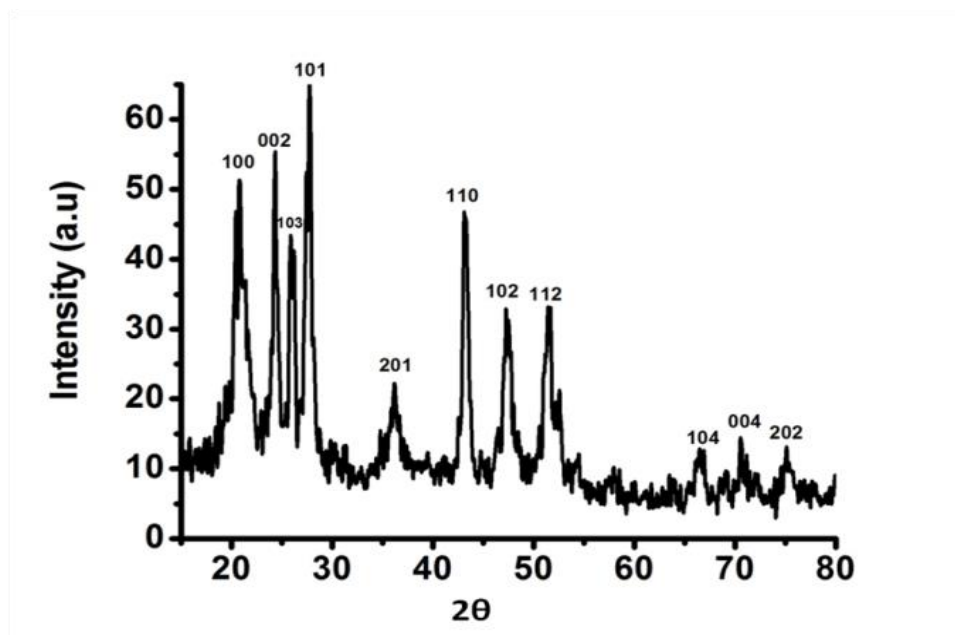


Figure 13: XRD patterns of HDA capped CdS nanoparticles synthesized from Cd-thiourea complexes, at 180 °C

(b) CdO nanoparticles prepared from urea complexes

The UV-Vis spectrum of CdO nanocrystals **Figure 14(a)** shows band edge around 380nm. The bulk crystalline of CdO usually observes the interband adsorption spectrum with a band edge around 539 nm. The large blue shift relative to the bulk CdO is attributed to quantum

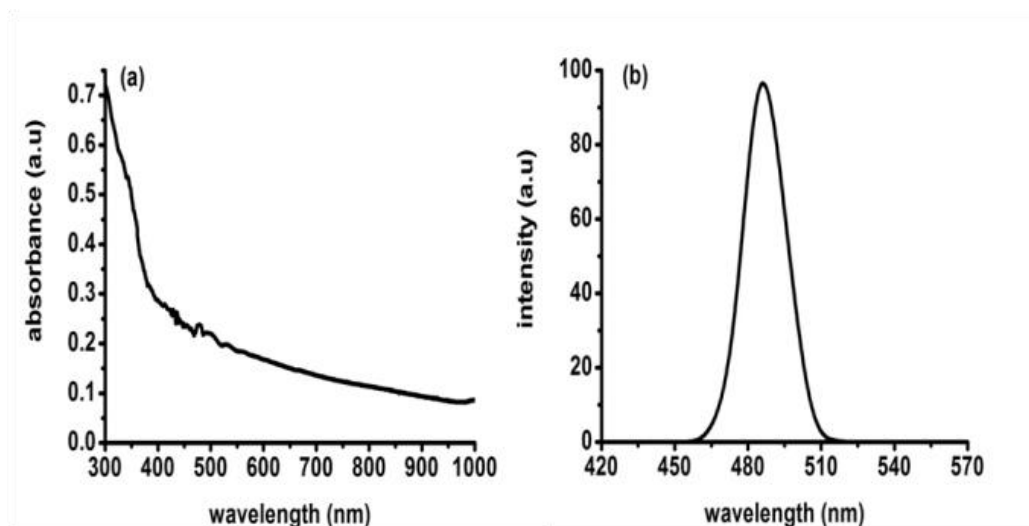


Figure 14: (a) Absorption spectrum and (b) emission spectrum of CdO nanoparticles synthesized from Cd-Urea complex

confinement. Ghosh and co-workers reported that the bulk exciton Bohr radius of CdO is not available in the literature and is therefore difficult to conclude as to which confinement regime the CdO nanocrystals belongs [264]. Wu *et al* [265] have reported the photoluminescence spectra of CdO suggesting that the band around 480 nm arises from transition between conduction and valence band. In **Figure 14(b)** we show the photoluminescence spectra excited at a wavelength of 200 nm. The excitonic band was observed at 490 nm which is red-shifted to UV-vis spectrum. The red-shift can also be explained by the work reported by Wu *et al*.

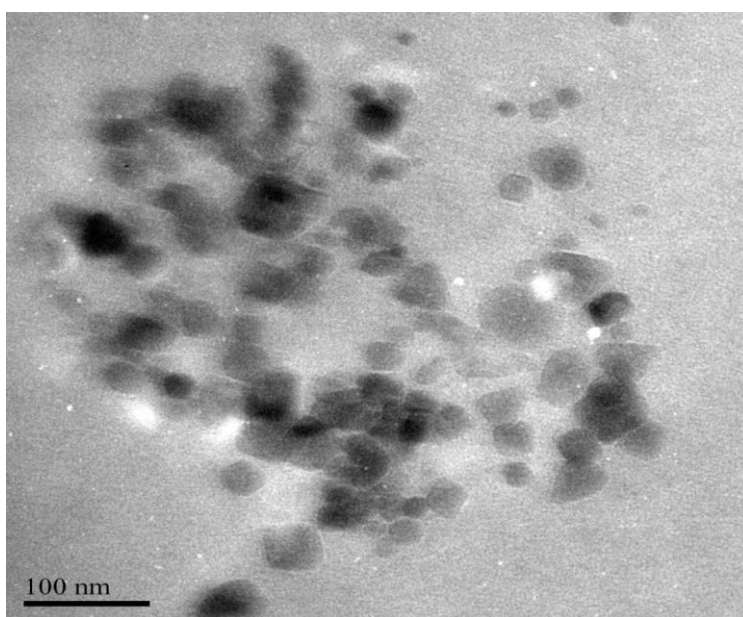


Figure 15: TEM image of CdO nanoparticles prepared at 180°C, 1g precursor: 6g HDA from the Cd-urea complex

The TEM images of CdO nanoparticles prepared from Cd-Urea complex are shown in **Figure 15**. The particles obtained are irregular in shapes with size ranging from 4 to 15 nm in size.

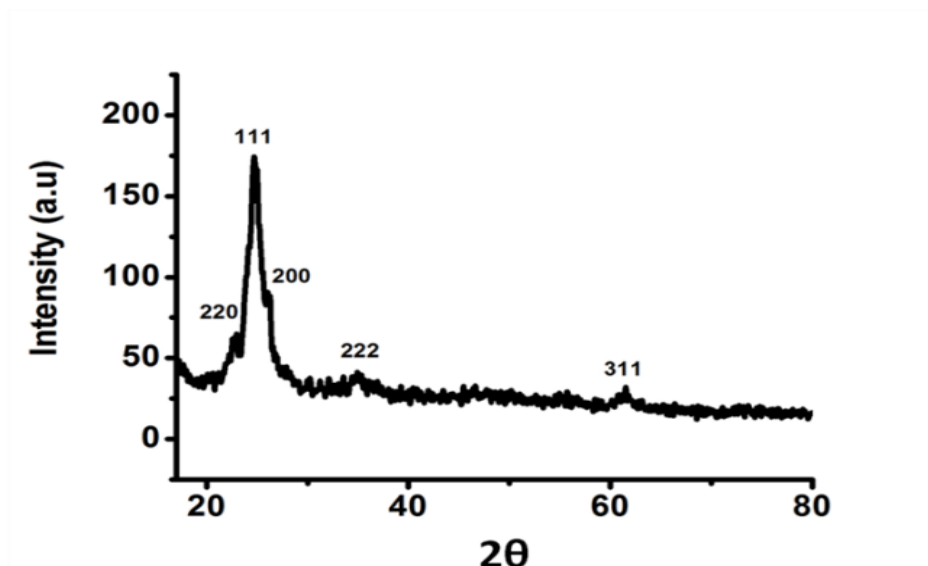


Figure 16: XRD patterns of HDA capped CdO nanoparticles synthesized from Cd-urea complexes, at 180 °C

Figure 16 shows the XRD patterns of CdO nanoparticles. Cubic structures CdO have been confirmed from their corresponding XRD patterns. The above experimental results clearly imply that CdO can be successfully obtained by employing Cd-thiourea as the precursor.

(c) CoS nanoparticles prepared from thiourea complexes

UV vis spectra of CoS prepared from cobalt thiourea complex **Figure 17(a)** gave an excitonic absorbance bands at 423 ± 10 nm and 349 ± 5 nm with a tail extending towards the longer wavelength as a results of quantum size effect. The absorption band gaps are blue shifted to a high energy compare with bulk cobalt oxide due to reduced particle size of the material. CoS exist in several number of transition state. Gupta *et al* [266] proposed that the two maxima in absorbance are because of bulk (extended state to extended state) state transition and surface (localized state to extended state) transitions. The surface states include the localized states because of defect in bulk in addition to the surface states. The optical transition to and from the surface states will produce maxima at higher wavelengths [266]. The emission maxima in

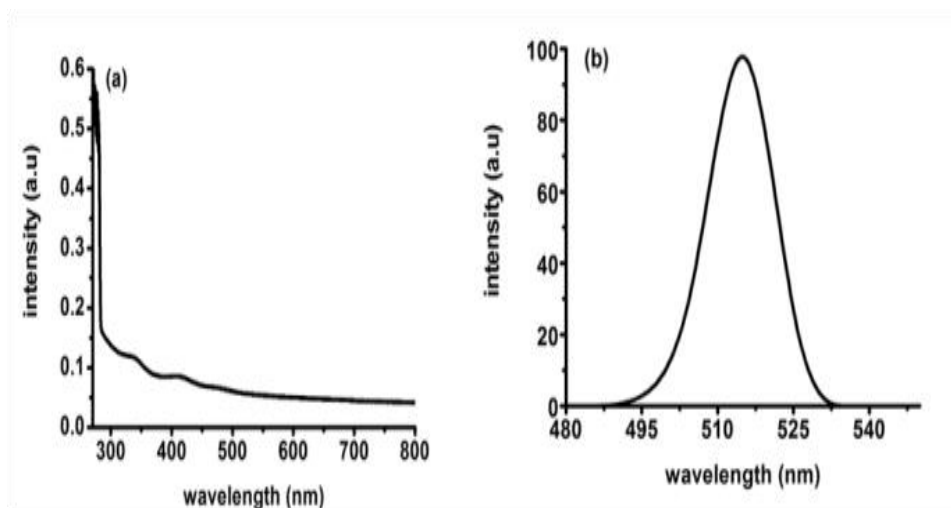


Figure 17: (a) Absorption spectrum and (b) emission spectrum of CoS nanoparticles synthesized from Co-thiourea

Figure 17(b) are red shifted from their respective band edges of the absorption spectra. The emission peak has a narrow shape which indicates the monodispersity and good passivation of the particles. **Figure 18** show CoS nanoparticles prepared from Co-thiourea complex.

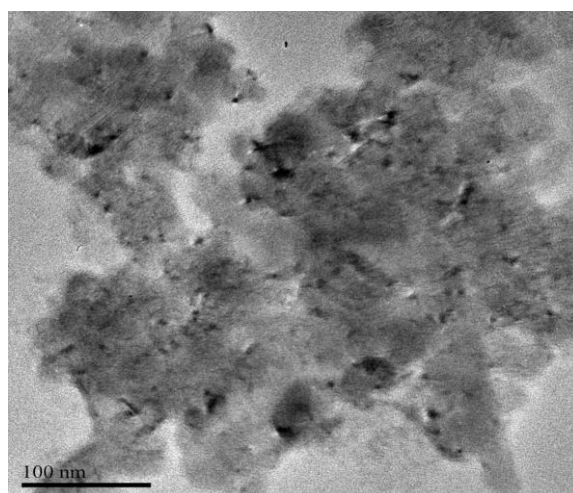


Figure 18: TEM image of CoS nanoparticles prepared at 180°C, 1g precursor: 6g HDA from the Co-thiourea complex

The particles are agglomerated and spherical shape depicted in the agglomeration environment. The particles are 2 to 3 nm in diameter. These features are confirmed by optical properties with narrowing of the emission peak in favor of small particles.

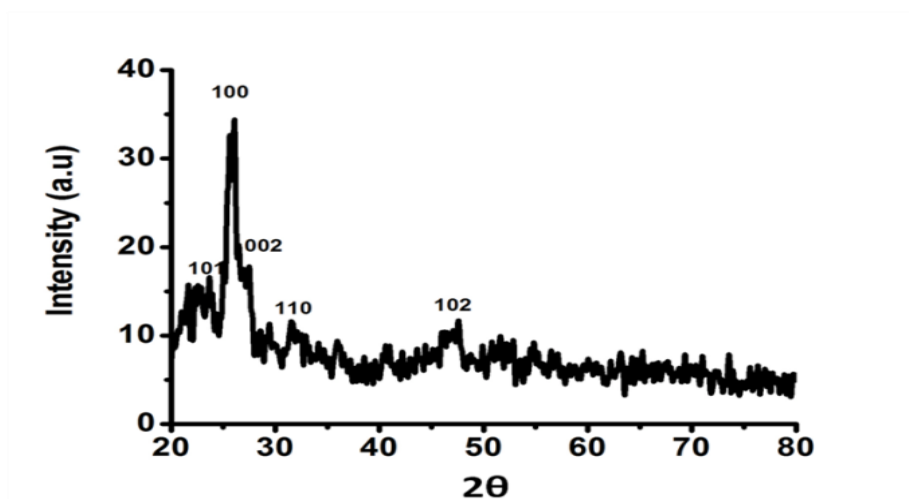


Figure 19: XRD patterns of HDA capped CoS nanoparticles synthesized from Co-thiourea complexes, at 180 °C

Figure 19, shows diffraction peaks of CoS which can be indexed to a face centered-cubic of cobalt sulfide (Co_9S_8), Diffraction peaks shows a lot of impurities which might be as results of insufficient washing of nanoparticles or recurring of impurities from the complex.

(d) CoO nanoparticles prepared from urea complexes

Optical properties of cobalt oxide in **Figure 20 (a)** were recorded using UV vis spectroscopy observing a broad excitonic absorbance peak at 661 ± 10 nm with a tail extending towards the

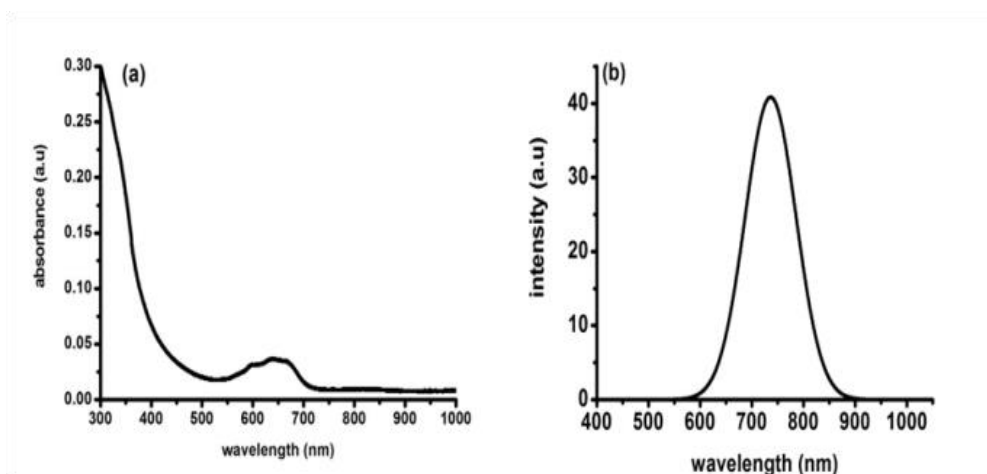


Figure 20: (a) Absorption spectrum and (b) emission spectrum of CoO nanoparticles synthesized from Co-Urea

longer wavelength as a results of quantum size effect. The broadening of excitonic absorption band is because of the particle size. The absorption band gaps are blue shifted to a high energy compare with bulk cobalt oxide. The blue shift phenomenon of the absorption edge has been ascribed to a decrease in particle size. It is well known in case of semiconductors that the band gap between the valence and conduction band increases as the size of the particles decreases in the nano-scale range. The magnitude of the shift depends on the size of the semiconductor material. In **Figure 20 (b)** we observe the red-shift in emission maxima of cobalt oxide to its absorption band edge as expected. **Figure 21** depicts the TEM images of

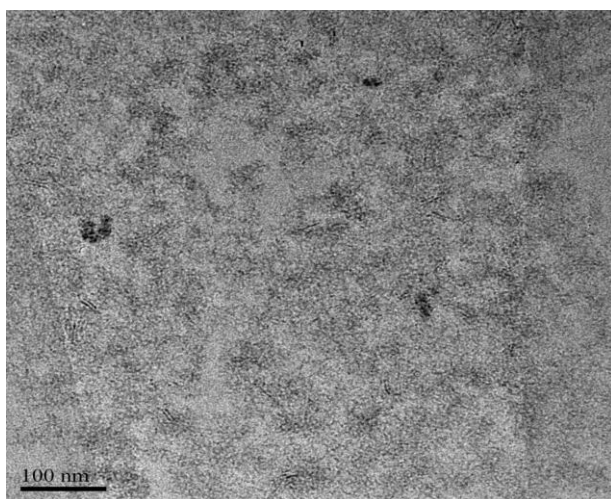


Figure 21: TEM image of CoO nanoparticles prepared at 180°C, 1g precursor: 6g HDA from the Co-urea complex

CoO nanoparticles capped with HDA. The image show particles that appear spherical to rod shaped with agglomeration due to their small size and high surface energy. It was difficult to measure the size of the particles because of that aggregation. This is in agreement with the PL width of more than 150 nm showing tendency for agglomeration of particles. In the cadmium urea complex there was no agglomeration observed and this can be attributed to stability of decomposition.

Figure 22 shows the XRD patterns of the nanoparticles prepared at 180 °C. Figure 22 shows five major peaks which are characterized by the (001), (100), (001), (002) and (012) reflections of hexagonal CoO.

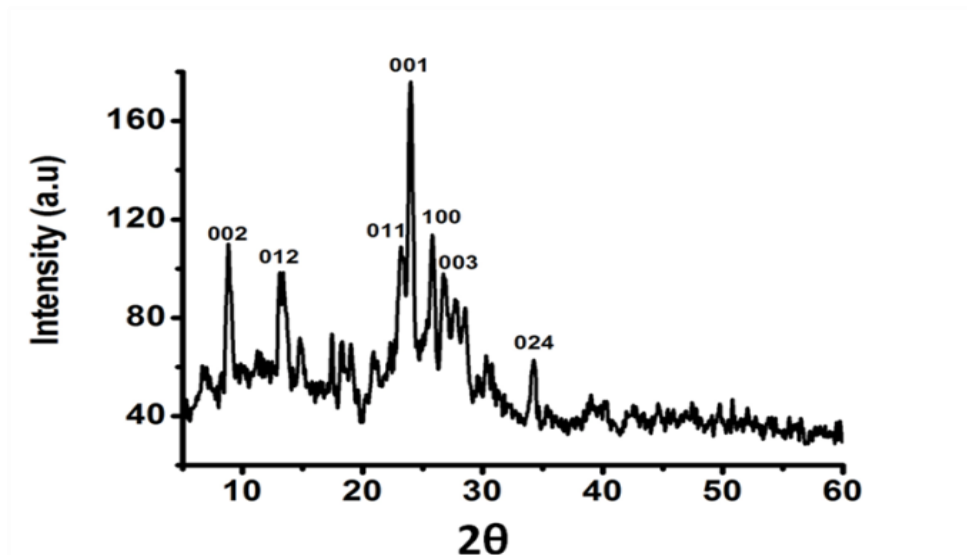


Figure 22: XRD patterns of HDA capped CoS nanoparticles synthesized from Co-thiourea complexes, at 180 °C

SECTION B

Synthesis of core-shell nanoparticles and use of single-precursors on urea and thiourea, cobalt and cadmium complexes

4.4 Introduction

Core-shell semiconducting nanocrystals (CSSNCs) are a class of materials which have properties intermediate between those of small, individual molecules and those of bulk, crystalline semiconductors. They are unique because of their easily modular properties, which are a result of their size. These nanocrystals are composed of a quantum dots semiconducting core material and a shell of a distinct semiconducting material. The core and the shell are typically composed of type II–VI, IV–VI, and III–V semiconductors, with configurations such as CdS/ZnS, CdSe/ZnS, CdSe/CdS, and InAs/CdSe (typical notation is: core/shell) [267]. Organically passivated quantum dots have low fluorescence quantum yield due to surface related trap states[268]. CSSNCs address this problem because the shell increases quantum yield by passivating the surface trap states[268]. In addition, the shell provides protection against environmental changes, photo-oxidative degradation, and provides another route for modularity[268, 269]. Precise control of the size, shape, and composition of the core and shell enable the emission wavelength to be tuned over a wider range of wavelengths than with either individual semiconductor. These materials have found applications in biological systems and optics[270, 271].

Recently, there has been work reported on the core-shell nanomaterials, unfortunately only few work has been done on the core-shells. Steckel and core-workers [272], reported CdS (core) QDs overgrown with a ZnS shell using the classical organometallic approach with hazardous reagents diethylzinc and hexamethyldisilthiane as precursors, yielding a blue

emission in the range of 460–480 nm with the full width at half maximum of 24–28 nm and quantum yields (QYs) of 20–30% [272]. Protiere and Reiss [91] used the air-stable monomolecular precursor zinc ethylxanthate in combination with zinc stearate to synthesize the monodispersed CdS/ZnS core/shell QDs exhibiting efficient blue emission in the range of 440–480 nm with QYs of 35–45%. Very recently, another monomolecular precursor zinc diethyldithiocarbamate was applied for the synthesis of stable purple/blue emitting CdS/ZnS core/shell QDs with their emission peak tunable between 375 and 475 nm and the maximum QY of 50% [273].

Tsuji *et al* [274] reported the preparation of Au–Ag core–shell nanostructures with different sizes and morphologies by growing silver layers onto Au seeds using a microwave mediated polyol reduction. Ma *et al* [275] prepared cubic Au–Ag core–shell nanoparticles in aqueous medium by depositing silver with ascorbic acid on gold seeds prepared in the presence of different capping agents. The latter have been widely used in the preparation of Au–Ag core–shell nanostructures either to tailor the particle size/morphology or to improve dispersion stability. However, Ma *et al* [275] concluded that capping agents tend to interfere with the epitaxial deposition of silver atoms and the formation of continuous shells. Murugadoss *et al* [276] synthesized high quality and water-soluble ZnS/CdS/ZnO and ZnO/ZnS/CdS core/shell nanoparticle through a simple chemical method, it was mentioned that nanoparticles exhibit strong blue emission at 470 nm and 490 nm for ZnS/CdS/ZnO and ZnO/ZnS/CdS, respectively.

In this work, the synthesis of the core-shells nanoparticles was achieved by employing the single source precursor method. The single-source molecular precursor method [94, 95, 277] (an individual molecule acting as the source of both metal and chalcogen in nanoparticle

synthesis) route offers the distinct advantages of mildness, safety, and simplified fabrication procedure and equipment, when compared with the most popularly employed successive-ion-layer adsorption and reaction method for shell growth [273, 278] in which the use of multiple sources requires exact control over stoichiometry. The properties of these semiconductor nanoparticles were thoroughly studied and reported. Since semiconductor nanoparticles or quantum dots core-shells have become an interesting subject all over the world because of their unique enhanced properties. In this work we report attempts to synthesize coreshell nanomaterials using single-source precursor route by combining two complexes, Cd and Co bonded to urea and thiourea ligands separately in order to establish the formation of the coreshell combinations, CdS/CdO, CdS/CoS, CoS/CoO. The ratio of one complex is varied while all other conditions are kept constant to establish if the nanomaterials formed are of coreshells nature, individual sulfide or oxide nanoparticles.

4.5 Experimental section

4.5.1 Reagents

Cobalt (II) chloride hexahydrate, cadmium (II) chloride, urea, thiourea obtained from Sigma Aldrich, were used as purchased. Acetone, methanol and n-butyl alcohol (analytical grade) were used without further purification and distilled water was also used as solvents.

4.5.2 Instrumentation

(a) Optical characterization

Absorption spectra of the particles were measure using a Perkin Elmer Lambda 20 UV-VIS Spectrophotometer. The samples were place in quartz cuvettes (1-cm path length) with toluene as the solvent. Emission spectra of the particles were recorded on a Perkin Elmer LS 45

photoluminescence (PL) spectrometer with a xenon lamp at room temperature. The samples were placed in glass cuvettes (1 cm) with toluene as solvent.

(b) X-ray diffraction analysis

X-ray diffraction (XRD) patterns on powdered samples were carried out in the 2θ on a D8 diffractometer. Samples were placed in silicon zero background sample holder. Measurements were taken using a glancing angle of incidence detector at an angle of 2° , for 2θ values over $20^\circ - 60^\circ$ in steps of 0.05° with a scan speed of $0.01^\circ 2\theta.s^{-1}$.

(c) Electron microscopy

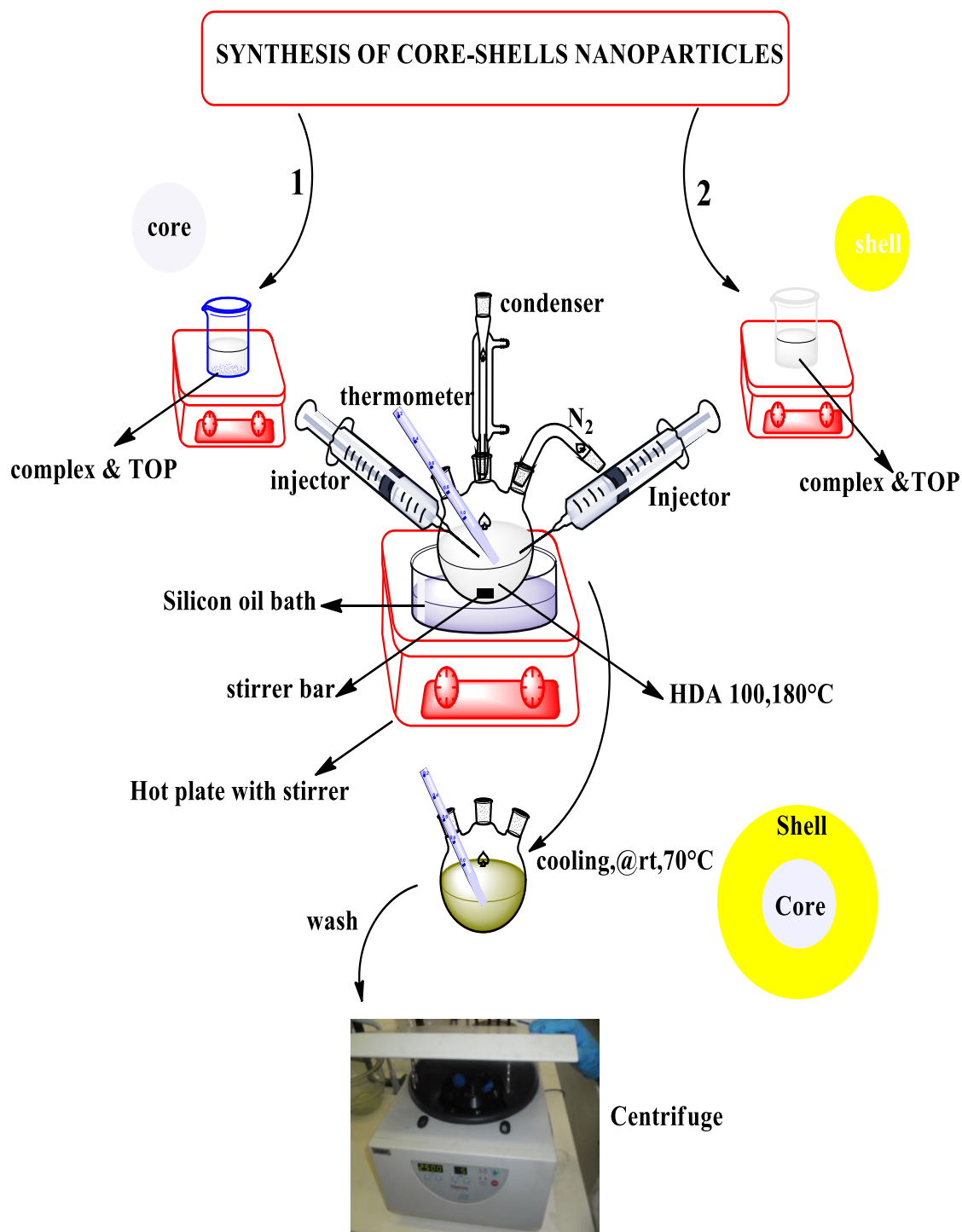
The images were obtained using high resolution transmission electron microscope (HRTEM Joel JEM-2100 microscope) operating at 200 kV. The samples were prepared by placing a drop of dilute solution of sample in toluene on to a copper grid. The sample was allowed to dry completely at room temperature.

4.5.3 Methodology

4.5.3.1 Preparation of core-shells nanoparticles from a mixture of two precursors.

In a typical experiment, 6.0 g hexadecylamine (HDA) was degassed and heated to 180°C under nitrogen. The precursors (0.5 g Co-thiourea and 0.5 g Co-urea) was separately dispersed in 5 ml trioctylphosphine (TOP) and injected into the hot solution starting with a precursor to serve as the core and followed by the shell. The reaction was maintained at optimal temperature of 180°C for 1 hour. The solution was cooled to approximately 70°C . After cooling the reaction

mixture, an excess of acetone was added the solid was isolated by centrifugation. The solid was further washed several times with acetone and dry at room temperature.



Scheme 9: Schematic representation for the synthesis of core-shell nanomaterials.

Table 4: General variation of concentration and temperature in the preparation of core-shells nanoparticles from complex I, II, III & IV

HDA (g)	Precusors	Temperature(°C)	Time(minutes)
6	1:1	180	60
6	1:2	180	60
6	1:3	180 & 100	60

Complex (I) – cobalts thiourea, (II) cobalts urea, (III) cadmium urea and (IV) cadmium thiourea.

4.6. Results and Discussions

Physical and chemical properties of semiconducting materials can be control and manipulated by tuning of their size and shapes. Controlling the concentration of the precursor is a major factor on both size and shape of nanoparticles with high concentration profoundly favouring larger size [279]. The effect of concentration on shape is quite complex, however suggested that chemical potential of nanoparticles are related to the formation of nanoparticles with different size and morphology [86]. The chemical potential of the reaction environment is mainly determined by the monomer concentration at a fixed temperature. Therefore, when the concentration of precursor increases, the reaction system deviates towards kinetic control, resulting in multiple shapes of nanoparticles being formed. Core shell semiconductor nanocrystal properties are based on the relative conduction and valence band edge alignment of the core and the shell. Core-shells nanocrystals are classified in three type:

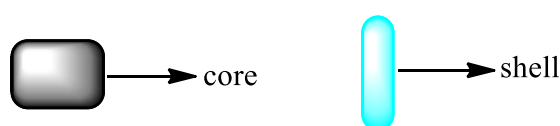
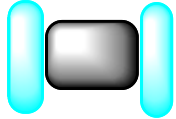
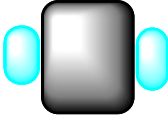



Table 5: Types of core-shells nanoparticles

Type I	Reverse type I	Type II
		
electron and holes tend to localize within the core	electron and holes tend to localize within the core	one carrier is localized in the shell while the other is localized in the core
bandgap of core is smaller than that of the shell	the core has a wider bandgap than the shell	bandgap of the core can be high or low than the shell
conduction and valence band edges of the core lie within the bandgap of the shell	conduction and valence band edges of the shell lie within those of the core	valence and conduction band edge are both lower or higher than the band edges of the shell

Core-shell semiconductor nanocrystals (CSSNCs) can be grown by using single source precursor methods with an appropriate control of the reaction kinetics [280]. Using this method which results in a relatively high control of size and shape, semiconductor nanostructures could be synthesized in the form of dots, spheres, rods and other forms which show interesting optic and electronic size-dependent properties [280]. Since the synergistic properties resulting from the intimate contact and interaction between the core and shell, CSSNCs can provide novel functions and enhanced properties which are not observed in single nanoparticles [281].

4.6 (a) Synthesis of coreshell nanomaterials based on urea and thiourea cadmium complexes

The cadmium complexes of urea and thiourea were synthesized and characterized as described in chapter 1 were subsequently used to prepare nanoparticles in which a mixture of the two complexes are added into HDA to generate either a mixture CdS & CdO, exclusively CdS or CdO or coreshell nanomaterials with CdS as the core and the CdO as the shell or vice versa. The hexadecylamine was heated to about 180 °C and the precursors heated for about an hour. CdS nanoparticles has dominant characteristic optical features and hence the study involves the variation of the two complexes of urea and thiourea from 1:1, 1:2 and 1:3 mole ratio to understand the changes from the dominant features of CdS. Table 6 shows reaction conditions for the preparations of CdO:CdS core-shells nanoparticles by using various concentrations of complex III & IV, while keeping all the other parameters the same.

Table 6: Variation of concentration in the preparation of CdO:CdS core-shells nanoparticles from complex III & IV

HDA (g)	CdO:CdS	Temperature(°C)	Time(minutes)
6	1:1	180	60
6	1:2	180	60
6	1:3	180	60

UV- visible absorption spectra of CdO-CdS core-shells showed absorption band at 431 nm with band edges at about 450, 460, 470 nm respectively for 1:1, 1:2 and 1:3 ratios. **Figure 23(a)**. Observation of absorption band due electronic transition indicates that particles have narrow size distribution as results of early stage formation of nanoparticles and indication of irregular shapes from a lower concentration and more uniform shapes at a higher concentration.

The phenomena can also be explained by means of absorption band in which at a low concentration is less visible and as the concentration is increased becomes more profound. The band edges are red-shifted from a low (mono-dispersed) to high (poly-dispersed) concentration due to increase in particle size. The absorption bands have features similar to CdS prepared using cadmium thiourea complex as seen in **Figure 11**.

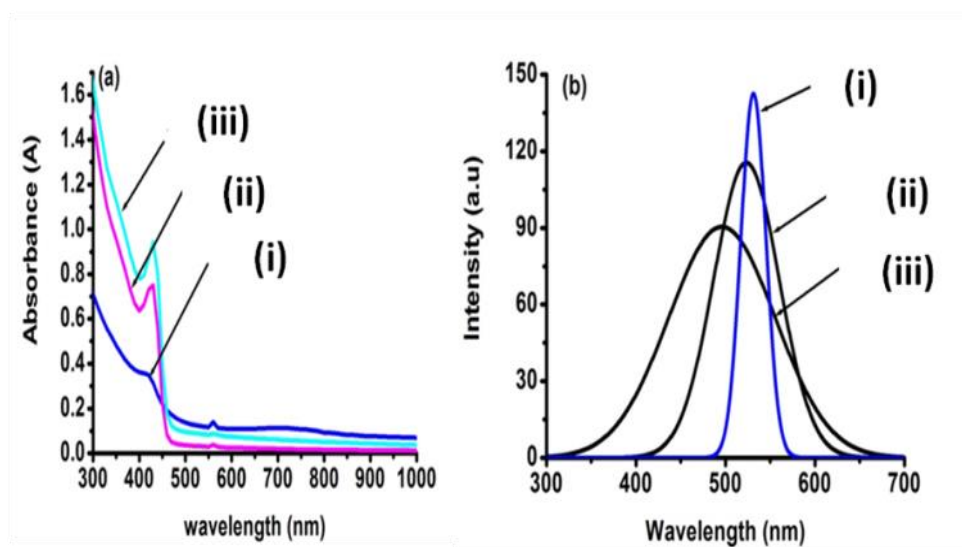


Figure 23: (a) Absorption spectra (i(1:1), ii(1:2) and iii(1:3)) and (b) emission spectra(i(1:1), ii(1:2) and iii(1:3)) of CdO-CdS nanoparticles synthesized from Cd-Urea and Cd-thiourea complexes.

Table 7: Band edges and emission maxima

Ratio (m/m)	Material	Band edge (nm)	Emission maxima (nm)
1:1	CdO-CdS	450	482
1:2	CdO-CdS	460	520
1:3	CdO-CdS	470	630

There are two types of emissions known for semiconductor nanoparticles namely excitonic and trapped emission. The excitonic emission usually gives sharp peaks near their band edges whereas trapped emission is always characterized by broad peaks with large Stokes shift. The narrowing of the peaks is observed as the monomer concentration is increased due to excitonic type of emission **Figure 23(b)**. These were caused by a faster growth as a result of increased concentration. The emission peaks for the sample prepared at low concentration have a broad shape which indicates the monodispersity and good passivation of the particles. However, for the nanoparticles prepared at high concentration, the emission is very narrow which indicate that the particles are polydispersed. Photoluminescence emission maxima of the samples were observed (**table 7**) and are red shifted from their respective band edges of the absorption spectra.

The red shift can be explained by spreading the electrons over the entire QDs while the hole remains confined in the core [282]. This red-shifting could have the origin in the deficiency of electrons in the core, directly leading to a decreased electron density, as a result of transferring the electrons from core to the shell, in addition to the change in the dielectric properties due to the nanoshell (medium effect), the interfacial proximity effects and quantum constraints [283, 284]. It is understood that the reduced electron density certainly lowers the frequency of the surface plasmon and therefore, the red-shifting of the resonance [284]. The same factor of the electron deficiency of the core due to the shell of oxide coating could result in the drop in absorption intensity. Other contributions include the shadowing effect of the shell and the background of non-characteristic absorption. The emphasize is that an accurate treatment of the optical properties of core-shell nanoparticles may need to meticulously tackle the interfacial proximity effects ensuing in such nanosystems, in addition to the popular calculation strategy based on the dimension and shape of the nanostructure and the properties of the

medium, the shell material and the core composition[283-286]. **Figure 24(a-c)** shows TEM images for the CdO-CdS coreshell nanoparticles by varying concentration of precursors. From the images we observe a mixture of rods and spherical shapes from nanoparticles prepared at 1:1 and 1:2 with the rods width ranging from 3 to 8 nm and length ranging from 15 to 28 nm. The diameters and width for 1:1 being smaller and elongating when the concentration is increased to 1:2. However we observed interesting phenomenon on nanoparticles prepared at 1:3. The particles are also in spherical morphology

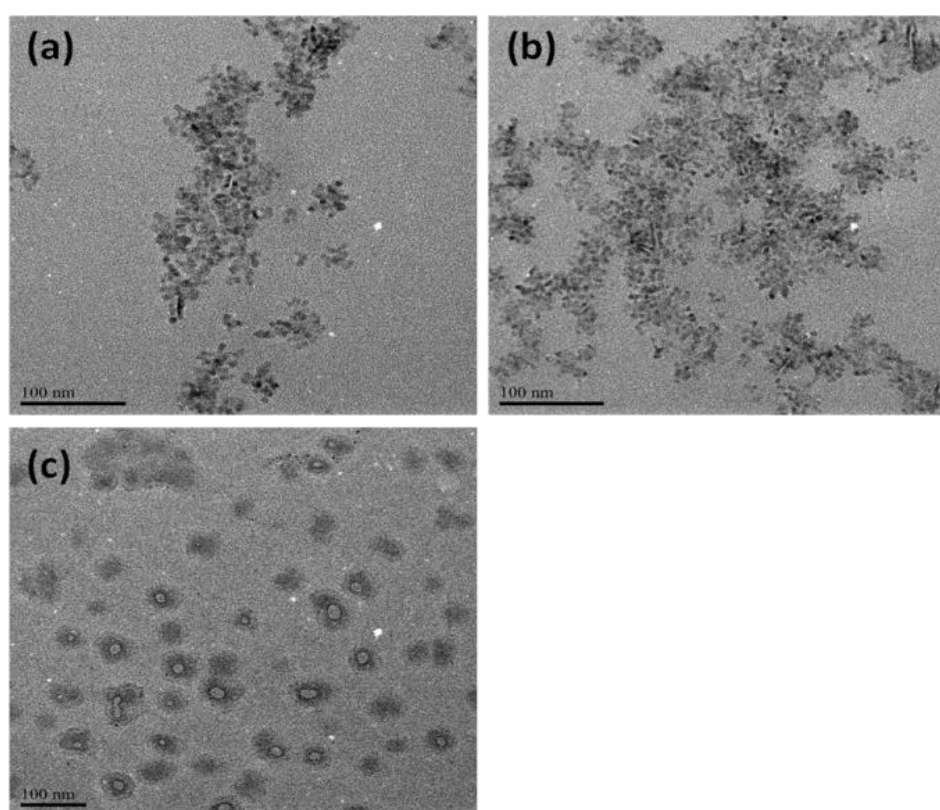


Figure 24: TEM images of CdO-CdS nanoparticles prepared at 180°C (a) 1:1, (b) 1:2, (c) 1:3 precursors: 6g HDA from the Co-urea and Cd-thiourea complexes

with the ring/hollow cavities and the shell covering the cavity. These are not perfect spheres as they possess rough edges making diameters large to about 50 nm. The coreshells formed in the study is assumed to be a reverse type I coreshell nanoparticles. Comparing the bulk band edges of CdO and CdS are 539 and 515 nm respectively. In the study CdO precursor was

injected first to serve as a core and followed by CdS precursor after 60s to serve as a shell hence we assume the coreshell nanoparticles will follow the same trend during thermolysis, the hollow cavity being that of CdO and the shell of CdS. The behavioral condition of TEM was confirmed by the absorption spectra **Figure 23(a)** because when the concentration of precursors was increased the particles increases as well.

The PL spectra **Figure 23(b)** also support this evidence with the broader peaks favouring the larger particles. The XRD patterns of the CdO-CdS coreshell nanoparticles in **Figure 25** range from cubic to hexagonal phase, however with the predominance of hexagonal phase. Patterns can be indexed to the hexagonal phase. The peaks at $2\theta = 25^\circ$ to 35° can be indexed to 100, 002 and 101 planes and other peaks confirm the structure to be hexagonal in nature. The UV Vis absorption features are dominated by the presence of CdS nanoparticles as shown in Figure 11 and 21. The emission spectra of 1:1 ratio of urea and thiourea complexes show very narrow emission compared to the other ratios. This is indicative of narrowing of the maximum due to the coreshell formation of materials. The absorption features are also supported by the XRD patterns which are significant peaks due to CdS nanoparticles.

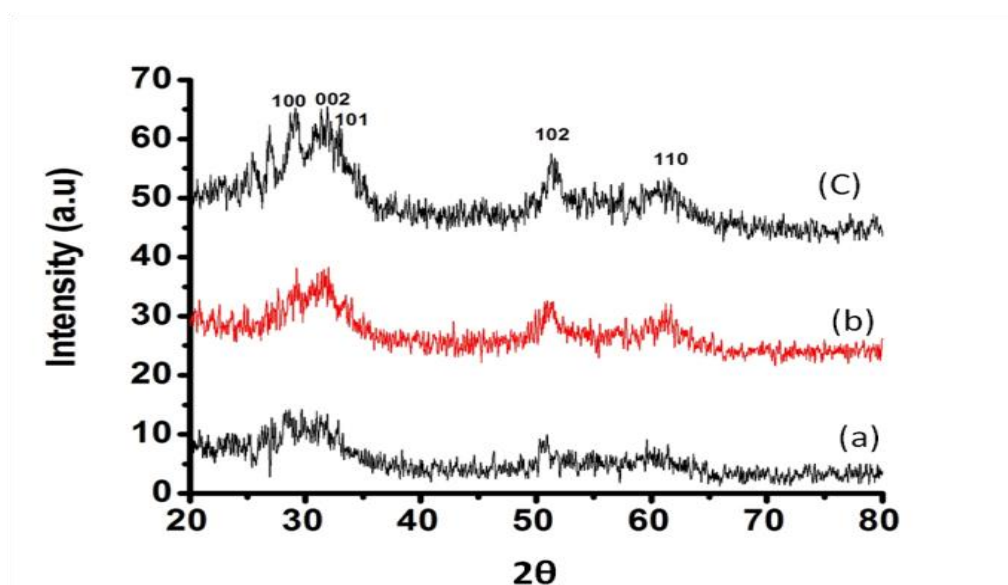


Figure 25: XRD patterns of HDA capped CdO-CdS coreshell nanoparticles synthesized from Cd-urea and Cd-thiourea complexes in the ratio (a) 1:1, (b) 1:2 and (c) 1:3

The hexagonal phase can be attributed to CdS nanoparticles which exists either as the cubic, orthorhombic or hexagonal phases. The existence of mixture of cubic and hexagonal phase with predominance of one over the other was reported by Bawendi *et al* [263]. Both spectra show reasonable broadened peaks, with the higher concentration samples having slightly sharper peaks than the lower concentration samples. This also in consistent with UV-visible spectra with the predominance of CdS nanoparticles features and the increase in particle size with increase in concentration.

4.6 (b) Synthesis of core-shells nanomaterials based on urea and thiourea cobalt and cadmium complexes.

Table 8: Variation of concentration in the preparation of CoO:CdS core-shells nanoparticles from complex I & III

HDA (g)	CoO:CdS	Temperature(°C)	Time(minutes)
6	1:1	180	60
6	1:2	180	60
6	1:3	180	60

Figure 26(a) shows the UV-visible of CoO-CdS nanoparticles prepared by varying concentrations of complex I & III capped with HDA. We observe a blue shift in the optical spectra from a high to low concentration of precursors as a result of nanosize regime exhibiting quantum confinement effect. Their band edges are reported in **table 9**. Optical properties of CoO-CdS nanoparticles are reported in **Figure 26(a)** which is similar to those in **Section A**,

Figure 11(a) preparation of CdS nanoparticles. The similarity can be concluded that the characteristic optical properties favour those of CdS due to the following: (i) Firstly, due to the amount of precursors used, in this study CdS is more than CoO source which might be the reason optical spectrum favour the characteristics of CdS nanoparticles. (ii) Secondly, electron affinity between sulphur and oxygen. Electron affinity increases upward for the group and from left to right across periods of a periodic table because the electrons added to energy levels becomes closer to the nucleus, thus a stronger attraction between the nucleus and its electrons. Atomic radius for oxygen is 0.073 and 0.102 nm for sulphur.

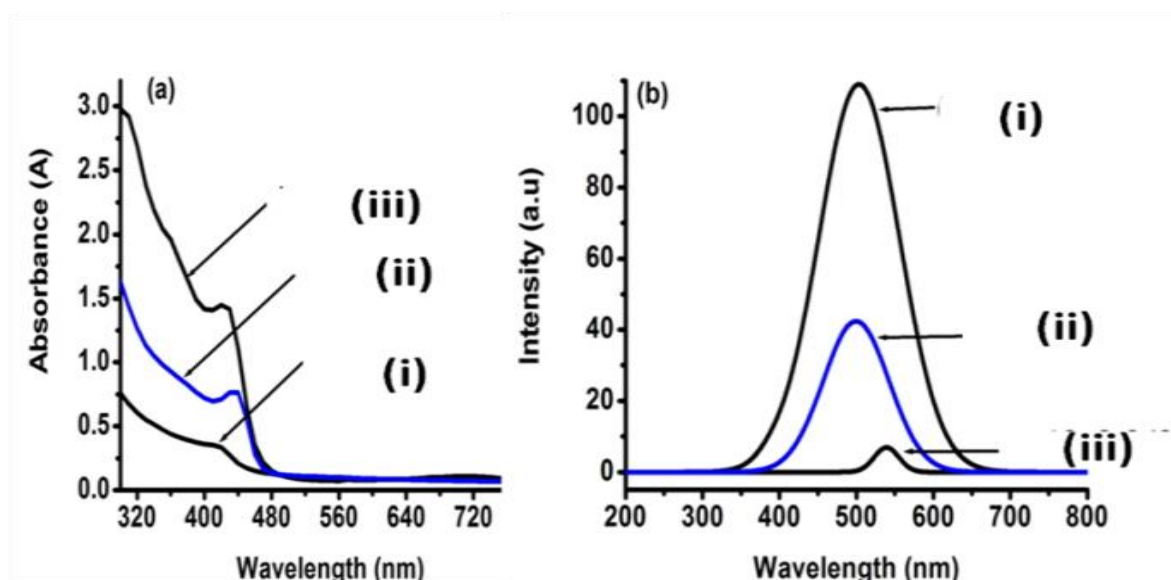


Figure 26: (a) Absorption spectra (i(1:1), ii(1:2) and iii(1:3)) and (b) emission spectra(i(1:1), ii(1:2) and iii(1:3)) of CoO-CdS nanoparticles synthesized from Co-Urea and Cd-thiorea complexes

Table 9: Band edges and emission maxima

Ratio (m/m)	Material	Band edge (nm)	Emission maxima (nm)
1:1	CoO-CdS	448	506
1:2	CoO-CdS	481	501
1:3	CoO-CdS	481	541

Even though expectation is for oxygen to attract electrons more readily than sulphur because of its higher electronegativity, however it is the smaller size of the oxygen atom which explains it, the mutual repulsion of the electrons in a smaller space in oxygen is explained. (i) Due to small size and high electron density of oxygen compare to sulphur inter-electronic repulsion is higher in oxygen, resulting in less energy being released when an electron is added to oxygen. (ii) Due to lesser stability after electrons is added (ii) due to inter-electronic repulsion in the small oxygen atom. However in this study during injection of precursors electron affinity of atoms were not considered because injection was done randomly. Photoluminescence spectra are red-shifted from the respective absorption band-edges. The emission maxima for the various samples were reported in **Table 9**. The peaks are single and smooth, an indication of efficient surface passivation and single morphology.

TEM is a very useful technique in characterizing the size and shape of the nanoparticles. CoO-CdS nanoparticles using Co-urea and Cd-thiourea complexes as precursors have been prepared in HDA at a varied concentration. The arrangement of nanoparticles in 1:2 and 1:3 is not clearly understood, but could be as result of the amount and choice of the capping agent used. The manner in which the capping group attaches itself to the particle could have influence on the other surrounding particles, thus affecting the mode of arrangement of the particles. The particles are in a mixture of rod and spherical and some percentages of bipodal, tripodal and tetrapodal morphologies in each sample for 1:1 and 1:3, with dimensions about 2 to 3 nm in width, 18 to 30 nm in length and 3 to 5 nm in diameter and are monodispersed, however spherical for 1:1 with a diameter ranging from 3 to 6 nm and are polydispersed (**Figure 27(a-c)**). Adam and Peng [287, 288] recently elucidated profoundly the mechanism for the shape evolution of nanocrystals in solution. They mentioned that the formation of elongated nanocrystal was a high kinetics driven reaction, and a shape evolution from long rods to short

rods and even spherical particles was a results of the reaction system shifting from kinetic driven control to thermodynamic driven control due to the situation change of nanacrystals and their reaction environments (high precursor concentration supplies the reaction system with high kinetic drive, while high reaction temperature provides it with high thermal energy (KT) and accelerates reaction rate).

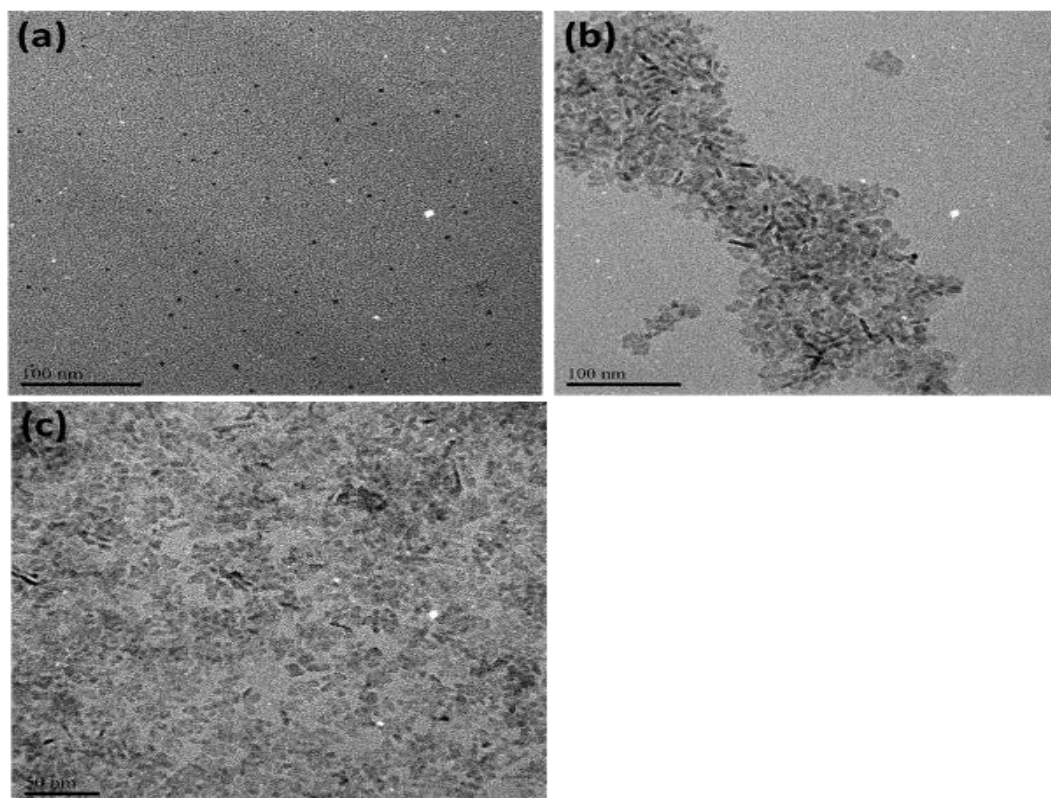


Figure 27: TEM images of CoO-CdS nanoparticles prepared at 180°C (a) 1:1, (b) 1:2, (c) 1:3 precursors: 6g HDA from the Co-urea and Cd-thiourea complexes

The particles in 1:2 and 1:3 showed similar morphology except the 1:1 and are consistent with the absorption spectra results as shown in **Figure 26(a)**. The XRD patterns CoO-CdS coreshell nanoparticles **Figure 28** were consistent with those of hexagonal CdS prepared from Co-urea and Cd-thiourea complexes. However there are some cubic phase which can be attributed to CoO nanoparticles. The predominance of the hexagonal phase is indicated by the planes indexed as 100, 002 and 101 and the other peaks confirming the structure to be hexagonal in

nature. This is caused by the amount of CdS source used during synthesis which is higher than CoO source. This is also inconsistent with the UV-visible spectra predominantly showing CdS features.

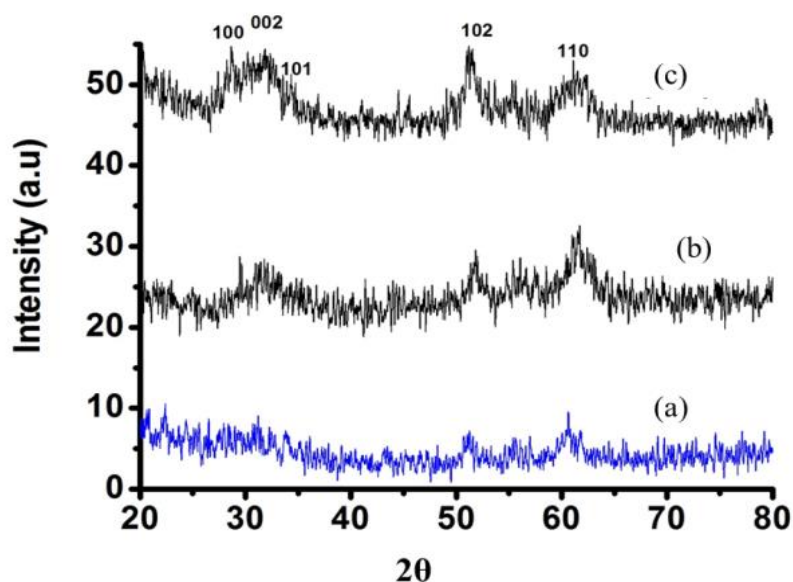


Figure 28: XRD patterns of HDA capped CoO-CdS core-shell nanoparticles synthesized from Co-urea and Cd-thiourea complexes in the ratio (a) 1:1, (b) 1:2 and (c) 1:3

4.6 (c) Synthesis of core-shells nanomaterials based on thiourea and urea cobalt and cadmium complexes

Table 10: Variation of concentration in the preparation of CoS:CdO core-shells nanoparticles from complex I & IV

HDA (g)	CoS:CdO	Temperature(°C)	Time(minutes)
6	1:1	180	60
6	1:2	180	60
6	1:3	180	60

The absorption and emission spectra of cobalt sulfide nanoparticles prepared at different concentrations of complex I & IV (**Table 10**) are shown in **Figure 29(a & b)**. The spectra shows an absorption peak at 758, 730, 706 nm from a low to high concentration respectively. The band edges are reported in **table 11** which are red-shifted as a result of increase in concentration and particles growth.

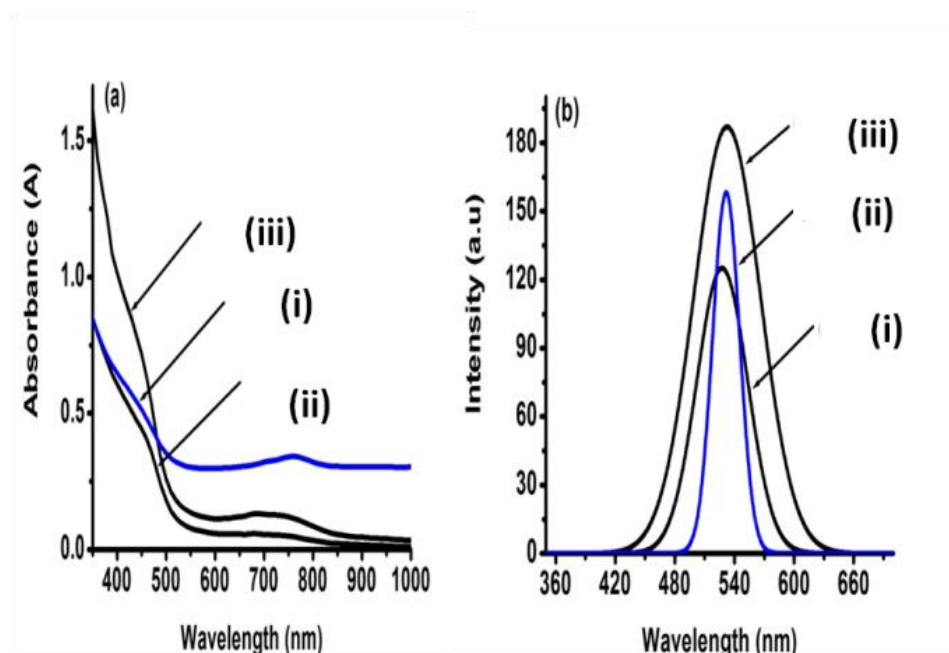


Figure 29: (a) Absorption spectra (i(1:1), ii(1:2) and iii(1:3)) and (b) emission spectra(i(1:1), ii(1:2) and iii(1:3)) of CoS-CdO nanoparticles synthesized from Co-thioreia and Cd-Urea complexes

Table 11: Band edges and emission maxima

Ratio (m/m)	Material	Band edge (nm)	Emission maxima (nm)
1:1	CoS-CdO	504	528
1:2	CoS-CdO	526	532
1:3	CoS-CdO	530	534

The absorption maxima in absorbance can also be as a results of bulk (extended state to extended state) state transition and surface (localized state to extended state) transitions of the interaction of two precursors (complex I & IV). The surface states include the localized states because of defect in bulk in addition to the surface states. The optical transition to and from the surface states will produce maxima at higher wavelengths. The photoluminescence spectra exhibit close to band edges emissions. The peaks are smooth however narrow for nanoparticles prepared at 1:1 and 1:3 ratios which indicates monodispersity of the well passivated particles. Nanoparticles prepared at 1:2 ratios show broad emission maxima indicating polydispersity. The photoluminescence maxima are red-shifted from their respective band edges (**table 11**). TEM images of the CoS-CdO coreshells nanoparticles prepared by varying concentration are showed in **Figure 30(a-c)**. The particles are in rods for nanoparticles prepared at 1:1 with the width ranging from 2 to 3 nm and length from 10 to 18 nm, bipodal, tripodal and tetrapodal for 1:2 with length ranging from 7 to 15 nm and a width from 1 to 2 nm and a mixture of rods and spheres for the nanoparticles prepared at 1:3 with length ranging from 15 to 20 nm, width ranging from 3 to 5 nm and diameter 3 to 6 nm. The trend is inconsistence with the respective absorption band edges absorption witnessing the increase in particles size with the increase in concentration of the precursors. The 1:2 ratio gave a narrowed PL peak indicative of the formation of coreshell nanomaterials, which in the TEM images also show intense darker core with lighter shell structure on the outer phere of the nanomaterials in rod, bipod shaped structures. **Figure 31** show the diffraction peaks for both samples synthesized from different concentration can be indexed to a hexagonal phase.

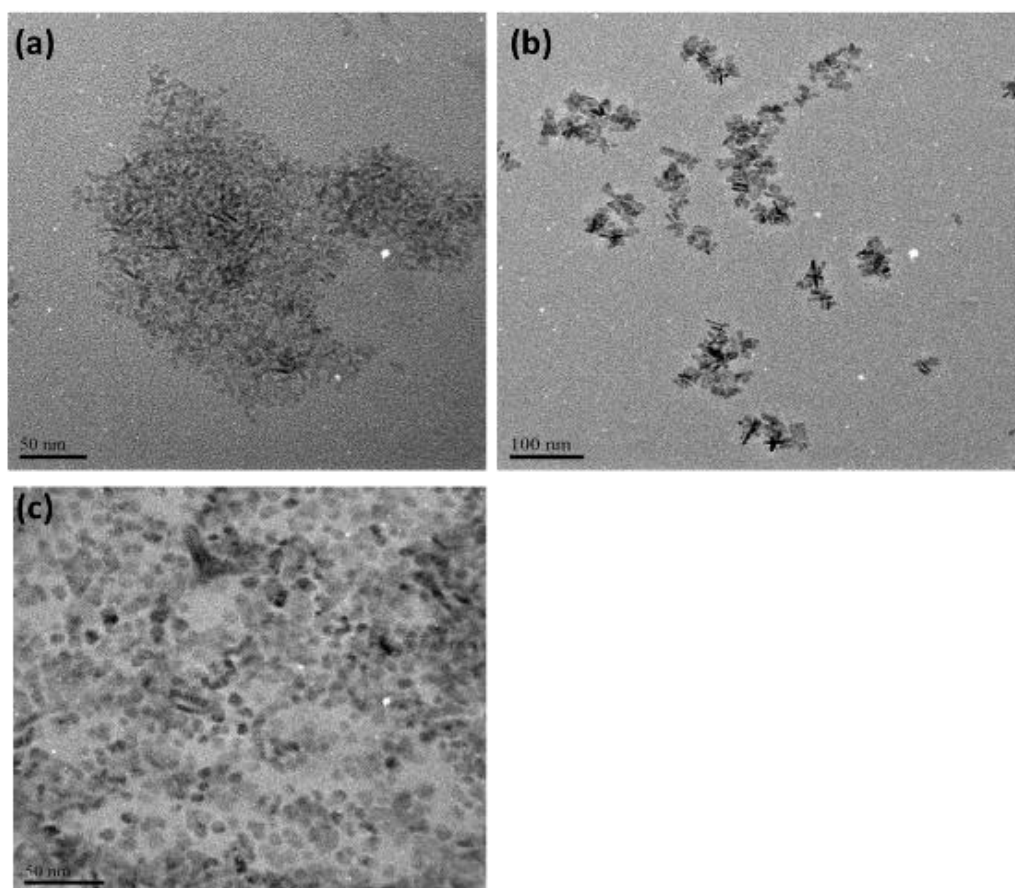


Figure 30: TEM images of CoS-CdO nanoparticles prepared at 180°C (a) 1:1, (b) 1:2, (c) 1:3 precursors: 6g HDA from the Co-thiourea and Cd-urea complexes

The patterns are well defined, characterized by the 100, 101, 110 and 102 plane at $2\theta = 20^\circ$ to 35° reflection of Co_{1-x}S . The broadening of the peaks at low concentration indicates small particles and as the concentration increased slightly sharper peaks indicating the growth in particle size as seen on the TEM images (**Figure 30**). No impurity peaks are observed, which indicates that pure CoS-CdO coreshell nanomaterials are produced by the single source precursor method.

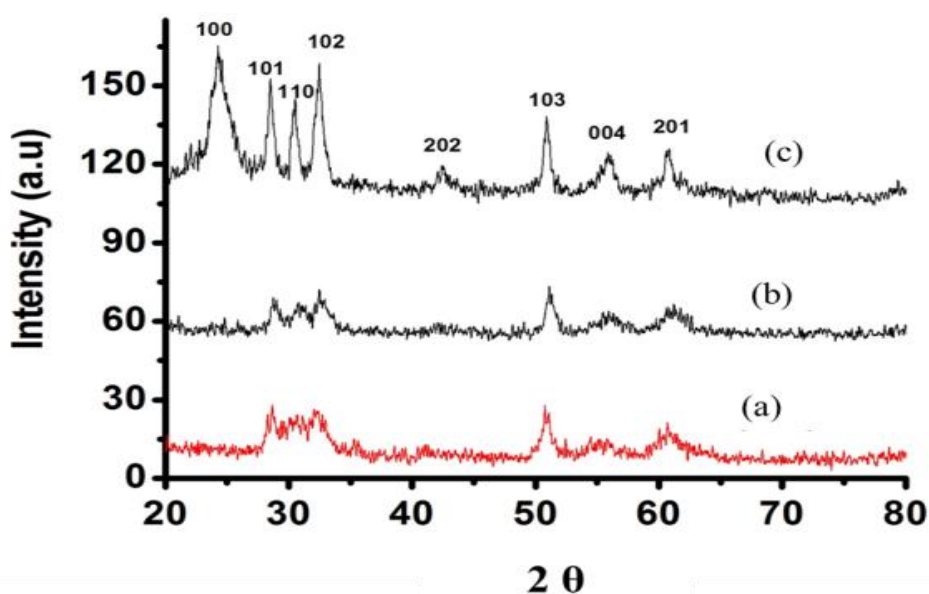


Figure 31: XRD patterns of HDA capped CoS-CdO core-shell nanoparticles synthesized from Co-thiourea and Cd-urea complexes in ratios of 1:1(a), 1:2(b) and 1:3(c)

4.6 (d) Synthesis of core-shells nanomaterials based on urea and thiorea cobalt complexes

Table 12: Variation of concentration in the preparation of CoO:CoS core-shells nanoparticles from complex II & I

HDA (g)	CoO:CoS	Temperature(°C)	Time(minutes)
6	1:1	180	60
6	1:2	180	60
6	1:3	180	60

The absorption spectra of CoO-CoS nanoparticles prepared by varying concentration of the reaction (**Table 12**) are reported in **Figure 32(a)**. The spectra show an absorption peak at 655, 765 and 671 nm for 1:1, 1:2 and 1:3 respectively. However for the nanoparticles prepared at 1:1 the absorption peak is not well define because of the early formation of nanoparticles and

as the concentration of the precursors was increased the peak was more visible. The spectra for 1:2 and 1: show exclusively CoS features as results of large contents used in the experiment. The band edges are reported in **Table 13** which are red-shifted from low to high concentration as a result of particles size growth as the concentration increases. Photoluminescence spectra for nanoparticles prepared at 1:1 are red-shifted from the respective band edges (**Table 13**). However the emission spectrum for the particles prepared at 1:2 and 1:3 are blue shifted from the respective band edges. The blue shift in emission spectra is not a characteristic of nanoparticles but could be explained using the reasoning of

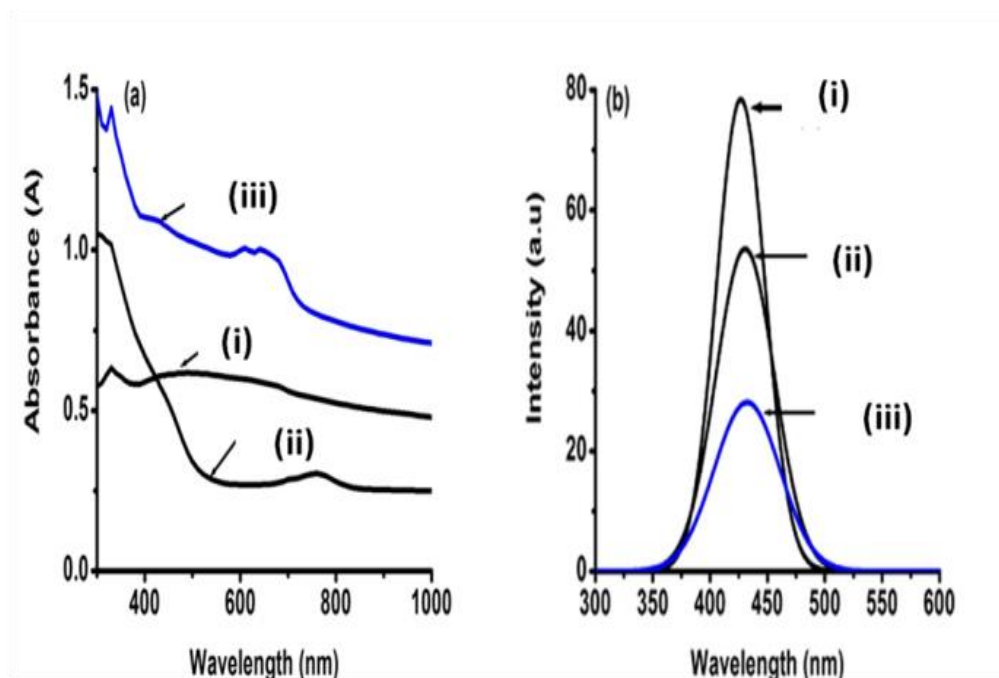


Figure 32: (a) Absorption spectra(i(1:1), ii(1:2) and iii(1:3)) and (b) emission spectra(i(1:1), ii(1:2) and iii(1:3)) of CoO-CoS nanoparticles synthesized from Co-urea and Co-thiourea complexes.

Table 13: Band edges and emission maxima

Ratio (m/m)	Material	Band edge (nm)	Emission maxima (nm)
1:1	CoO-CoS	365	427
1:2	CoO-CoS	509	431
1:3	CoO-CoS	810	433

Cheon et al. [37, 73] reported that not only the size of the nanoparticles has an influence on the emission but shape also plays an important role [289]. In the case of rods, length and the width both have a contribution in the resultant band-edges. Taking into account the general definition of nanoparticles only accounts for diameter of the particles, therefore a rod with a diameter within 20 nm and length than that can still be considered a nanoparticles. Even though the diameter of a particle is small, the length of the particles results in increased or decreased emission energy. Therefore the blue shift can be explained by the notion that the morphology of the particle has a great influence on the photoluminescence properties of the nanoparticles. With spherical particles, the diameter of the particle can be related to the whole size of the particles, whereas with rod or wire like particles, the diameter does not account for the length of the particles. The TEM images (**Figure 33**) clearly witness this phenomenon as from a low concentration particles are irregular and agglomerated for 1:1 and 1:2 which makes it difficult to determine the particle size, due to the amount of the capping molecule used.

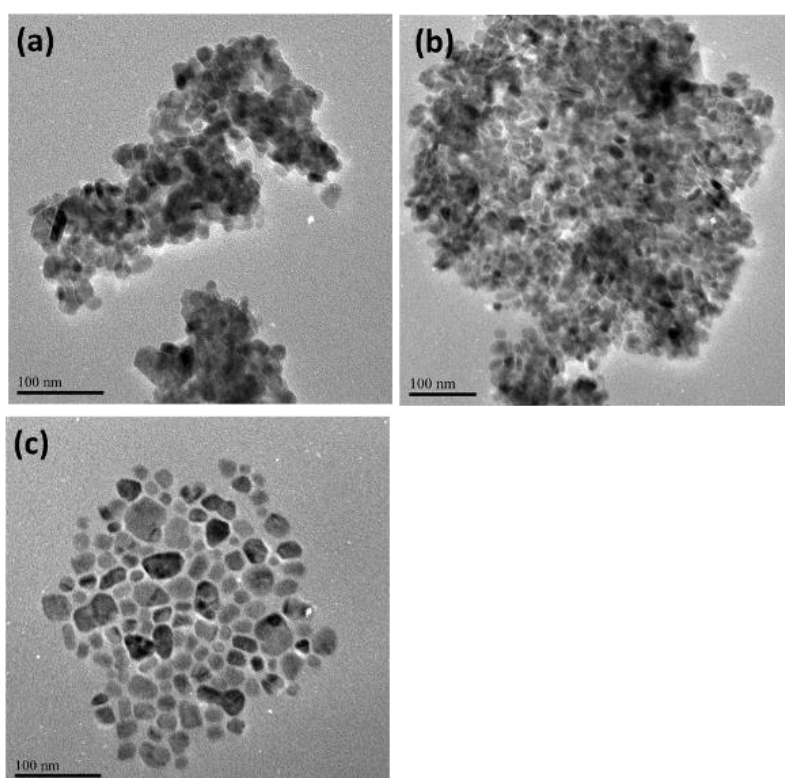


Figure 33: TEM images of CoO-CoS nanoparticles prepared at 180°C (a) 1:1, (b) 1:2, (c) 1:3 precursors: 6g HDA from the Co-urea and Co-thiourea complexes

As the concentration of precursors was increased to 1:3 particles are well dispersed and are irregular in shapes ranging from 15 to 50 nm. The TEM images are inconsistent with the absorption spectra in which particles increases when the concentration of the precursors was increased and the emission peaks further evidence this with broad peaks favouring large particles. The XRD patterns of CoO-CoS core-shell nanoparticles prepared at the lowest and highest precursor concentration are shown in **Figure 34**. The XRD patterns of the core-shell from low to high concentration exhibit the orthorhombic phase predominantly of Co_4S_3 high content used compare to CoO. The peaks are broadened at a low concentration indicating small particles, whereas peaks are slightly sharper at high concentration indicating the growth and crystallinity of particles and this phenomenon is in consistent with TEM images.

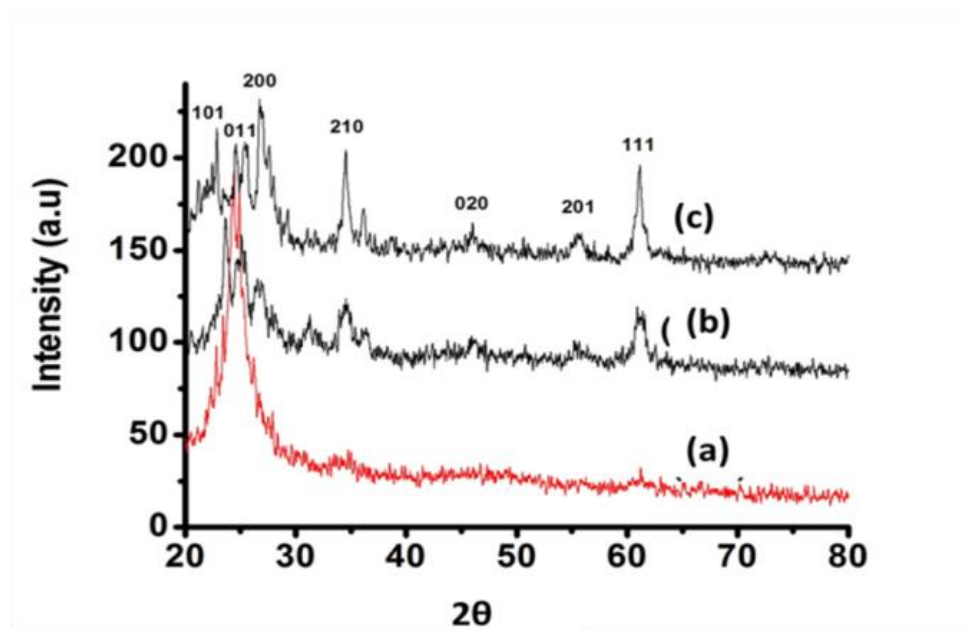


Figure 34: XRD patterns of HDA capped CoO-CoS core-shell nanoparticles synthesized from Co-urea and C-thiourea complexes in the ratio 1:1(a), 1:2(b) and 1:3(c)

4.6.1 Effect of temperature

There are several parameters that has effect on the shape, size and phase of nanoparticles during synthesis. Temperature is one of the major factors that influence particle growth, with an increase of temperature of the reaction more likely favouring larger particle size [290]. It has been reported by Moloto *et al* [259] that the growth process of nanoparticles involves a delicate balance between kinetic and thermodynamic control. The control of temperature during the nucleation process can result to a crystalline phase of one compound being more favourable over the others, however stable phase is highly dependent on its environment [291]. In this part of the study, the effect of temperature for (1:3) CdO-CdS core-shells nanoparticles was investigated, due to the formation of the hollow cavity core-shell nanomaterials at high temperature of 180°C.

4.6.1 (a) Synthesis of core-shells nanomaterials based on urea and thiourea cadmium complexes

Table 14: Effect of temperature in the preparation of CdO:CdS core-shells nanoparticles from complex III & IV

HDA (g)	CdO:CdS	Temperature(°C)	Time(minutes)
6	1:3	100	60

When urea and thiourea cadmium complexes was thermolysed at 100 °C, the band edge is higher compare to when was thermolysed at 180 °C with corresponding red-shift in the PL emmission maximum (**Figure 35**). The band edge was observed at 510 nm with the emmission maximum at 570 nm with the excitation at the band edge. The emission maximum is reasonable broad which is in consitent with larger particle size. This can be seen

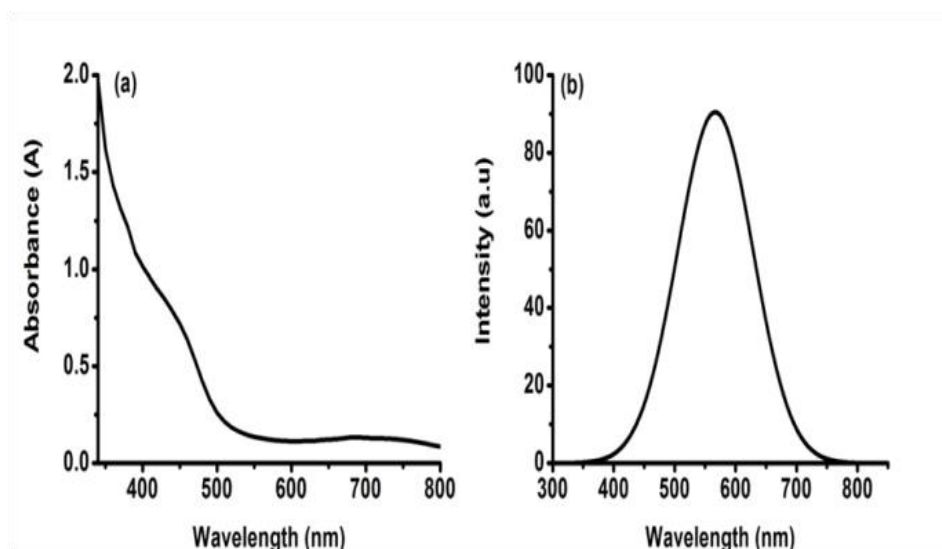


Figure 35: (a) Absorption spectrum and (b) emission spectrum of CdO-CdS nanoparticles synthesized from Cd-urea and Cd-thiourea complexes

Table 15: Band edge and emission maxima

Ratio (m/m)	Material	Band edge (nm)	Emission maxima (nm)
1:3	CdO-CdS	510	570

from TEM images with diameter of the particles ranging from 140 to 145 nm (**Figure 36**). The particles as shown in the Figure 33 tend to form multiple layers of onion ring shapes with a hollow cavity. This change at this lower temperature is unexpectedly giving higher band edge and emission maximum and the arrangement of onion rings bring the change as the multiple layers enlarges the particle diameters. This can be attributed to the unbalanced thermodynamic and kinetics as well as the relative stability of the complexes which are comparable in their thermolysis. The absorption band edge features are dominated by the presence of CdS, which is a lower band gap material. The urea complex thermally decompose faster and has two patterns of decomposition compared to thiourea complex as shown by their TGA curves in Figure 9. This could results in fast formation of CdO followed by gradual layers of CdS alternating with CdO.

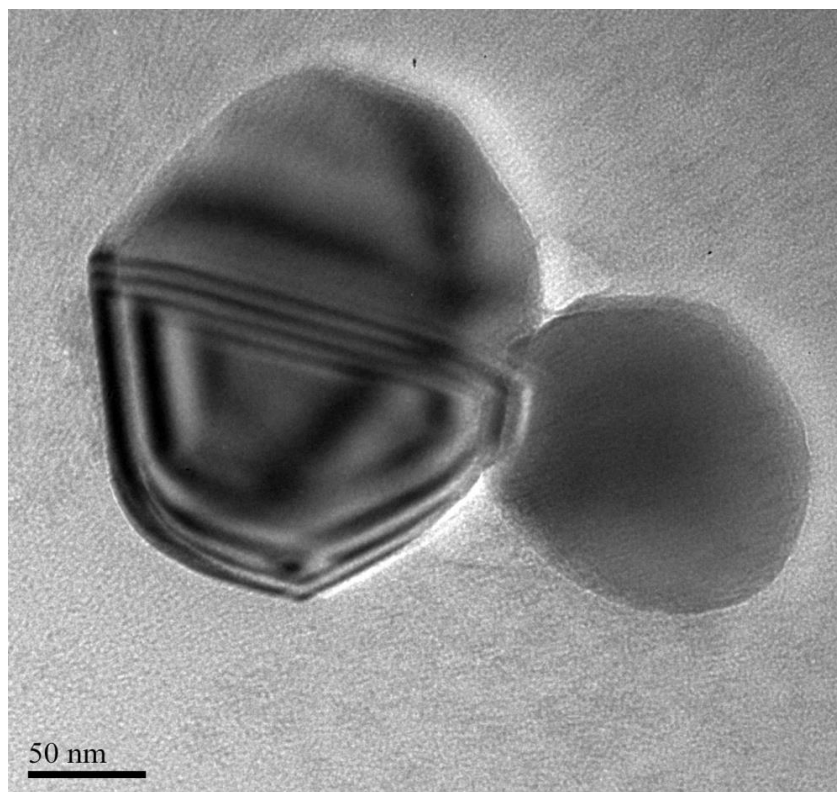


Figure 36: TEM images of CdO-CdS particles prepared at 100°C, 1:3 precursors: 6g HDA from the Cd-urea and Cd-thiourea complexes

The TEM images of the samples was in a mixture of hexagonal and spherical shapes with sheets like onion morphology, another type of core-shell nanoparticles. In the experiment CdO source/precursor was injected first to serve as the core followed by CdS precursor as a shell. The core-shells formed in this regard can be associated with the reverse type I, because the band edge of the core (CdO) is higher than that of shell (CdS). The XRD patterns of CdO-CdS core-shells particles are consistent with the one thermolysed at 180 °C with the predominance of hexagonal phase (**Figure 37**). The 100, 101, 002 planes are the most intense in all samples and are clearly distinguishable in the patterns as planes of hexagonal CdS phase due to high amount used in the experiment. The narrowing of the peaks on the diffractogram is consistent with the larger particles evidence from TEM.

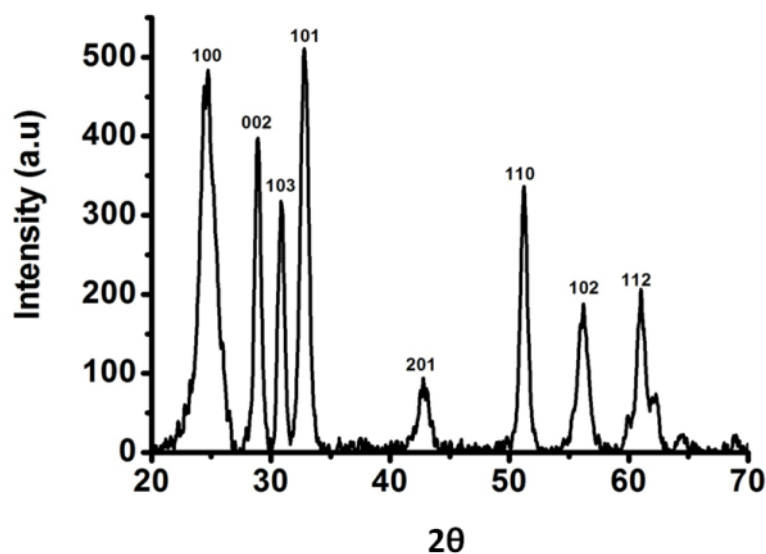


Figure 37: XRD patterns of HDA capped CdO-CdS core-shell nanoparticles synthesized from Cd-urea and Cd-thiourea complexes, at 100 °C

4.7 Conclusion

The high quality nanoparticles and core-shell (CdS-CdO, CoO-CoS, CoO-CdS and CoS-CdO) nanomaterials were successfully synthesized by the single-source precursor method exhibited strong absorptions and emissions. The absorption peaks of the normal nanoparticles (CoS, CoO, CdS and CdO) are highly blue shifted from the same bulk material. The PL maxima of the normal nanoparticles are blue shifted from their respective band edges whereas of the core-shells are red-shifted from low to high concentration as results of quantum confinement. The PL improvement indicated the complete elimination of surface defects and increasing of the crystalline nature of nanoparticles. The core-shells on one set of experimental condition, 1:3 CdO-CdS, with a ring/hollow cavity, spherical morphology and well dispersed nanoparticles with size about 50 nm was successfully synthesized. Low temperature (100°C) study was also conducted in which TEM images revealed a mixture of hexagonal and spherical shapes with onion-like sheets. The study provides a good indication of tuning the visible absorption and emission of the nanoparticles and the core shells.

4.9 Summary

Cobalt and cadmium complexes based on urea and thiourea were successfully synthesised for their use as single source precursor for the preparation of the metal sulphide and oxide nanoparticles. All complexes were obtained in reasonable yields, easy to prepare and very stable. The complexes were analysed by several spectroscopic techniques such as FTIR, TGA and Elemental analysis. The prepared complexes coordinate with the ligands through sulphur and oxygen which was advantageous in the formation of metal sulphide/oxide nanoparticles. A single-source precursor method was employed for thermolysis of the synthesised complexes to give metal sulphide/oxide nanoparticles. A synthetic procedure for the synthesis of normal and core-shell nanoparticles whose emission spans most of the visible spectrum is described in the study. These samples were analyzed optically and structurally using numerous techniques such as TEM, UV- visible, PL and XRD. Morphology demonstrated an increase in the size of the nanoparticles with increasing precursor concentration as well as an increase in the size distribution. The absorption band edges of the normal nanoparticles is blue shifted to their bulk band-edges whereas the absorption band edges of the core-shells nanoparticles are red-shifted from low to high concentration all as results of quantum confinement.

Photoluminescence spectra show a red shift from their respective band edges, however 1:2 & 1:3 CoO-CoS is blue shifted from their respective band edges as results of irregular shapes and agglomeration of nanoparticles. In the case of rods, length and the width both have a contribution in the resultant band-edges. Taking into account the general definition of nanoparticles only accounts for diameter of the particles, therefore a rod with a diameter within 20 nm and length than that can still be considered a nanoparticles. Therefore the blue shift can be explained by the notion that the morphology of the particle has a great influence on the

photoluminescence properties of the nanoparticles. With spherical particles, the diameter of the particle can be related to the whole size of the particles, whereas with rod or wire like particles, the diameter does not account for the length of the particles. XRD matches well with TEM, broader and narrow peaks favouring small and larger particles respectively.

In the study core-shells nanoparticles were successfully synthesised, with hollow cavity and spherical nanoparticles under the experimental conditions CdO-CdS (1:3) at 180°C, while other ratios and precursors were no evidence of the formation of core-shells. The effect of temperature was also investigated on CdO-CdS (1:3) nanoparticles at 100°C. A mixture of hexagonal and spherical shape with sheets like onion morphology was observed from TEM images. The core-shells formed in this study are assumed to be reverse type I core-shells nanoparticles. The bulk band edges of CdO and CdS are 539 and 515 nm respectively. In the study CdO precursor was injected first to serve as a core and followed by CdS precursor after 60s to serve as a shell hence we assume the coreshell nanoparticles will follow the same trend during thermolysis, the hallow cavity being that of CdO and the shell of CdS.

4.10 Recommendations and future work

There are numbers of properties that require a special attention for further exploration to produce coresells with high intensity luminescence. There are only few reports on core-shell nanomaterials and provide room to prepare materials with improved luminescence, quantum yields, increased fluorescence lifetimes, and benefits related to the tailoring of the relative band-gap positions between the two materials. Relevant precursors for the synthesis of metal chalcogenides material have to be carefully selected as different precursors have different applications.

Based on the study more things need to be explored:

1. Injection time between the first precursor (to serve as shell) and the second precursor (to serve as a shell).
2. To study the affinity of different chalcogenides elements on a specific metal by comparing the band edges, this will help in understanding the suitable choice of precursor to serve as core or shell.
3. Investigate the behaviour of the core-shells nanoparticles at higher temperature.
4. Investigate the behaviour of core-shells nanoparticles in different capping agent.
5. Understanding how polarity and the salt affect the morphology of the particles, because the precursor type and the solvent polarity influence the shape of the particles.
6. Understand interaction of two precursors as they grow during thermolysis of core-shells nanoparticles.
7. Identification of the instrument to verify material forming a core, shell and sheets on the formed core-shells nanoparticles.

4.8 References

1. Berkowitz A.E, Kodama R.H, Salah A, Makhlouf F.T, Parker F.E, Spada E.J and McNiff Jr S. Phys. Rev. Lett, 1992. 68: p. 3745
2. Flomenbom O, Amir R. J, Shabat D and Klafter J. J. Lumin, 2005. **111**: p. 315.
3. Guillot M, Eisler S, Weller K, Merkle H.P, Gallani J. L and Diederich F. Org. Biomol. Chem. 2006. **4**: p. 766.
4. Zhu H.W, Xu C.L, Wu D.H, Wei B.Q, Vajtai R and Ajayan P. M. Science. 2002 **296**: p. 884.
5. Dekker, C, Shannon W. Anderson, Margaret H. Christ, Henri Phys today, 1999. **52**: p. 22.
6. Zhao Y, Kim Y. H, Dillion A. C, Heben M. J and Zhang S. B. Phys. Rev.Lett, 2005. **95**: p. 155-504.
7. Fahlman B.D and Barron A.R. Adv. Mater. Opt. Electron. 2000. **10**:p. 223.
8. Marcus M.A, Brus L.E, Murray C, Bawendi M.G, Prasad A and Alivisatos A.P. Appl. Phys. 1992. **1(4)**. p. 323–335.
9. Kittel, C., Introduction to Solid State Physics, John Wiley & Sons Inc, 2005.
10. Efros A and Rosen M. Annu. Rev. Mater. Sci, 2000. **30**: p. 475.
11. Steigerwald M.L and Brus L.E. Acc. Chem. Res, 1990. **23**: p. 183.
12. Dabbousi B. O, Rodriguez-Viejo J, Mikulec F. V, Heine J. R, Mattoussi H, Ober R, Jensen K. F and Bawendi M. G. J Phys Chem. 1997. **101**: p. 9463-9475.
13. Murray C.B, Norris D.J and Bawendi M.G. J. Am. Chem. Soc, 1993. **115**: p. 8706.
14. Chemsiddine A and Weller H. Phys. Chem, 1993. **97**: p. 636.
15. Micic O.I, Sprague J.R, Curtis C.J, Jones K. M and Machol J.L. J.Phys. Chem. 1995. **99**: p. 7754.

16. Nirmal M, Murray C.B and Bawendi M.G. Phys. Rev, 1994. **50**: p. 2293.
17. Youn H.C, Baral S and Fendler J.H. J. Phys. Chem, 1988. **92**: p. 6320.
18. Mews A, Eychmuller A, Giersig M, Schooss D and Weller H. J.Phys. Chem. 1994. **98**: p. 934.
19. Mangin D, Puel F and Veessler S. Org Proc R & D, 2009. **13(6)**: p. 1241.
20. Kashchiev D. Cluster Properties. In Nucleation basic theory and application, 2001.
21. Sugimoto T., Adv. Colloid. Interf. Sci, 1987. **28**: p. 65.
22. Shah P. S, Holmes J. D, Johnston K. P and Korgel B. A. J. Phys. Chem. 2002. **106(10)**: p. 5020
23. Lamer V.K and Dinegar R.H. J. Am. Chem. Soc., 1950. **72(11)**: p. 4847.
24. Lifshitz M and Slyozov V.V. J. Phys.Chem. Solids, 1961. **19**: p. 35.
25. Wagner C, Schuster J, Schulz S.E, Fuchs F and Zienert A. Elektrochem, 1961. **65**: p. 581.
26. Markov I.V. Crystal Growth for beginners, 2nded, Singapore: World Scientific. 2003. **546**: p. 723.
27. Sugimoto T, Talapin, D.V, Lee J. S, Kovalenko M. V and Shevchenko E. V. Adv. Colloid Interface Sci., 1987. **28**: p. 165.
28. Alivisatos A.P. J. Phys. Chem, 1996. **100**: p. 13226.
29. Buffat P and Borel J.P. Phys. Rev. 1976. **13(6)**: p. 2287.
30. Kreibig U and Vollmer M. Optical Properties of Metal Clusters, Springer. 1995.
31. Alivisatos A.P, Marcus M.A, Brus L.E, Murray C, Bawendi M.G and Prasad A, Science, 1996. **271**: p. 933.
32. Kamat P.V and Tvrđy K. J. Phys. Chem. 2002. **106**: p. 7729.
33. Yu P. Fundamentals of Semiconductors: Physics and Materials Properties, Springer. 1999.

34. Talapin D.V, Lee J. S, Kovalenko M. V and Shevchenko E. V. Chem. Rev. 2010. **110**: p. 389.
35. Knox R.S. Theory o f Excitons; New York: Academic Press, 1963.
36. Brus L.E. J. Chem. Phys, 1984. **80**: p. 4403.
37. Wang Y and Herron N. J. Phys. Chem, 1991. **95**: p. 5120.
38. Henglein A. Chem. Rev. 1989. **89**: p. 1861.
39. Henglein A. and Gratzel M. Chem. Rev, 1995. **95**: p. 49.
40. Ma X, Shi W and Li B. Semicond. Sci. Technol, 2006. **21**: p. 713.
41. Pankove J.L. Optical Process in Semiconductors, Dover Publications Inc.: New York, 1970.
42. Jarrold M.F, Creegan K. **M**. Science, 1991. **252**: p. 1991.
43. Brus L.E and Krishnan R. J. Phys. Chem, 1986. **90**: p. 3393.
44. Sharma M, Kumar S and Pandey O.P. Digest Nanomaterials and Biostructures, 2008. **3(4)**: p. 189.
45. Skoog D.A, West D.M and Holler T.J. Analytical Chemistry. **7**: p. 506 and 601.
46. Weller H, Koch U, Gutierrez M and Henglein A. Phys. Chem, 1987. **91**: p. 88.
47. Talapin D.V, Rogach L, Kornowski A, Haase M and Weller H. Nano. Lett, 2001. **1**: p. 207.
48. Hässelbarth A, Eychmuller A, Eichberger R, Giersig M, Mews A and Weller H. J. Phys. Chem., 1993. **97**: p. 5333.
49. Zhou H.S, Honma I, Komiyama H and Haus J. W. J. Phys. Chem, 1993. **97**: p. 895.
50. Zhou H.S. Sasahara H. Honma I., Komiyama H., and Haus J. W., Chem. Mater, 1994. **6**: p. 1534.
51. Eychmüller A., Hässelbarth A and Weller H. J. Lumin, 1992. **53**: p. 113.

52. Kortan A.R, Hull R, Opila R. L, Bawendi M. G, Steigerwal M. L and Carroll J. P. J. Am. Chem. Soc, 1990. **112**: p. 1327.
53. Hoener C.F. Allan K. A., Bard A. J, Campion A, Fox M. A, Mallouk T. E, Webber S. E and White J. M. J. Phys. Chem, 1992. **96**: p. 3812.
54. Reiss P, Bleuse J and Pron A., Nano Lett, 2002. **2**: p. 781.
55. Dabbousi B.O, Rodriguez-Viejo J, Mikulec F. V, Heine J. R, Mattoussi H, Ober R, Jensen K. F and Bawendi M. G. J. Phys. Chem, 1997. **B 101** p. 9463.
56. Bruchez M.P, Moronne M, Gin P, Weiss S and Alivisatos A. P. Science, 1998. **281**: p. 2031.
57. Han M, Gao X, Su J. Z and Nie S. Nat. Biotechnol, 2001. **19** p. 631.
58. Zhang D, Wang Y, Xiao Y, Qian S and Qian X. Tetrahedron, 2009. **65**: p. 8099.
59. Bardajee G.R, and Hooshyar Z. Colloids Surf. A: Physicochem. Eng. Aspects, 2011. **387**: p. 92.
60. Mahmoud W.E. Sens. Actuators, 2012. **B 164** p. 76.
61. Mews A, Eychmuller A, Giersig M, Schoob D and Weller H. J. Phys. Chem, 1994. **98**: p. 934.
62. Yang Y, Chen O, Angerhofer A and Cao Y. C. J. Am. chem. soc, 2008. **130 (46)**: p. 15661.
63. Sapoval B and Hermann C. Physics of semiconductors, 1993.
64. Shim, M, Wang C and Norris D.J. Guyot-Sionnest, P. MRS Bulletin, 2001, p. 1122
65. Shim M and Guyot-Sionnest P. Nature, 2000. **407**: p. 981.
66. Wang C.J and Shim M and Guyot-Sionnest P. Science, 2001. **291**: p. 2390.
67. Yu D, Wang C.J and Guyot-Sionnest P. Science, 2003. **300**: p. 1277.
68. Erwin S.C. J.Nature, 2005. **436**: p. 91.
69. Bhargava R.N. Phys. Rev. Lett, 1994. **72**: p. 416.

70. Norberg N.S. J. Am. Chem. Soc, 2004. **126**: p. 9387.
71. Murray C.B, Norris D.J and Bawendi M.G. J Am Chem Soc 1993. **115(19)**: p. 8706.
72. Cozzoli P.D. Chem Mater, 2005. **17(6)**: p. 1296.
73. Dabbousi B.O. J Phys Chem, 1997. **101(46)**: p. 9463.
74. Brus L.E. J Chem Phys, 1983. **79(11)**: p. 5566.
75. Trindade T and OBrien P.A. Adv Mat, 1996. **8(2)**: p. 161.
76. Trindade T, OBrien P and Zhang X.M. Chem Mater, 1997. **9(2)**: p. 523.
77. Nair P.S and Scholes G. D. J Mater Chem, 2002. **12(9)**: p. 2722.
78. Malik M.A, O'Brien P and Revaprasadu N.A. Chem Mater, 2002. **14(5)**: p. 2004.
79. Murcia M.J, Chem Mater, 2006. **18(9)**: p. 2219.
80. Green M and O'Brien P. Adv Mater, 1998. **10**: p. 527.
81. Green M and O'Brien P. J Mater Chem, 1999. **9**: p. 243.
82. Brennan J.G. J Chem Soc, 1989. **111**: p. 4141.
83. Wells R.L. Organometallics 1993. **12**: p. 2832.
84. Stoll S.L, Gillan E.G and Barron A.R. Chem Vap Deposition, 1996. **2**: p. 182.
85. Trindade T. Polyhedron, 1999. **18**: p. 1171.
86. Ramasamy K. Phil. Trans. R. Soc., 2010. **368**: p. 4249.
87. Lee S.M, Cho S.N and J. Cheon. Adv. Mater, 2003 **15**: p. 441.
88. Christian P and O'Brien P. J. Mater. Chem, 2008. **18**: p. 1689.
89. An J. J. Phys.Chem Mater, 2007. **111**: p. 18055.
90. Jun S, Jang E and Lim J.E. Nanotechnology, 2006. **17**: p. 3892.
91. Protiere M and Reiss P. Nanoscale Res. Lett, 2006. **1**: p. 62.
92. Chen D. Chem. Mater, 2010. **22**: p. 1437.
93. Cumberland S.L. Chem. Mater, 2002. **14**: p. 1576.
94. Tong H. and Zhu Y.J. Nanotechnology, 2006. **17**: p. 845.

95. Nair P.S and Scholes G.D. Mater. Chem, 2006. **16**: p. 467.
96. Li J.J. J.Am. Chem. Soc, 2003. **125**: p. 12567.
97. Mukherjee R. Coord. Chem. Rev., 2000. **203**: p. 151.
98. Ghebghoub F and Barkat D. J. Coord. Chem, 2009. **62**: p. 1449.
99. Hamid A.A.A. J. Coord. Chem, 2010. **3**: p. 731.
100. Hachemaoui A, Belhamel K and Bart H.J. J. Coord. Chem, 2010. **63**: p. 2337.
101. Trofimenko S. J. Am. Chem. Soc, 1996. **88**: p. 1842.
102. Atwood D.A, Matlock M.M and Howerton B.S. Water Res., 2003. **37**: p. 579.
103. Parkin G. Chem. Rev, 2004. **104**: p. 699.
104. Kantekin H. J. Coord. Chem, 2010. **63**: p. 1921.
105. Tshuva E.Y and Lippard S.J. Chem. Rev, 2004. **104**: p. 987.
106. Walkes M.P. J. Inorg. Biochem, 2000. **79**: p. 241.
107. Pons J. Inorg.Chem. Commun., 2007. **10**: p. 1554.
108. Wöhler and Ann, Physik, 1828. **12**: p. 253.
109. Tonn J. Chem. Eng, 1955. **62**: p. 186.
110. Moore P. Chem. & Eng. News, 1959. **37**: p. 84.
111. Franz A. J. Org. Chem, 1961. **26**: p. 3304.
112. Heinig R. SOFW J, 1996. **122(14)**: p. 998.
113. Gnewuch C.T and Sosnovsky G. Chem. Rev, 1997. **97(3)**: p. 829.
114. Finar I.L. Organic Chemistry”, Longman group limited, London, 1973: p. 460.
115. Srinivasa I. Technology, 1970. **7(12)**: p. 27.
116. Kaganskii I.M and Babenko A.M. Zh. Prikl. Khim, 1970. **43(11)**: p. 2390.
117. Zhang Y. Huaxue Shijie, 1996. **37(4)**: p. 178.
118. Chuncong H., Chem. Abs., 1990. **113**: p. 888.
119. Pandey A.D. Chem. Abs., 1993. **118**: p. 607.

120. Crispoldi A. Chem. Abs., 1993. **119**: p. 831.
121. Hachemaoui A, Belhamel K and Bart H.J. J. Coord. Chem, 2010. **63**: p. 2337.
122. Gentile P. S. Inorg. chim.acta., 1972. **6(c)**: p. 296.
123. Sagatys D. S. polyhedron., 1992. **11(1)**: p. 49.
124. Lewinski K, Sliwinski J and Lebioda L. Inorg. chem., 1983. **22(16)**: p. 2339.
125. Kryatov S. V. chemical communicationa., 2000. **11**: p. 921.
126. Bhoopathy T. J, Baskaran M and Mohan S. Indian J. Phys., 1988. **62 B (1)**: p. 47.
127. Yamaguchi A, Penland R. B and Mizushima S. J. Amer. Chem. Soc., 1958. **80**: p. 527.
128. Duncan J.L, Aitken G. B, Quillan G.P.M. Spectochim.Acta, Part A, 1970. **27**: p. 1197.
129. Aitken G. B, Duncan J. L and Quillan G.P.M. J. Chem. Soc. A., 1971. **2695**: p. 1-56.
130. Hadzi D, Kidric J and Knezevic Z. V. Spectochim.Acta,Part A., 1976. **32**: p. 693.
131. Sib S. B and Ghosh P.N. J. Mol. Str., 1983. **101**: p. 69.
132. Kellner L. Proc. Roy. Soc., 1941. **A 117**: p. 456.
133. Waldron R. D and Badger R.M. J. Chem. Phys., 1950. **18**: p. 566.
134. Andrew E. R and Hyndman D. proc. Roy. Soc., 1953. **A 66**: p. 1187.
135. Yamaguchi A, Miyazawa T and Shimanouchi T. Spectochim.Acta., 1957. **10**: p. 170.
136. Stewart J.E, Marcus M.A and Brus L.E. J. Chem. Phys., 1957. **26**: p. 248.
137. Penland R. B, Mizushima S and C. Curran. J. Amer. Chem. Soc., 1957. **79**: p. 1575.
138. Svatos G. F, Curran C and Quaglian J.V. Phys. Lett. 1965. **77**: p. 6159.
139. El-Bahy G.M.S, El-Sayed B.A and Shabana A.A. Vib. Spectrosc, 2003. **31**: p. 101.
140. Yamaguchi A, Penland R.B and Mizushima S. J.Am. Chem. Soc, 1958. **80**: p. 527.
141. Lopes J.G.S. J. Raman Spectrosc, 2004. **35**: p. 131.
142. Selvakumar S. Mater. Chem. Phys, 2007. **103**: p. 153.
143. Krishnakumar V and Nagalakshmi R. Spectrochim. Acta Part A, 2005. **61**: p. 499.
144. Jayalakshmi D and Kumar J. Cryst. Res. Technol, 2006. **41**: p. 37.

145. Alia J.M, Edwards H.G.M and M.D. Stoev, *Spectrochim. Acta Part A*, 1999. **55** p. 2423.
146. Yu S.H. *J. Mater. Chem*, 1999. **9**: p. 1283.
147. Yamaguchi A. *J. Am. Chem. Soc*, 1958. **80**: p. 527.
148. Miyazawa T, Shimanouchi T and Mizushima S. *J. Chem. Phys*, 1956. **24**: p. 408.
149. Miyazawa T, Shimanouchi T and Mizushima S., *J. Chem. Phys*, 1958. **29**: p. 611.
150. Wyckoff R.G and Corey R.B, *J Am Chem Soc*, 1932. **18**: p. 386.
151. Kumle W.D and Fohler G.M. *J. Am. Chem. Soc*, 1942. **64**: p. 1944.
152. Sandell E.B. *Colorimetric Determination of Trace Elements*, Interscience, New York, 1959: p. 199.
153. Bourne S and Koch K.R. *J. Chem. Soc. Dalton Trans.*, 1993: p. 2071.
154. Kumar K.S, Singh S.K and Pandeya S.N. *Bolletino Chimico Farmaceutico.*, 2001. **140**: p. 238.
155. Ku`zu`kgu` zel I. *Bioorg.Med. Chem. Lett.*, 2001. **11**: p. 1703.
156. Venkatachalam T.K, Sudbeck E.A, and Uckun F.M. *Tetrahedron Lett.*, 2001. **42**: p. 6629.
157. Vasilev G, Tafrdzhiski I and Masher N.P. *Dokl. Bolg. Akad.Nauk.*, 1974. **27**: p. 1121.
158. Campo R. *J. Inorg. Biochem.*, 2002. **89**, p 11.
159. Giuliani A.M. *J. Chem. Soc., Dalton Trans.*, 1975: p. 492.
160. Sidall T.H and Stewart W.E. *J. Org. Chem.*, 1967. **32**: p. 3261.
161. Tompa A.S, Barefoot R.D and Price E. *J. Phys. Chem.*, 1969. **73**: p. 435.
162. Kessler H and Leibfritz D. *Tetrahedron Lett.*, 1970. **19**: p. 595.
163. Lane T.J and Yamaguchi A. *J. Am. Chem. Soc.*, 1959. **81**: p. 3824.
164. Vassilev G, Koleva V and Ilieva M. *J. Mol. Struct.*, 1982. **82**: p. 35.
165. Kavalek J, Fiedler P and Papouskova Z. *Collect. Czech.Chem. Comm.*, 1982. **47** p. 35.
166. Mido Y, Okada H and Fujita N. *J. Mol.Struct.* , 1997. **415**: p. 215.

167. Joy V.T and Srinivasan T.K.K. *Spectrochim. Acta.*, 1999. **A55**: p. 2899.
168. Rosenheim A and Meyer V.J. *Z. Anorg. Chem.* , 1906. **49**: p. 13.
169. Mido Y, Kitagawa I and Hashimoto M. *Spectrochim. Acta.*, 1999. **A55**: p. 2623.
170. Yamaguchi A, Penland R.B and Mizushima S.. *J. Am. Chem. Soc.*, 1958. **80**: p. 527.
171. Flint C.D and Goodgame M. *J. Chem. Soc. A.*, 1966: p. 744.
172. Adams D.M and Cornell J.B. *J. Chem. Soc.* , 1967. **A**: p. 884.
173. Marcos C. Alia J.M., Adovasio V.. *Acta Crystallogr.*, 1998. **C54**: p. 1225.
174. Shen X. Shi X., Kang B.. *Polyhedron.*, 1998. **17**: p. 4049.
175. Rivest R and Can. *J. Chem. Phys.*, 1962. **40**: p. 2234.
176. Pakawatchai C, Thanyasirikul Y and Saepae T. *Acta Crystallogr.*, 1998. **C54**: p. 1750.
177. Cox M.J and Tiekink E.R.T. *Kristallogr.*, 1999. **214**: p. 670.
178. Griffith E.H, Hunt G.W and Amma E.L. *J. Chem. Soc.*, 1976. **Chem.Comm.**: p. 432.
179. Bott R.C, Bowmaker G.A and Davis C.A. *Inorg. Chem*, 1998. **37**: p. 651.
180. Okaya Y and Knobler C.B. *Acta Crystallogr*, 1964. **17**: p. 928.
181. Gash A.G, Griffith E. H and Spofford W. A. *J Am Chem Soc*, 1973.
182. Wharf I, Can, Gramsted T and Makhiji R. *J. Chem*, 1976. **54**: p. 3430.
183. Moloto M.J, Revaprasadu N and Moloto N *Polyhedron*, 2003. **22**: p. 595.
184. Moloto N, Malik M. A, Moloto M.J and O'Brien P. *Polyhedron*, 2007. **26**: p. 3947.
185. Yamaguchi A, Penland R. B and Mizushima S. *J Am Chem Soc*, 1958. **80**: p. 527.
186. Kaganskii I.M and Babenko A.M. *Zh. Prikl. Khim*, 1970. **43(11)**: p. 2390.
187. Kim Y.K, Williard J.W and Frazier A.W. *J. Chem. Eng. Data*, 1988. **33(3)**: p. 306.
188. Srinivasa I, Vishivanathapuram K and Mishra M. B. *Technology*, 1970. **7(12)**: p. 27.
189. Gentile P.S, Carfagno P and Haddad S. *Inorg. Chim. Acta*, 1972. **6C**: p. 296.
190. Sagatys D.S, Bott R. C and Smith G. *Polyhedron*, 1992. **11(1)**: p. 49.
191. Lewinski K, Sliwinski J and Lebioda L. *Inorg. Chem*, 1983. **22(16)**: p. 2339.

192. Kryatov V, Nazarenko A. Y and Robinson P. D. Chem. Comm, 2000. **11**: p. 921.
193. Bhoopathy T.J, Baskaran M and Mohan S. Indian J. Phys, 1988. **62B(1)**: p. 47.
194. Yamaguchi A, Penland R. B, Mizushima S. J, Carfagno P and Haddad S Am. Chem. Soc, 1958. **80**: p. 527.
195. Duncan J.L, Waldron R.D. and Badger R.M. Spectrochim. Acta, 1970. **27A**: p. 1197.
196. Aitken G.B, Duncan J.L and Quillan G.P.M. J. Chem. Soc, 1971. **A**: p. 2695.
197. Hadzi D, Kidric J and Knezevic Z. V. Spectrochim. Acta, 1976. **32A**: p. 693.
198. Bala S.S and Ghosh P.N. J. Mol. Struct, 1983. **101**: p. 69.
199. Kellner L, Saito Y, Machida K and Uno T. Proc. Roy. Soc, 1941. **177A**: p. 456.
200. Waldron R.D and Badger R.M. J. Chem. Phys, 1950. **18**: p. 566.
201. Andrew E.R and Hyndman D. Proc. Phys. Soc, 1953. **66A**: p. 1187.
202. Yamaguchi A, Miyazawa T and Shimanouchi T. Spectrochim. Acta, 1957. **10**: p. 170.
203. Stewart J.E, Aitken, G.B, Duncan J.L and Quillan G.P.M. J. Chem. Phys, 1957. **26**: p. 248.
204. Penland R.B, Mizushima S and Curran C. J. Am. Chem. Soc, 1957. **79**: p. 1575.
205. Svatos G.F, Curran C and Quagliano J.V. J. Am. Chem. Soc, 1955. **77**: p. 6159.
206. Paoletti P and Vacca A. Trans, faraday Soc, 1964. **60**: p. 50.
207. Orgel L.E. an introduction to transition metal chemistry, methuen,london. 1967.
208. Clark R.J.H and Willams C.S. Inorg. chem, 1965. **4**: p. 350.
209. Goldstein M and Unsworth W.D. Spectrochim.Acta,, 1972. **28A**: p. 1107.
210. Nakamoto K. infrared spectra of inorganic and coordination compound, wiley, london. 1970.
211. Yamaguchi A, Miyazawa T and Shimanouchi S. Spectrochim.Acta,, 1957. **10**: p. 170.
212. Duncan J.L, El-Bahy, G.M.S, El-Sayed B.A and Shabana A.A. Spectrochim.Acta,, 1971. **27A**: p. 1197.

213. Saito Y, Machida K and Uno T. Spectochim.Acta,, 1971. **27A**: p. 991.
214. Hadzi D, Kidric J and Kenzevic Z. V. Spectochim.Acta,, 1976. **32A**: p. 693.
215. Diaz G and Campos M. spetrosc. Lett, 1981. **14**: p. 365.
216. Arenas J.F, Marques F and Cardenete A. sectrochim. Acta, 1984. **40A**: p. 1033.
217. Bhoopathy T.J, Baskaran M and Mohan S., Indian J. Phys, 1988. **62B**: p. 47.
218. Williams D.R, Bruchez M.P, Moronne M, Gin P, Weiss S and Alivisatos A. P. Chem. Rev, 1972. **3**: p. 202.
219. Maslowska J and Baranowska A. J. Thermal Anal, 1984. **29**: p. 309.
220. Jona E and Sramko T. chem Zvesti, 1966. **20**: p. 569.
221. Spitsin V.I and Kolli I.D. Russ. J. Inorg. Chem, 1964. **9**: p. 99.
222. Maslowska J and hruscinska E.C. Polish J. Chem, 1978. **52**: p. 1261.
223. Hullavarad N.V, Hullavarad S.S and Karulkar P.C. J. Nanosci. Nanotechnol, 2008. **8**: p. 3272.
224. Tiwari S and Tiwari S. Cryst Res Technol, 2006. **41**: p. 78.
225. Sanz M, Hullavarad N. V, Hullavarad S. S, and Karulkar P. C. J. Appl. Chem C, 2011. **115**: p. 3203.
226. Steigerwald M.L, Allivisatos A. P, Gibson J. M, Harris T. D, Korten R, Muller A. J, and Thayer A. M. j. Am. Chem. Soc, 1988. **110**: p. 3046.
227. Moloto N. J, Moloto M. J, Coville N. J and Sinha R. S. Nanosci. Nanaotechnol, 2010. **10 (9)**: p. 5594.
228. Greenwald S. Acta Crystallogr, 1953. **6**: p. 396.
229. Smith W.L and Hobson A.D., Acta Crystallogr, 1973. **B29** p. 362.
230. Roth W.L, J. Phys. Chem, 1964. **25** p. 1.
231. Mahendiran, R. and Raychaudhuri A.K., Phys. Rev, 1996. **B54**: p. 16044.

232. Respaud M, Frontera J, Garcí'a-Muñoz L, Aranda M.A.G, Raquet B, Broto J. M, Rakoto H, Goiran M, Llobet A and Rodri'guezCarvajal J. Phys. Rev, 2001. **B64**: p. 214401.
233. Taskin A.A, Lavrov A. N, Ando Y. Phys. Rev. Lett, 2003. **90**: p. 227201.
234. Akahoshi D and Ueda Y. J. Solid State Chem, 2001. **156**: p. 355.
235. Ramasamy K, Maneerprakorn W, Mohammad A, Malik M.A and O'Brien P. Phil. Trans. R. Soc., 2010. **A368**: p. 4249.
236. Smith G.B, Ignatiev A and Zajac G. J. Appl. Phys, 1980. **51**: p. 4186.
237. Whitney T.M, Jiang J. S, Searson P and Chien C. Science, 1993. **261**: p. 1316.
238. Yue G.H, Yan P. X, Fan X. Y, Wang M. X, Qu D. M, Wu Z. G, Li C and Yan D. Electrochem,Solid State lett, 2007. **10**: p. D29-D30.
239. Feng Y.G, He T and Alonso-Vante N. Chem. Mater, 2008. **20**: p. 26.
240. Yu Z, Du J, Guo S, Zhang J and Matsumoto Y. Thin Solid Films, 2002. **415**: p. 173.
241. Ortega-Borges R and Lincott D. J. Electrochem. Soc, 1993. **140**: p. 3464.
242. Deshmukh L.P and Holikatti S.G. J. Phys. D: Appl. Phys, 1994. **27**: p. 931.
243. Basu P.K and Pramani K.P. J. Mater. Sci: Lett., 1986. **5**: p. 1216.
244. Okli N.D and okoli N.C. J. Natural Sci. Res, 2012. **2**: p. 5.
245. Deshmukh L.P and Mane S.T. Nano materials and Biostructures, 2011. **6**: p. 931.
246. Sifuentes C, Barmenkov Y, Strodumov A, Filipov V and Lipovskii A. Opt. Eng, 2000. **39**: p. 2182.
247. Stegeman G.I and Seaton C.T. J. Appl. Phys, 1985. **58**, p.234
248. Ezema F.I and Osuji R.U. Chalcogenides Lett, 2007. **4**: p. 69.
249. Mishack E and Ekuma F. chalcogenide Lett, 2010. **7**: p. 31.
250. Khaorapapong N and Ogawa A.O.M. App. Clay sci, 2011. **51**: p. 182.

251. Ramasamy K, Maneerprakorn W, Malik M. A and O'Brien P. Phil. Trans. R. Soc., 2010. **A368**: p. 4249.
252. Sun Z.X, Li F. Y, Xu L, Liu S. P, Zhao M. L and Xu B. B. J. Phys. Chem C, 2012. **116**: p. 6420.
253. Ganesh T, Mane R. S, Cai G, Chang J.H and Han S.H. J. Phys. Chem C, 2009. **113**: p. 7666.
254. Ke D.N, Liu S. L, Dai K, Zhou J. P, Zhang L. N and Peng T. Y. J. phys. Chem C, 2009. **113**: p. 16021.
255. Li T.L, Lee Y.L and Teng H. Energy & Environmental Science, 2012. **5**: p. 5315.
256. Jie J.S, Zhang W. J, Jiang Y, Meng X. M, Li Y. Q and Lee S. T. Nano Letters, 2006. **6**: p. 1887.
257. Yildiz H.B, Tel-Vered R and Willne I. Angewandte Chemie, 2008. **120**: p. 6731.
258. Jun Y, Choi J and Cheon J. Angew. Chem. Int., 2006. **45**. p. 665
259. Moloto N, Revaprasadu N, Moloto M. J, O'Brien P, and Helliwell M. Polyhedron, 2007. **26**: p. 3947.
260. Hoyer P, Baba N and Masuda H. appl. phys. Lett, 1995. **66**. p. 534.
261. Wang Y and Herron N.J. J. Phys. Chem, 1988. **92**: p. 4988.
262. Klick C.C, Michael C, Andreas V and Alivisatos A. P. Phys. Rev, 1953. **89**: p. 274.
263. Bawendi M.G, Steckel J. S, Zimmer J. P, Sullivan S. C, Stott N. E and Bulovic V. J Am Chem Soc, 1989. **91**: p. 7282.
264. Ghosh M and Rao C.N.R. Chemical Physics Letters, 2004. **2004**: p. 493.
265. Wu X, Tsuji M, Miyamae N, Lim S, Kimura K, Zhang X, Hikino S, and Nishio M. J. Mater. Res, 1998. **13**: p. 604.
266. Gupta R.K, Sinha A. K, Sekhar B. N. R, Srivastava A. K, Singh G and Deb S. K. Appl. Phys A, 2011. **103**. p. 122

267. Alexandre R, Ceco D, Karolina I and Andrey V. Phys. Eng. Asp, 2004. **245**. p. 232
268. Reiss P, Protière M and Li L. core/shell semcond nano cryst, 2009. **5(2)**. p.244
269. Michael C, Andreas V and Alivisatos A.P. J. Am. Chem. Soc, 1997. **119(30)**. p. 89
270. Bruchez M, Moronne M, Gin P and Weiss S. Science 1998. **281(5385)**. p.67
271. Makhal A, Yan H, Lemmens P and Pal S. K. J. Phys. Chem, 2010. **114(1)**. p.766
272. Steckel J.S, Zimmer J. P, Sullivan S. C, Stott N. E, Bulovic V and Bawendi M. G. Angew. Chem. Int. Ed, 2004. **43**: p. 2154.
273. Chen D, Zhao F, Qi H, Rutherford M and Peng X. G. Chem. Mater, 2010. **22**: p. 1437.
274. Tsuji M, Miyamae N, Lim S, Kimura K, Zhang X, Hikino S and Nishio M. Cryst.Growth Des, 2006. **6**. p. 877
275. Ma Y, Li W, Cho E. C, Li Z, Yu T, Zeng J, Xie Z and Xia Y. ACS Nano, 2010. p. 766
276. Murugadoss G. Journal of Luminescence, 2012. **132**. p. 112
277. Cumberland S.L, Hanif K. M, Javier A, Khitrov G. A, Strouse G. F and Woessner Chem S.M. Mater, 2002. **14**: p. 1576.
278. Li J.J, Wang Y. A, Guo W. Z, Keay J.C, Mishima T. D, Johnson M. B and Peng X. G. J. Am. Chem. Soc, 2003. **125**: p. 12567.
279. Cheng Z, Wang S, Wang Q and Geng B. Cryst. Eng. Comm, 2010. **12**: p. 144.
280. Trallero-Giner C, Comas F, Marques G, Tallman R and Weinstein B. Phys. Rev, 2010. **82 (20)**: p. 5426.
281. Tiejun Z, Meihua L, Zhihua Z, Hao G, Chin Y, Shong W and Bo L. Adv Mat, 2010. **22(3)**: p. 403.
282. Peng X.G, Schlamp M. C, Adavanich A. V and Alivisatos A. P. J. Am. Chem. Soc, 1997. **119**: p. 7019.
283. Daniel M.C, George C, Diaspro A, Manna L and Cingolani R. Chem. Rev, 2004. **104** p. 293.

284. Korobchevskaya K. Appl. Phys. Lett, 2011. **99**: p. 011907.
285. Bohren C.F and Huffman D.R. Absorption and Scattering of Light by Small Particles, Wiley, New York, 1983.
286. Mulvaney P, Liz-Marzan L.M and Giersig M. J. Mater. Chem, 2000. **10**: p. 1259.
287. Peng X, Manna L, Yang W, Wickham J, Scher E. C, Kadavanich A and Alivisatos A. P. Nature, 2000. **404**: p. 59.
288. Adam Z and Peng X.G. J Am Chem Soc, 2001. **123**: p. 1389.
289. Jun Y, Jung Y and Cheon J. J Am Chem Soc, 2001. **123**: p. 5150.
290. Moloto N, Revaprasadu N, Musetha P. L and Moloto M. J. J Nanosci and nanotech, 2008. **9**: p. 1.
291. Lee S.M, Cho S.N and Cheon J. Adv. Mater, 2003. **15**: p. 441.